Velocity Measurement by Doppler Sonar Using Coherent Method

LIU, PENG

(Degree)
博士（工学）
(Date of Degree)
2015-09-25
(Date of Publication)
2016-09-01
(Resource Type)
doctoral thesis
(Report Number)
甲第6492号
(URL)
https://hdl.handle.net/20.500.14094/D1006492

Doctoral Dissertation

Velocity Measurement by Doppler Sonar Using Coherent Method

(コヒーレント方式を用いた
ドップラーソーナーによる速度計測に関する研究)

July 2015

Graduate School of Maritime Sciences
Kobe University

LIU PENG
(刘　鹏)

SUMMARY

Here we present a combined method of conventional and coherent Doppler sonar systems (CMDS) to provide accurate marine velocity information. The dissertation is divided into four chapters, background, sonar system, combined method of Doppler sonar and conclusions.

Chapter 1 describes the background of velocity measurement systems in water. The purpose of CMDS is to measure velocity accurately and precisely for surface and underwater vessels. Conventional Doppler sonar (CNDS) can provide velocity without velocity ambiguity, but it needs some seconds to provide valuable reading velocity. Coherent Doppler sonar (CHDS) can measure the velocity with an accuracy of about 1 cm/s, but velocity ambiguity seriously limits its general application. Therefore, CMDS is proposed in order to take advantage of both CNDS and CHDS to provide accurate and precise velocity with a short time lag. A further brief description of the dissertation's structure can be found at the end of this chapter.

Chapter 2 introduces existing Doppler sonar systems, CNDS and CHDS, in detail. Firstly, types and usages of sonar systems are introduced briefly. Then the fundamentals of CNDS are explained and the equations used to calculate velocity using CNDS are shown. CNDS calculates velocity using measured frequency information directly based on the Doppler effect. After introducing the measurement method of CNDS, error analysis of CNDS is also discussed. Thirdly, velocity measurement by CHDS is introduced. Phase change between two adjacent pulses is used to calculate moving velocity. But because the measured phase is limited from $-\pi$ to π, velocity ambiguity occurs. Several methods have

been proposed to solve this problem. One method is to introduce dual time intervals. This method can extend the range of maximum measureable velocity several times, but it decreases the data rates and increases measurement error. Although a data processing technique is used to make the measurement as precise as the single time interval method, measureable velocity range is still limited when using the dual time interval method. Multiple frequency method is also used to enlarge the measureable velocity range without decreasing the data rates, but system device needed is expensive. The alternating dual time interval and dual frequency method has also attempted to solve the problem of velocity ambiguity, but despite enlarging the range it was unable to solve the velocity ambiguity. Although, these previous methods could extend the measureable velocity several times larger, none of them could cancel it. At the end of this chapter error analysis using CHDS is explained.

In Chapter 3, CMDS is introduced as a solution to cancel the velocity ambiguity. Firstly, basic CMDS is presented using the measurement results of CNDS and CHDS. However, the result of this basic CMDS method is affected by the value of measured velocity. A velocity shift technique is introduced to solve this problem. CMDS using fixed ambiguity velocity only works well at the range of high SNRs. At the range of low SNRs it contains lots of impulsive noise due to a wrong estimation of integer factor. Accordingly adaptive algorithm is employed to provide accurate and precise velocity information for CMDS at a wide range of SNRs.

Chapter 4 discusses measurement error of CMDS. After introducing the definition of measurement error, the measurement error of CMDS is deduced by the error of CNDS and CHDS. The effect of velocity shift technique and adaptive algorithm are also analyzed. In the end, simulations and experiments of CMDS were carried out to evaluate its performance. Simulations were carried out with white Gaussian noise and the results of CMDS fitted the theoretical analysis well. Experiments were carried out in a large shallow water tank. Under the situation of fixed projector and hydrophone, the noise in the received signals could be considered as white Gaussian noise, and the measurement results fitted the theoretical results well. The projector which moves forward and backward, caused a vibration to be generated from the bar and frame of the experimental platform. The vibration caused the results of CNDS to be much noisier than in the stable situation, which made the CMDS, using adaptive algorithm, do not work well at the range of high SNRs. According to the simulation and experiment results CMDS can provide accurate and precise velocity at a wide range of SNRs in white Gaussian noise.

In Chapter 5, conclusions based on the theoretical and experiment results of the proposed CMDS are explained. Future considerations and proposals are also discussed to improve the performance of CMDS.

CONTENTS

LIST OF FIGURES AND TABLES

ACRONYMS

SDME	Speed and Distance Measurement Equipment
SOLAS	Safety of Life at Sea
EM log	Electro-Magnetic log
INS	Inertial Navigation System
GPS	Global Positioning System
VI-GPS	Velocity Information GPS
CMDS	Combined Doppler Sonar
CNDS	Conventional Doppler Sonar
CHDS	Coherent Doppler Sonar
SNR	Signal to Noise Ratio

NOTATIONS

A	Amplitude of received signal
$a_0(t)$	Envelop of transmitted signal
c	Wave speed in the medium
$C\,(t)$	Cross-correlation of two complex signals
D	Distance change of measured object during time interval τ
E	Energy of the received signal
f_0	Transmitted carrier frequency
f_r	Received frequency
$f_{r\,I}$	Frequency of front beam in CNDS
$f_{r\,II}$	Frequency of rear beam in CNDS
f_d	Doppler shift
f_D	Doppler shift between the front and rear received beams in CNDS
$I(t)$	In-phase component
$N_0/2$	Noise power per Hertz for noise waveform
$N_a(t)$	White Gaussian noise
N, n	Integer value
n_0	True value of integer factor n
n_e	Estimated integer factor
Δn_e	Estimated integer error
$P_{(\Delta n_e)}$	Probability of Δn_e occurring
$P_{t(\Delta n_e)}$	Probability of Δn_e occurring using velocity shift
$p_t(\varepsilon_t)$	Probability density function of the error factor, ε_t

$Q(t)$	Quadrature component
$R_r(t)$	Received target signal without noise
$R(t)$	Received target signal with thermal and environmental noise
$R_f(f)$	Fourier transform of received signal
$\mathbb{R}(t)$	Received signal in complex domain
Δr	Maximum measureable space range of CHDS
$S(t)$	Transmitted signal
$S_f(f)$	Fourier transform of transmitted signal
t_0	Time delay generated by the distance between the transmitter and target
v	Moving velocity of measured object
v_s	Speed of signal source
v_r	Speed of receiver
$v_{s,r}$	Relative speed of signal source and observer,
v_n	Velocity measured by CNDS
v_{n0}	Velocity measured by CNDS without noise
v_h	Velocity measured by CHDS
v_{h0}	Velocity measured by CHDS without noise
Δv	Maximum measureable velocity of CHDS, ambiguity velocity
Δv_u	Maximum value of the range of ambiguity velocity
Δv_s	Search step used to find optimum ambiguity velocity
Δv_a	Optimum range of ambiguity velocity
α	Angle of depression of the beam in CNDS
τ	Time interval between two adjacent pulses
$\sigma_{\Delta f}$	Root mean square error in estimating Doppler shift
σ_n	Standard deviation of velocity measured by CNDS
σ_h	Standard deviation of velocity measured by CHDS

σ_m	Standard deviation of velocity measured by CMDS
σ_{mt}	Standard deviation of velocity measured by CMDS using variable shift
σ_{ha}	Standard deviation of velocity measured by CHDS using the optimum range of ambiguity velocity
σ_{ma}	Standard deviation of CMDS using the optimum range of ambiguity velocity
ϵ_Δ	Integrated squared difference of spectral between transmitted and received signals for CNDS
ϵ	Measurement error of phase
ε_n	Measurement error of CNDS
ε_h	Measurement error of CHDS
ε_t	Error factor used to decide a wrong integer factor
φ	Phase change between two adjacent pulses
$\tilde{\varphi}$	Measurement value of the phase change φ
φ_{i-est}	Estimated phase by $\tilde{\varphi}$
φ_{ori}	Original phase
λ	Sound wave length
$p(\varphi)$	Probability density function of phase measurement
$p_d(\varphi)$	Probability density function of the phase difference between two adjacent pulses
γ_b	Signal to noise ratio of the band-limited signal
ω_0	Angular velocity of transmitted signal
ω_d	Angular velocity generated by Doppler effect

CHAPTER 1

BACKGROUND

Since the mid 1970's, Doppler Docking Sonar has been installed on very large vessels to provide velocities with the accuracy of 1 cm/s over ground and in three directions: fore/aft movement and side movements at bow and stern. Furthermore, Docking Speed and Distance Measurement Equipment (SDME) usually fixed on dolphins have been developed. Because of sonic disturbance, Docking SDME on dolphin was developed to use laser instead of underwater ultrasonic. Tracking laser equipment was then applied on a docking guidance system [1]. For Very Large Crude Oil Carrier (VLCC), velocity information is frequently and effectively used to maneuver adequately and safely. Therefore, at the 2000 International Convention for the Safety of Life at Sea (SOLAS) vessels more than 50,000 gross tonnes were recommended to be equipped with two axes SDME [2], [3], [4]. In addition, there are also many benefits for usual navigators on the vessels less than 50,000 gross tonnes to use the precise velocity information. With precise velocity information, a decrease in the probability of collisions with other ships or piers and improvement of the workload safety is possible.

Normally, electro-magnetic (EM) log, inertial navigation system (INS), Global Positioning System (GPS) and Doppler sonar systems are used to measure the velocity of moving vessels at sea. The EM log can only provide the velocity through water. The velocity measured by EM log is also limited to the area around the sensor. The handbook of the EM log (EML 500) indicates its accuracy as 0.1 m/s [5]. The velocity information GPS (VI-GPS) system can provide accurate velocity information relative to the earth with an accuracy of 0.01 m/s [6], [7], [8], [9]. Unfortunately GPS signal cannot be transmitted into water, so the VI-GPS is limited to the surface and above where it can receive the GPS signal. It also has an intrinsic disadvantage in that we cannot always receive a GPS satellite signal due to obstacles, such as mast or antenna. INS can also provide the velocity if the initial velocity is known, but the accumulative error seriously affects the final results. The accuracy of the INS of SEANAVTM for velocity is 0.91 m/s [10]. The Doppler sonar system can measure the velocity of objects both on the sea surface and in the water. Both the velocity relative to ground and water can be provided by the Doppler sonar system. However, the velocity information of the conventional Doppler sonar system includes a time lag of not a few seconds [11].

Most navigators of small vessels which are less than 500 gross tonnes do not rely on Doppler sonar. But about 30 – 40 % of navigators on vessels from 3,000 gross tonnes to 5,000 gross tonnes do rely on Doppler sonar. 80 % of navigators on vessels larger than 50,000 gross tonnes depend on Doppler sonar [7]. According to this data, it is important to provide accurate and precise velocity with short time lag by Doppler sonar for navigators.

The combined Doppler sonar (CMDS) system is proposed in this dissertation. Both conventional Doppler sonar (CNDS) and coherent Doppler sonar (CHDS) are used in the CMDS system. Adaptive algorithm is also introduced to decrease the measurement error at a wide range of signal to noise ratio (SNR). Error analyses are carried out to evaluate the performance of CMDS. According to the results of the simulation and experiments, CMDS can provide accurate and precise velocity with a short time lag and no velocity ambiguity.

The structure of this dissertation is as below:

Chapter 1 details the background and the structure of this dissertation.

Chapter 2 introduces the existing Doppler sonar systems. Before introducing CMDS, CNDS and CHDS are elaborated on. Measurement methods of CNDS and CHDS are explained in detail. Some improved methods of CHDS are also discussed. Error analysis of CNDS and CHDS are shown to evaluate their performance.

Chapter 3 describes in detail the method of combined Doppler sonar. First, with the knowledge of CNDS and CHDS, the expressions of CMDS are deduced. Then technique of variable shift is introduced to erase the effect of the value of measured velocity. Finally, an adaptive algorithm is proposed to decrease the measurement error of CMDS at a wide range of SNRs.

Chapter 4 discusses measurement error of CMDS. After introducing the definition of measurement error, theoretical analysis of combined Doppler sonar is deduced based on the error of CNDS and CHDS. Both simulation and experiments are carried to evaluate the performance of CMDS at different SNRs.

Chapter 5 summarizes the performance of velocity measurement by CMDS and discusses future work.

References

[1] M. Shimizu, Y. Ueno, “A Tracking Laser Ranging Equipment and Its Application to a Docking Guidance System,” Journal of the Society of Instrument and Control Engineers, Vol. 12, No. 8, pp.688-695, 1973.

[2] K. Tatsumi, T. Kubota, H. Fujii, N. Kouguchi and Y. Arai, “Ship’s Speed Information Standards in Docking/Leaving Maneuvering Based on Questionnaire Survey,” The Journal of Japan Institute of Navigation, Vol. 118, pp.31-37, Mar. 2008.

[3] “Maritime Bureau，Ministry of Land Infrastructure and Transport: International Convention for the Safety of Life at Sea, 2000,” Kaibundo-Shuppan, Jun. 2002.

[4] “IMO Resolution MSC. 96(72): Adoption of amendment to performance standards for devices to indicate speed and distance,” May 2000.

[5] “General Specification of EML500,” Yokogawa Denshikiki Co., Ltd. Dec. 2002.

[6] Y. Yoo, Y. Nakama, N. Kouguchi and C. Song, "Experimental Result of Ship’s Maneuvering Test Using GPS," Journal of Navigation and port research, 33(2), pp.99-104, 2009.

[7] K. Tatsumi, H. Fujii, T. Kubota, S. Okuda, Y. Arai, N. Kouguchi and K. Yamada, “Performance Requirement of Ship’s Speed in Docking/Anchoring Maneuvering,” Proceeding of International Association Institute of Navigation IAIN 06, Jeju South Korea, pp.67-73, 2006.

[8] Y. Aray, E. Pedersen, N. Kouguchi and K. Yamada, “The Availability of VI-GPS for Ship-Operation,” Proceedings of ANC 2010 in Inchon, KOREA, pp.88-95, Nov. 2010.

[9] Y. Arai, A. Hori, S. Okuda and K. Yamada, “Strategic Application of Two Axes Velocities Information for Ship Maneuvering,” Proceedings of IAIN Congress,

Stockholm, 2009.

[10] S. Beiter, R. Poquette, B.S. Filipo and W. Goetz, "Precision Hybrid Navigation System for Varied Marine Applications," Position Location and Navigation Symposium, IEEE, pp.316-323, 1998.

[11] R. Pinkel, "On Estimating the Quality of Doppler Sonar Data," Current Measurement, Proceedings of the 1982 IEEE Second Working Conference, Vol. 2, pp.113-116, 1982.

CHAPTER 2

SONAR SYSTEMS

2.1 Introduction

2.1.1 Types of sonar system

Of all known radiation sources, it is sound that travels best in water. Light and radio waves are attenuated in seas of turbid and saline water, greater than sound, which is a form of mechanical energy. Therefore, sound is normally used in the ocean exploration. The science of sonar consists of the uses of underwater sound, and systems using underwater sound in a variety of ways are called sonar systems [1].

Sonar systems can be divided into two types: active sonar systems and passive (or listening) sonar systems. If sound is generated by one component of the system, this kind of sonar is called active sonar system. Sound waves generated by a projector travel through the water to the objective, and are reflected as sonar echoes and are detected by a hydrophone. The hydrophone is a device which converts sound into electric signals. Then the converted electric signals from the hydrophone are amplified and processed to provide the information which is used to control or display depending on how the sonar system was intended to be used. If the sound used is radiated by the target, this kind of sonar is called passive or listening sonar system. In the passive sonar system only one-way transmission of sound is involved, and only the hydrophone is used to establish the system. However, in practiced applications, such as telemetry, communication and control applications, a hybrid form of sonar system using a projector and a hydrophone is employed at both ends of the communication paths.

2.1.2 Uses of sonar system

The first practical application of underwater sound was submarine bell, used by ships for offshore navigation. After the disaster as the collision of “Titanic”, echo ranging systems were developed to detect icebergs for safe passage. During World War Ⅰ a number of military applications of sonar systems were developed. This research and development continued and now there are great advances in the commercial uses of underwater sound, which listed in Table 2-1 [1].

2.2 Doppler Sonar System

Doppler sonar system has been developed to provide velocity information for vessels and submarines. CNDS needs a few seconds time delay to provide velocity information with the desired accuracy. A long time lag means a large risk of collision for navigators. CHDS which can provide precise velocity with short time lag has been developed, and it has been used in various applications, such as wave and turbulence measurements [2]. However, CHDS has an intrinsic disadvantage, velocity ambiguity [3]. Velocity ambiguity means that it can only provide accurate velocity information in a limited range, which seriously limits its general application.

2.2.1 Conventional type

The basic block diagram of CNDS is shown in Figure2-1. It consists of four basic parts, a transmitter, a receiver, a signal processing unit and a display [4]. The transmitter sends ultrasonic waves through the water when trigged, which also initiates a time-measuring system in the signal processing unit. The receiver is required to pick up and amplify

Table 2-1 Commercial uses of sonar

Function	Description
Depth Sounding	
Conventional depth sounders	Send short pulses downward and time the bottom return
Subbottom profilers	Use lower frequencies and a high-power impulsive source for bottom penetration
Side-scan sonars	Sidewise-looking sonars for mapping the sea bed at right angles to a ship' track
Acoustic speedometers	Use pairs of transducers pointing obliquely downward to obtain speed over the bottom from the Doppler shift of the bottom returns. Another method uses the time-delay correlogram of the bottom return between halves of a small split transducer
Fish finding	Forward-looking active sonars for spotting fish schools
Fisheries aids	For counting, luring, or tagging individual fish
Divers' aids	Small hand-held sonar sets for underwater object location by divers
Miscellaneous uses	Acoustic flow meters and wave-height sensors
Control	Sound-activated release mechanisms; well-head flow control devices for underwater oil wells
Communication and telemetry	Use a sound beam instead of a wire link for transmitting information
Position marking	
Beacons	Transmit a sound signal continuously
Transponders	Transmit only when suitably interrogated

the low level return echo from targets for use in the signal processing unit. The transducers, projector and hydrophone are connected with the transmitter and receiver respectively. In the signal processing unit of CNDS, Doppler shift will be detected and velocity will be calculated. Normally fast Fourier transform is used to measure the frequency information. Then with the comparison of spectrum between transmitted and received signals, Doppler shift can be determined. Then the measured velocity is presented in several ways, such as electro-sensitive recording paper, a spinning neon display and LCD which is normally used in modern devices.

(1) Conventional method

The Doppler effect (also called Doppler shift) was first proposed in 1842 by the Austrian physicist Christian Doppler [5]. It is the change in frequency of a wave (or other periodic event) for an observer moving relative to its source. For waves that propagate in a medium, such as sound waves, the Doppler effect is affected by motion of the wave source,

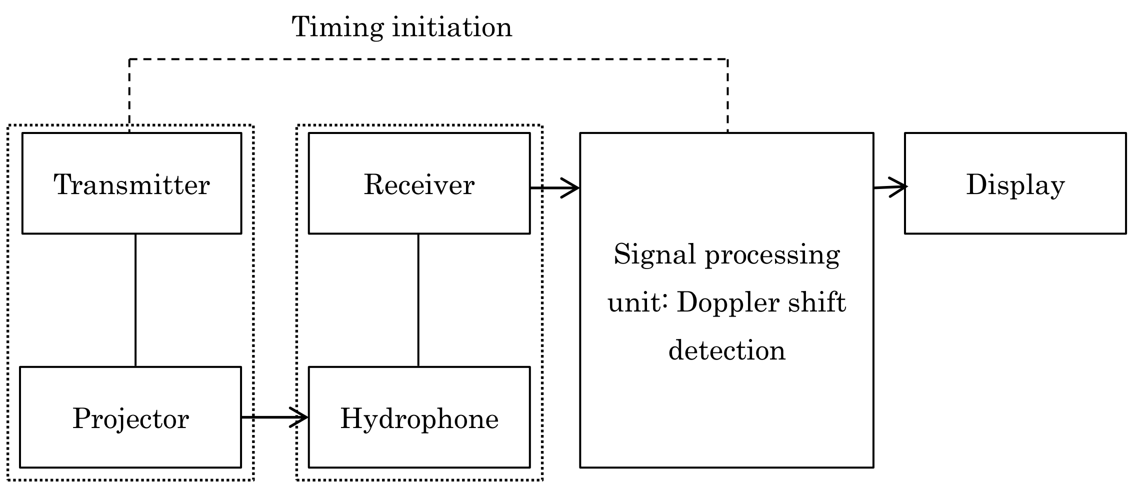

Figure 2-1 Block diagram of CNDS.

motion of the observer, and motion of the medium. For waves, such as light or gravity which do not require a medium, only the relative velocity between the observer and the wave source affects the Doppler effect.

If the source emitting waves through a medium with a frequency f_0 moves with a speed of v_s, and the observer moves with a speed of v_r, then the frequency f_r of received waves can be expressed as

$$f_r = \frac{c + v_r}{c + v_s} f_0 \quad , \tag{2-1}$$

or, alternatively:

$$f_0 = (1 + \frac{v_{s,r}}{c + v_r}) f_r \quad , \tag{2-2}$$

where v_s is positive if the source is moving away from the observer, and negative if the source is moving towards the observer. v_r is positive if the observer is moving towards the source, and negative if the observer is moving away from the source. c represents the wave speed in the medium. $v_{s,r}$ is the relative speed of source and observer, which can be expressed as $v_{s,r} = v_s - v_r$.

The above formula works for sound waves, if and only if, the speed $v_{s,r}$ between the wave source and receiver relative to the medium is slower than the wave speed c. And also the above formula assumes that the movements of the wave source and receiver are either directly approaching or receding from each other.

In line with the Doppler effect, CNDS was developed to measure the velocity of vessels and submarines. We will now introduce CNDS used to measure the speed of a local vessel [6], [7], [8].

Figure 2-2 shows the structure of CNDS. In this figure, the projector and hydrophone are located in the same place, and the moving velocity of the vessel is set as v. In order to obtain a fixed reference point, usually there is a stationary reflecting surface ahead of the vessel. A beam is deflected downwards at α degree to the vertical and a reflection is obtained from the bottom. Based on the expression of Doppler effect, the received frequency by hydrophone can be expressed as:

$$f_r = f_0 \frac{c + v \times cos\alpha}{c - v \times cos\alpha} \quad , \tag{2-3}$$

where f_0 is the frequency of transmitted signal;

f_r is the frequency of received signal;

c is the sound speed in the water;

α is the angle of depression of the beam.

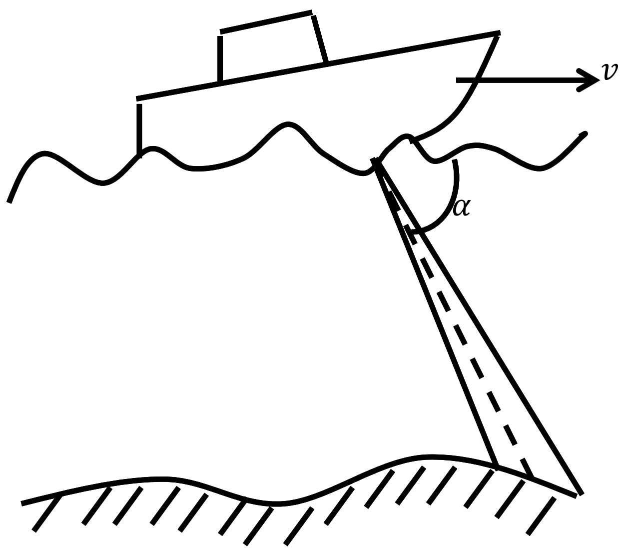

Figure 2-2 Schematic diagram of velocity measurement by Doppler effect.

And Eq. (2-3) can be simplified as

$$f_r = f_0 \frac{1+x}{1-x} \quad , \tag{2-4}$$

where x is defined as $(v \times cos\alpha)/c$. Then the frequency shift f_d caused by Doppler effect can be calculated as

$$f_d = f_r - f_0 = f_0 \frac{1+x}{1-x} - f_0 = f_0 \frac{2x}{1-x} \quad . \tag{2-5}$$

Because the moving speed of vessel v is much less than the propagation velocity of sound c in water, it caused value x which is far less than 1. Then Eq. (2-5) can be approximated to be:

$$f_d \approx 2x \times f_0 = \frac{2v \times cos\alpha}{c} f_0 \quad . \tag{2-6}$$

Unfortunately, the system is now sensitive to vertical motion, and generally speaking only the velocity in the horizontal direction is important for sailors.

In order to eliminate the vertical component, two sets of sonar systems with projector and hydrophone are introduced, shown in Figure 2-3. The angle of depression of the forward beam is α (beam Ⅰ), and the angle of the rear beam is $180° - \alpha$ (beam Ⅱ). u is the velocity in the vertical direction. The transmitted frequency f_0 of the projectors remains the same. Then the received frequencies of the front and rear beams can be shown as below:

$$f_{r\,I} = f_0 \frac{1+x_1}{1-x_1} \ ,$$

$$f_{r\,II} = f_0 \frac{1 - x_2}{1 + x_2} \ , \tag{2-7}$$

where

$$x_1 = \frac{v \times cos\alpha}{c} + \frac{u \times sin\alpha}{c} \ ,$$

$$x_2 = \frac{v \times cos\alpha}{c} - \frac{u \times sin\alpha}{c} \ .$$

The Doppler shift between the front and rear received beams is

$$f_D = f_{r\,I} - f_{r\,II} = f_0 \frac{4x}{(1 - x_1)(1 + x_2)} \ , \tag{2-8}$$

and the approximate value can be expressed as

$$f_D \approx 4x \times f_0 = \frac{4v \times cos\alpha}{c} f_0 \ . \tag{2-9}$$

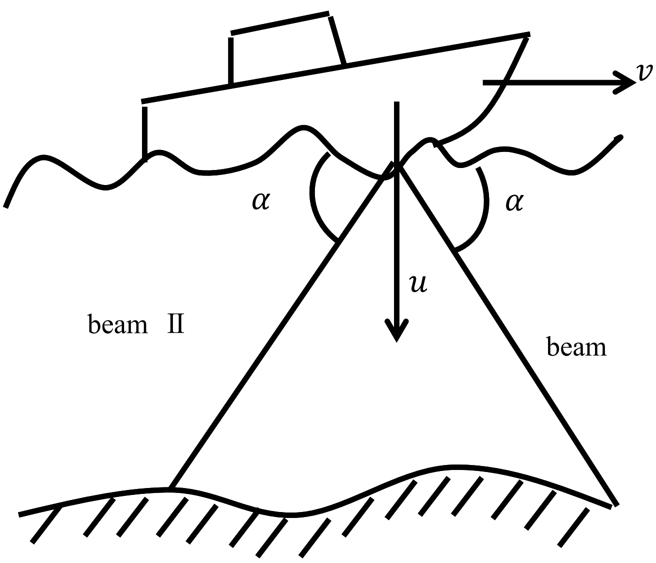

Figure 2-3 Velocity measurement system with two sets of projector and hydrophone.

(2) Error analysis of CNDS

Suppose the analytic form of the transmitted signal with a zero phase characteristic is

$$S(t) = a_0(t)e^{j\omega_0 t}, \tag{2-10}$$

the received target signal will be

$$R_r(t) = Aa_0(t - t_0)e^{j(\omega_0+\omega_d)(t-t_0)}\ , \tag{2-11}$$

where

$a_0(t)$ is the envelop of transmitted signal;

$\omega_0 = 2\pi f_0,\ f_0$ is the carrier frequency of transmitted signal;

A is the amplitude of received signal

ω_d is the frequency component generated by Doppler effect;

t_0 is the time delay generated by the distance between the transmitter and target.

For simplicity, we can let $t_0 = 0$, in which case the transmitted signal is expressed as

$$R_r(t) = Aa_0(t)e^{j(\omega_0+\omega_d)t}\ . \tag{2-12}$$

With the addition of thermal and environmental noise at the input to the receiving system, the total signal of receiver becomes

$$R(t) = R_r(t) + N_a(t)\ , \tag{2-13}$$

where $N_a(t)$ is an analytic random-noise characteristic of white Gaussian noise.

In order to estimate the Doppler shift, f_d, which exists between transmitted and received waveforms, it would seem reasonable to compare the spectra of these two waveforms. Based on Fourier transform, two waveforms of transmitter and receiver in time domain can be transformed to the frequency domain, which can be expressed as

$$S(t) \leftrightarrow S_f(f) \ , \tag{2-14}$$

$$R(t) \leftrightarrow R_f(f) \ . \tag{2-15}$$

The spectral integrated squared difference becomes

$$\epsilon_\Delta = \int_0^F \left|S_f(f-\Delta f) - R_f(f)\right|^2 df \ , \tag{2-16}$$

where F represents the maximum range of interest.

Accordingly, to get the minimum value of ϵ_Δ, the root mean square error in estimating Doppler shift can be obtained as [9]

$$\sigma_{\Delta f} = \frac{1}{\kappa\sqrt{2E/N_0}} \ , \tag{2-17}$$

where E is the energy of the received signal;

$N_0/2$ is the noise power per Hertz for noise waveform;

$$\kappa^2 = \frac{(2\pi)^2 \int_{-\infty}^{+\infty} t^2 |a_0(t)|^2 dt}{\int_{-\infty}^{+\infty} |a_0(t)|^2 dt} .$$

With the standard deviation of frequency shift, the standard deviation of measured velocity can be expressed as:

$$\sigma_n = \frac{\sigma_{\Delta f}}{f_0} c \,. \tag{2-18}$$

Because of the Gaussian white noise effect, the measurement velocity by CNDS also follows the Gaussian distribution, which is:

$$v_n \sim \mathcal{N}(v_0, {\sigma_n}^2) \,. \tag{2-19}$$

2.2.2 Coherent type

Pulse-to-pulse coherent method was used to provide velocity information in atmospheric radar observation [10] [11] and laser-Doppler anemometer [12] [13]. Then this method was introduced in sonar systems to carry out measurements of fluid turbulence [14] [15]. The basic structure of CHDS, shown in Figure 2-4, is similar to the CNDS, but in the signal processing unit, CHDS detects the phase difference between adjacent received pulses instead of the Doppler shift of each received pulse [16].

(1) Coherent method

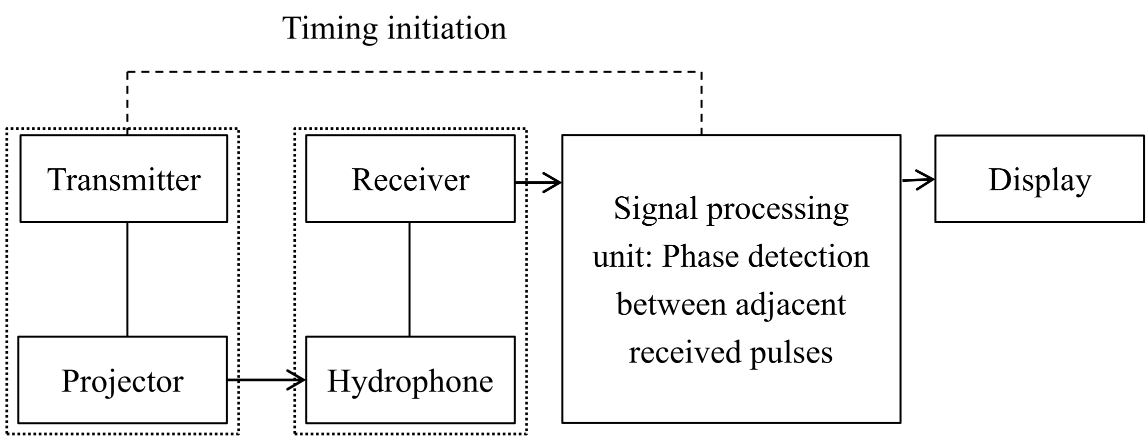

Figure 2-4 Block diagram of CHDS.

In some applications, such as the velocity measurement of water or turbulence, a pulse width of several milliseconds is required to allow a meaningful evaluation of the Doppler frequency shift for CNDS, but such a signal time window is still too short to provide the frequency resolution needed to observe the exact spectrum of Doppler frequency shifts. Therefore, the useful measurements have been performed using pulse-to-pulse CHDS. CHDS systems rely on the measurement of phase change between two adjacent coherent pulses. And this method can provide a velocity resolution of one centimeter per second [17], [18], [19], [20], [21].

In CHDS a phase change of two adjacent pulses is used to estimate the velocity. The process of phase calculation is shown in Figure 2-5.

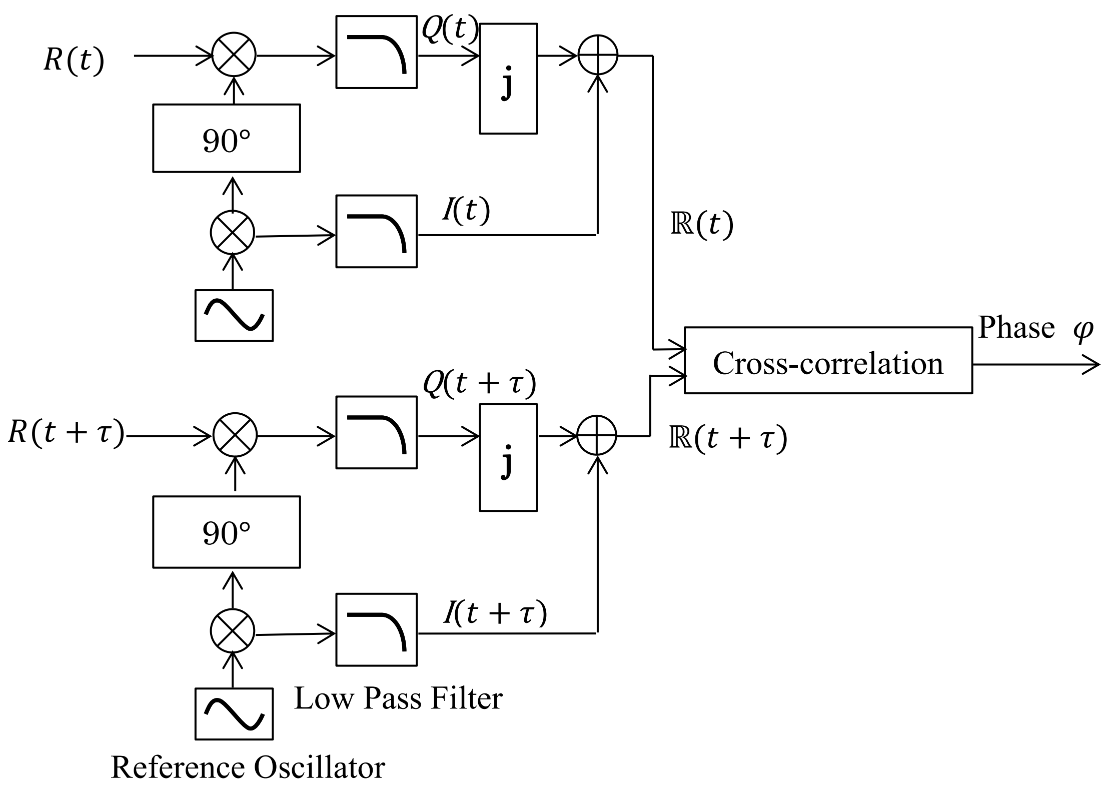

Figure 2-5 Phase calculation process.

Suppose that the two adjacent signals received at time interval τ are

$$R(t) = A_1 \cos(2\pi f_r t + \varphi_{ori}) \quad , \tag{2-20}$$

$$R(t+\tau) = A_2 \cos(2\pi f_r t + \varphi_{ori} + \varphi) \ , \tag{2-21}$$

where

φ_{ori} is the original phase;

A_1 and A_2 are amplitudes of received signals, and to simplify the analysis, the value of A_1 and A_2 are considered as 1.

φ is the phase generated by the movement of the object.

Then the known signals $\sin 2\pi f_0 t$ and $\cos 2\pi f_0 t$ are used to construct the quadrature and in-phase components of the received signals.

$$I(t) = \sin 2\pi f_0 t \cdot R(t)$$

$$= \frac{\sin[2\pi(f_r - f_0)t + \varphi_{ori}]}{2} + \frac{\sin[2\pi(f_r + f_0)t + \varphi_{ori}]}{2} \quad , \tag{2-22}$$

$$Q(t) = \cos 2\pi f_0 t \cdot R(t)$$

$$= \frac{\cos[2\pi(f_r - f_0)t + \varphi_{ori}]}{2} + \frac{\cos[2\pi(f_r + f_0)t + \varphi_{ori}]}{2} \quad , \tag{2-23}$$

$$I(t+\tau) = \sin 2\pi f_0 t \cdot R(t+\tau)$$

$$= \frac{\sin[2\pi(f_r - f_0)t + \varphi_{ori} + \varphi]}{2} + \frac{\sin[2\pi(f_r + f_0)t + \varphi_{ori} + \varphi]}{2} \quad , \tag{2-24}$$

$$Q(t+\tau) = cos\, 2\pi f_0 t \cdot R(t+\tau)$$

$$= \frac{cos[2\pi(f_r - f_0)t + \varphi_{ori} + \varphi]}{2} + \frac{cos[2\pi(f_r + f_0)t + \varphi_{ori} + \varphi]}{2} \ . \quad (2\text{-}25)$$

After the filtration of ideal low pass filter, the in-phase and quadrature components can be expressed as follows:

$$I'(t) = \frac{sin[\,2\pi(f_r - f_0)t + \varphi_{ori}]}{2} \ , \quad (2\text{-}26)$$

$$Q'(t) = \frac{cos[2\pi(f_r - f_0)t + \varphi_{ori}]}{2} \ , \quad (2\text{-}27)$$

$$I'(t+\tau) = \frac{\sin[\,2\pi(f_r - f_0)t + \varphi_{ori} + \varphi]}{2} \ , \quad (2\text{-}28)$$

$$Q'(t+\tau) = \frac{\cos[2\pi(f_r - f_0)t + \varphi_{ori} + \varphi]}{2} . \quad (2\text{-}29)$$

The complex signals consisting of in-phase and quadrature components are shown in the following equations:

$$\mathbb{R}(t) = I'(t) + jQ'(t) \ , \quad (2\text{-}30)$$

$$\mathbb{R}(t+\tau) = I'(t+\tau) + jQ'(t+\tau) \ . \quad (2\text{-}31)$$

Then the cross-correlation of two complex signals is

$$\mathbb{C}\,(t) = \mathbb{R}(t)\mathbb{R}^*(t+\tau)$$

$$= (I'(t)I'(t+\tau) + Q'(t)Q'(t+\tau)) + j(Q'(t)I'(t+\tau) - I'(t)Q'(t+\tau))$$

$$= a(t) + jb(t) \quad , \tag{2-32}$$

where

$\mathbb{R}^*(\mathrm{t}+\tau)$ donates the complex conjugate of $\mathbb{R}(\mathrm{t}+\tau)$, and

$$a(t) = I'(t)I'(t+\tau) + Q'(t)Q'(t+\tau)$$

$$= 0.25cos\varphi \quad , \tag{2-33}$$

$$b(t) = Q'(t)I'(t+\tau) - I'(t)Q'(t+\tau)$$

$$= 0.25sin\varphi \, . \tag{2-34}$$

According to $a(t)$ and $b(t)$, phase change can be calculated as in the equation shown below:

$$\varphi = tan^{-1}\frac{b(t)}{a(t)} \quad . \tag{2-35}$$

Because the projector and hydrophone are located in the same place, the transmitted signal travels as a round trip between the projector and the measured object. Then distance change of measured object during time interval τ can be expressed as

$$D = \frac{\varphi}{2\pi} \times \frac{c}{f_r} \times \frac{1}{2} \quad , \tag{2-36}$$

As the velocity of object is much less than c, f_r is approximate to f_0. Then the radial velocity which is calculated by the pair of reflected pulses can be expressed as

$$v = \frac{D}{\tau} = \frac{c\,\varphi}{4\pi\tau f_0} \quad . \tag{2-37}$$

Generally speaking, pulse-to-pulse CHDS is an accurate method for the measurement of velocity information, as only spectrum skewness that f_r is replaced by f_0, produces a small bias in the estimate. Here the difference between spectral estimate and the pulse-pair estimate is discussed [19].

For CNDS, a transmitted pulse with a long time period is needed to provide enough resolution of measured velocity by Fourier transform. Thus the velocity estimated from a Fourier transform of the received signal is a statistical result that includes all the velocity components occurring during the observation time. This property is also seen in the spectra, since all velocity components in each spectra will be involved in the total velocity statistics. Therefore, the velocity measured by CNDS will be affected by time fluctuation of measured target and large scale eddies traveling through the measurement scale. The spectral variance will thus increase continuously with time as new scales become part of the statistics, and its final value will include all of those scales that have contributed to the spectra. However, once the variance of a spectrum has been evaluated, application of the same procedure to other spectra observed later will not bring any variance contribution arising from variations with respect to the frequency content of previous spectra.

In examining the principle of pulse-to-pulse CHDS carefully, we see that the estimator evaluates the variance of a snapshot of the velocity distribution relating only to the motion of targets during the short pulse-to-pulse time interval. Therefore, it can be considered as an "instantaneous" velocity. Repeating the measurements involving successive pulse-pair samples leads to the evaluation of an average value of this short-term variance that does not include velocity fluctuations at time scales exceeding the short pulse-pair time interval. The method is thus insensitive to variations of the instantaneous velocity mean, such as that produced by eddies translating through the sonar pulse volume, occurring over times exceeding the pulse-pair time interval. This may be considered to be an advantage of the pulse-pair technique since the lower wave number (larger scale) involved in the variance measurements is unambiguously only related to pulse volume size.

A prescribed range of velocity measurement can be made by considering the time elapsed since a sound pulse was transmitted. The range from the transducer can be calculated as

$$r(t) = \frac{c \times t}{2} \quad , \tag{2-38}$$

where t the time since the pulse was transmitted. The maximum range is determined by the acoustic propagation conditions where backscatter can be detected. But in coherent sonar, the precondition is that backscatter between successive acoustic pulses should be correlated. This means that the maximum range of the CHDS system is typically determined by the time interval between adjacent acoustic pulse transmissions. If some pulses, separated in time by the time delay of transmitted pulse interval τ exist in the water, then the range ambiguity is introduced such that backscatter is received from multiple ranges at the same time

$$r = \frac{c(t + n\tau)}{2} \quad , \tag{2-39}$$

where n is an integer value. However, backscatter decreases significantly due to attenuation and beam spreading, therefore backscatter from the shortest range dominates in all components of received signal. Then the maximum measureable space range of CHDS can be expressed as:

$$\Delta r = \frac{c\tau}{2} \quad . \tag{2-40}$$

Velocity ambiguity occurs in CHDS because it uses phase change to determine velocity. Phase change can only be determined to within $\pm\pi$ according to the characteristic of *tan*$^{-1}$ function. Based on the maximum phase π measured by *tan*$^{-1}$ function, the maximum measureable velocity provided by CHDS is

$$\Delta v = \frac{c}{4f_0\tau} \ . \tag{2-41}$$

This maximum measureable velocity is called ambiguity velocity.

For instance, the signal frequency is 200 kHz, the time interval is 20 ms and the sound speed is 1500 m/s, then the maximum measureable space range of the CHDS is 15 m and the velocity ambiguity of CHDS is 0.094 m/s.

If we combine the velocity ambiguity and maximum measureable space range together, we can get the velocity-range expression

$$\Delta r \Delta v = \frac{c\tau}{2} \times \frac{c}{4f_0\tau} = \frac{c\lambda}{8} \quad , \tag{2-42}$$

where λ is the sound wave length. Because the space range used in CHDS is not long, the temperature, salinity and pressure do not change a lot, so the sound speed can be considered as constant. A constant sound speed and transmitted frequency direct a constant value of wave length. Therefore, the velocity-range is considered as a constant value related to the transmitted frequency and sound speed. According to this result, it is easy to find that the velocity ambiguity is inversely proportional to the maximum measureable space range for a CHDS. For instance, if we enlarge the time interval of 20 ms into 40 ms, the maximum measureable space range increases to 30 m, but the velocity ambiguity decreases to 0.047 m/s compared with 0.094 m/s. By cutting the time interval in half, the maximum space range is also shortened to half, while the velocity ambiguity is doubled. With this relationship between the maximum measureable space range and ambiguity velocity, we cannot provide large maximum measureable space range and ambiguity velocity simultaneously. This seriously restricts the general application of pulse-to-pulse CHDS.

Medical Doppler ultrasound and pulsed Doppler radar also use pulse-to-pulse coherent processing technique which is subject to the same limitation of range and velocity ambiguities. For medical applications, the short ranges allow sufficiently short pulse delays thereby avoiding velocity ambiguities except in extreme circumstances [22]. Pulsed radar does not generally encounter problems with range ambiguities but must deal with velocity ambiguities. In order to overcome this shortcoming, some methods have been developed. A simple way to deal with velocity ambiguity is to invert velocity using time history or prior knowledge of the observed target, but these approaches are not always practical or reliable. Dual time intervals have been introduced to enlarge the range of ambiguity velocity [23]. This method which is already used in weather radar system can enlarge the velocity range significantly without affecting the space range and the equipment requirements are not strict [24]. However, because new longer time intervals are introduced, data rates will decrease. Multiple frequency method has also been proposed [25]. This method can improve the scale of velocity ambiguity without decreasing the sampling rate. However, this method needs large projector bandwidth which is both complicated and expensive. In some radar systems, both dual time interval and multiple frequency are introduced to enlarge the range of ambiguity velocity [26].

(2) Dual time interval method

a. Basic method of CHDS using dual time interval method

For a moving object with a constant velocity, according to Eq. (2-37), the velocity can be determined by the measured phase φ, the carrier frequency f_0 and the time interval between adjacent pulses. Suppose that phase is measured by two different time intervals τ_1 and τ_2 ($\tau_2 > \tau_1$), it is easy to find the equation of phase change and time interval by Eq. (2-37):

$$\varphi_1 = \frac{4\pi f_0 \tau_1}{c} v \, ,$$

$$\varphi_2 = \frac{4\pi f_0 \tau_2}{c} v \, . \tag{2-43}$$

By taking the difference of φ_2 and φ_1, the velocity can be calculated as follows [23]:

$$\begin{aligned} v &= \frac{c}{4\pi f_0 (\tau_2 - \tau_1)} (\varphi_2 - \varphi_1) \\ &= \frac{c\varphi_2}{4\pi f_0 \tau_2} * \frac{\tau_2}{(\tau_2 - \tau_1)} - \frac{c\varphi_1}{4\pi f_0 \tau_1} * \frac{\tau_1}{(\tau_2 - \tau_1)} \\ &= v_2 * \frac{\tau_2}{(\tau_2 - \tau_1)} - v_1 * \frac{\tau_1}{(\tau_2 - \tau_1)} \quad , \end{aligned} \tag{2-44}$$

where v_1 and v_2 are the velocities measured by single time intervals τ_1 and τ_2, respectively.

The ambiguity velocity determined by Eq. (2-41) is given by

$$\Delta v_{1,2} = \frac{c}{4f_0(\tau_2 - \tau_1)} \quad . \tag{2-45}$$

In practice, τ_1 is usually an integer multiple of the time interval difference $(\tau_2 - \tau_1)$, which can be defined as

$$\tau_1 = N \times (\tau_2 - \tau_1) \ . \tag{2-46}$$

Then velocity measured by dual time interval method can be expressed as

$$v = v_2 \times (N + 1) - v_1 \times N \, . \tag{2-47}$$

According to Eq. (2-46), the relationship of the maximum amplitude velocity between single time interval (τ_1) and dual time interval (τ_1 and τ_2) can be expressed as

$$\frac{\Delta v_{1,2}}{\Delta v_1} = \frac{\tau_1}{\tau_2 - \tau_1} = N \ . \tag{2-48}$$

Eq. (2-45) shows that the ambiguity velocity can be arbitrarily large by making the difference of dual time intervals small. In this situation, the integer N shown in Eq. (2-48) can be infinite. However, this is impossible because of the noise. Suppose that τ_1 is constant, if the value of N becomes larger, then the uncertainty of the measured velocity will increase at the same time.

The space range determined by each time interval can be expressed as

$$\Delta r_1 = \frac{c\tau_1}{2},$$

$$\Delta r_2 = \frac{c\tau_2}{2} \, . \tag{2-49}$$

For the time interval, τ_2 is larger than τ_1, the range Δr_2 is also larger than Δr_1. The velocity is determined by reflected pulses from the measured object. If the object is located at a position larger than Δr_1 and less than Δr_2, the reflected signal during the short time interval τ_1 cannot be used. Therefore, the space range of dual time interval pulse-to-pulse CHDS is determined by the shorter time interval, which can be expressed as

$$\Delta r_{1,2} = min(\Delta r_1, \Delta r_2) \ . \tag{2-50}$$

Although this method can improve the velocity range, it cannot be enlarged infinitely, due to the error of phase measurement. According to Eq. (2-47) which contains uncertainties from the estimations of v_1 and v_2, it is inherently much noisier than the single time interval method. According to the basic knowledge of statistics, the relationship of the standard deviation between dual time interval method and normal method can be expressed as

$$\sigma_{hd} = \sqrt{(N+1)^2 {\sigma_{h2}}^2 + N^2 {\sigma_{h1}}^2} \ , \tag{2-51}$$

where σ_{hd} is the standard deviation of velocity measured by dual time interval method, σ_{h1} and σ_{h2} are the standard deviations of the velocities using single time interval τ_1 and τ_2 respectively. In order to have the same level of accuracy as single time interval method, a special processing technique is introduced in the following section.

The advantage of dual time interval method is that it increases the velocity ambiguity, but the introduction of longer time interval decreases the data rate at the same time. For example, τ_1 = 0.04 s, the data rate of τ_1 is 25 velocity samples per second. If we introduce another time interval τ_2 which is 0.06 s, then the data rate of dual time interval method changes to 19 velocity samples per second.

b. Processing technique for dual time interval method

As mentioned above, dual time interval method enlarges the velocity ambiguity at the cost of measure accuracy and data rate. To remedy the disadvantage of higher uncertainty, one technique which has been mentioned in [27] and [28] is adopted to improve the accuracy without affecting velocity ambiguity.

A fundamental problem in dealing with phase measurements is that it is impossible to measure the absolute value. The phases mentioned above are all absolute values, and it is necessary to convert them into measurable values.

The measurement value of the phase change φ which is measured at the time interval τ with the measurement error ϵ and phase wraps $2n\pi$ can be expressed as:

$$\tilde{\varphi} = \varphi + \epsilon + 2n\pi. \tag{2-52}$$

Then the difference of the phases measured by τ_1 and τ_2 can be described as below:

$$\begin{aligned}\widetilde{\varphi_{12}} &= \widetilde{\varphi_2} - \widetilde{\varphi_1} \\ &= \varphi_2 - \varphi_1 + \epsilon_2 - \epsilon_1 + 2(n_2 - n_1)\pi\,,\end{aligned} \tag{2-53}$$

where subscribes 1 and 2 indicate the value for time intervals τ_1 and τ_2. With the restriction of the ambiguity velocity defined by Eq. (2-45), we can find the inequality

$$|\varphi_2 - \varphi_1 + \epsilon_2 - \epsilon_1| \le \pi\,. \tag{2-54}$$

The technique to improve the velocity accuracy of dual time interval method to be as good as single time interval method is to determine the integer value of n in Eq. (2-52).

This can be realized by a velocity estimation based on the dual time interval method, because the absolute values of phases are linear related

$$\frac{\varphi_i}{\tau_i} = \frac{\varphi_j}{\tau_j} \ , \tag{2-55}$$

the value of an unknown phase of any time interval can be calculated by a certain phase at a certain time interval. Although it is impossible to get the absolute value of the phase, it can be well estimated by the measurement value, if the error is not large. The phase for the time interval τ_i (i = 1 or i = 2) can be estimated by the $\widetilde{\varphi_{12}}$, which can be expressed as:

$$\begin{aligned}
\varphi_{i-est} &= \|\widetilde{\varphi_{12}}\| \frac{\tau_i}{\tau_2 - \tau_1} \\
&= (\varphi_2 - \varphi_1 + \epsilon_2 - \epsilon_1) \frac{\tau_i}{\tau_2 - \tau_1} \\
&= \varphi_i + (\epsilon_2 - \epsilon_1) \frac{\tau_i}{\tau_2 - \tau_1},
\end{aligned} \tag{2-56}$$

where the operator $\| \ \|$ denotes the value of an argument constrained between $\pm\pi$ by appropriate additions or subtractions of 2π.

The difference between estimated value φ_{i-est} and measured value $\widetilde{\varphi_i}$ is

$$\begin{aligned}
\widetilde{\varphi_i} - \varphi_{i-est} &= \varphi_i + \epsilon_i + 2n_i\pi - \left(\varphi_i + (\epsilon_2 - \epsilon_1) \frac{\tau_i}{\tau_2 - \tau_1}\right) \\
&= \epsilon_i + 2n_i\pi - (\epsilon_2 - \epsilon_1) \frac{\tau_i}{\tau_2 - \tau_1} \ ,
\end{aligned} \tag{2-57}$$

when the error component $\epsilon_i - (\epsilon_2 - \epsilon_1) \times \tau_i/(\tau_2 - \tau_1)$ is less than π, the integer n_i can be calculated as:

$$n_i = Round(\frac{\widetilde{\varphi}_i - \varphi_{i-est}}{2\pi}), \tag{2-58}$$

where the operator $Round(\ )$ denotes the integer value which is the nearest one around operand. The absolute value of phase φ_i can be estimated by combining $\widetilde{\varphi}_i$ and n_i together according to Eq. (2-52), and the velocity can be calculated by Eq. (2-37) with the advantage that it only contains the uncertainty ϵ_i.

(3) Multiple frequency method

Suppose that a moving object with a constant velocity is measured by CHDS with a fixed time interval τ, then phase difference φ measured by two different carrier frequency f_1 and f_2 $(f_2 > f_1)$ can be expressed as:

$$\varphi_{1f} = \frac{4\pi\tau f_1}{c} v ,$$

$$\varphi_{2f} = \frac{4\pi\tau f_2}{c} v . \tag{2-59}$$

By taking the difference of φ_{2f} and φ_{1f}, the velocity can be calculated as below [25]:

$$v = \frac{c}{4\pi\tau(f_2 - f_1)}\left(\varphi_{2f} - \varphi_{1f}\right)$$

$$= \frac{c\varphi_{2f}}{4\pi\tau f_2} \times \frac{f_2}{(f_2 - f_1)} - \frac{c\varphi_{1f}}{4\pi\tau f_1} \times \frac{f_1}{(f_2 - f_1)}$$

$$= v_{2f} \times \frac{f_2}{(f_2 - f_1)} - v_{1f} \times \frac{f_1}{(f_2 - f_1)} , \tag{2-60}$$

where v_{1f} and v_{2f} are the velocities measured by single carrier frequency f_1 and f_2, respectively.

The ambiguity velocity determined by Eq. (2-60) is given by

$$\Delta v_{1,2f} = \frac{c}{4\tau(f_2 - f_1)} \quad . \tag{2-61}$$

In practice, f_1 is usually an integer multiple of the carrier frequency difference $(f_2 - f_1)$, which can be defined as

$$f_1 = N \times (f_2 - f_1) \, . \tag{2-62}$$

Then velocity measured by multiple carrier frequency can be expressed as

$$v = v_{2f} \times (N + 1) - v_{1f} \times N. \tag{2-63}$$

According to Eq. (2-62), the relationship of the maximum velocity amplitude between single carrier frequency (f_1) and multiple carrier frequency (f_1 and f_2) can be expressed as

$$\frac{\Delta v_{1,2f}}{\Delta v_{1f}} = \frac{\tau_1}{\tau_2 - \tau_1} = N. \tag{2-64}$$

Eq. (2-64) shows that the velocity ambiguity can be arbitrarily large by making the difference of carrier frequencies small. In the same situation as dual time interval method, because of noise affection, multiple carrier frequency method can extend the ambiguity several times. By introducing a new frequency, two measured phases are used to calculate the velocity of measured target, which will decrease the measurement accuracy. However, the technique used in dual time interval method can also be used in multiple carrier frequency method to keep the measurement results as precise as the method using single carrier frequency.

Multiple carrier frequency method does not introduce new time intervals, which means it does not decrease the data rate. However, a transmitter wide frequency band is needed, and is a much more expensive device.

(4) Alternating dual time interval dual frequency method

In some weather radar systems, both dual time interval and dual carrier frequency methods are used to enlarge the range of ambiguity velocity [26]. The signal used in these systems can be expressed as Figure 2-6. In Figure 2-6 f_1 and f_2 are different carrier frequencies, τ_1, τ_2 and $\Delta\tau$ are used to generate different time intervals. $\Delta\tau_0$ is the initial time shift between two different carrier frequencies. In weather radar systems, the difference of wavelengths in two channels $(\lambda_1 - \lambda_2)$ is much less than λ_1 (or λ_2).

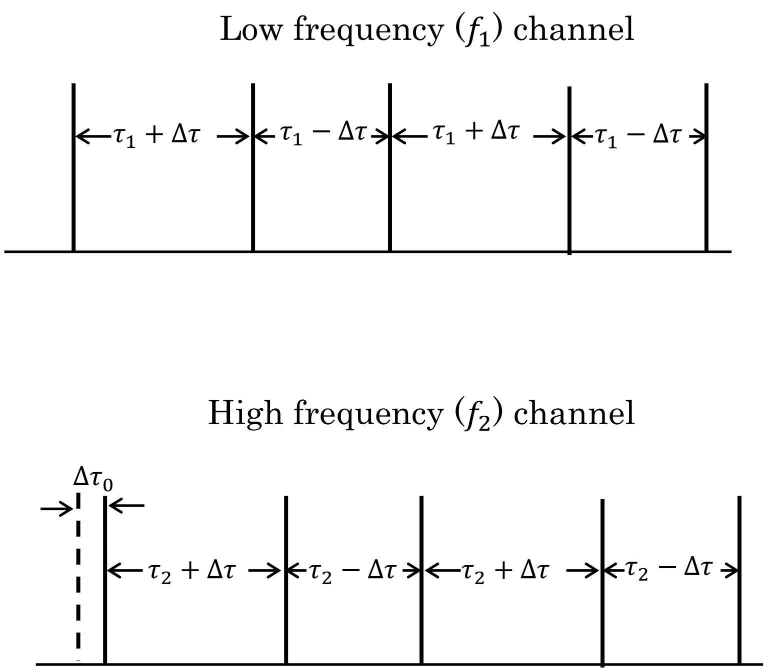

Figure 2-6 General alternating dual time interval sampling scheme for the two frequency channels.

According to these parameters the expression of measured velocity for alternating dual time interval dual frequency method is [26]

$$v = -\frac{\lambda_1}{8\pi\Delta\tau} arg(U_{\Delta\tau}), \tag{2-65}$$

where

$$U_{\Delta\tau} = \frac{1}{M-1}\sum_{m=0}^{M-2} \mathbb{C}_{12}\,(m)\,\mathbb{C}_{12}\,(m+1)\,;$$

$$\mathbb{C}_{12}\,(m) = \begin{cases} \mathbb{R}_1^*(t)\mathbb{R}_2(t), & m\ even \\ \mathbb{R}_1(t)\mathbb{R}_2^*(t), & m\ \ odd \end{cases};\text{for } m = 0,1,\ldots,M-1\,;$$

$\mathbb{R}_1$ and $\mathbb{R}_2$ denotes the complex signals from the two frequency channels;

M is the number of samples in the dwell time for each channel.

Taking advantages of both dual time interval method and dual carrier frequency method will make the range of ambiguity velocity even larger than a system using single method. However, it also makes the system more complicate to design and construct.

As discussed above, dual time interval method, multiple carrier frequency method and alternating dual time interval dual frequency method can only extend the range of ambiguity several times larger, and they cannot delete the velocity ambiguity completely. In order to provide a method of wide application which erases the effect of velocity ambiguity, we propose CMDS shown in next chapter.

(5) Error analysis of CHDS

For CHDS, the received signals are transferred into the complex domain, as shown in Figure 2-5**.** In this process, since the signal passes through the low pass filter, the SNR of the band-limited signal (γ_{b}) is improved significantly compared to the originally received signal.

For each received signal, the probability density function of phase ($p(\varphi)$), affected by the white Gaussian noise, can be expressed as [29], [30]:

$$p(\varphi) = \frac{e^{-\gamma_b}}{2\pi}\{1 + \sqrt{\pi\gamma_b}cos\varphi \times [1 + erf(\sqrt{\gamma_b}\, cos\varphi)]e^{\gamma_b cos^2\varphi}\}, \tag{2-66}$$

where $erf(x)$ is the error function, which can be expressed as [31]:

$$er\,f(x) = \frac{2}{\sqrt{\pi}}\int_0^x e^{-t^2}\,dt\,. \tag{2-67}$$

The probability density function of the phase difference between two adjacent pulses can then be expressed as [32]:

$$p_d(\varphi) = \int_{-\pi}^{\pi} p(\theta)p(\varphi - \theta)d\theta. \tag{2-68}$$

Based on the probability density function of the phase difference, the standard deviation of velocity measured by CHDS is:

$$\sigma_h = \frac{c}{4\pi f\tau} \times \sqrt{\int_{-\pi}^{\pi} \varphi^2 p_d(\varphi)d\varphi}\ , \tag{2-69}$$

$$= \frac{\Delta v}{\pi} \times \sqrt{\int_{-\pi}^{\pi} \varphi^2 p_d(\phi)d\phi}\ . \tag{2-70}$$

References

[1] R.J. Urick, “Principles of Underwater Sound,” McGraw. Hill Book Co., pp.1-8, 1983.

[2] F. Veron and W.K. Melville, “Pulse-to-Pulse Coherent Doppler Measurements of Waves and Turbulence,” Journal of Atmospheric and Oceanic Technology, Vol.16, pp.1580-1597, Nov. 1999.

[3] R.G.A. Craig, C. Loadman, B. Clement, P.J. Rusello and E. Siegel, “Characterization and Testing of a New Bistatic Profiling Acoustic Doppler Velocimeter: The Vectrino-II,” Proceedings of the IEEE/OES/CWTM 10th Working conference on Current Measurement Technology, 2010.

[4] G.E. Beck, “Navigation Systems: A Survey of Modern Electronic Aids,” Van Nostrand Reinhold London, pp.292~298, 1971.

[5] V.C. Chen, “The Micro-Doppler Effect in Radar,” ARTECH HOUSE, pp2~3, 2011.

[6] G.E. Beck, “Navigation Systems: A Survey of Modern Electronic Aids,” Van Nostrand Reinhold London, pp298~303, 1971.

[7] Tyoonpabinran henshuiinkai, “Tyoonpabinran,” Maruzen Kabusikikaisha, pp.501~502, 1999. (Japanese Language)

[8] D. Hurther and U. Lemmin, “A Correction Method for Turbulence Measurements with a 3D Acoustic Doppler Velocity Profiler,” Journal of Atmospheric and Oceanic Technology, Vol. 18, pp.446~458, Mar. 2001.

[9] W.S. Burdic, “Radar Signal Analysis,” Prentice-Hall, Inc., pp.166~167 1968.

[10] R. R. Rogers, B. R. Tripp, “Some Radar Measurements of Turbulence in Snow,” Journal of Applied Meteorology, Vol. 2, pp.603~610, Oct. 1964.

[11] R. C. Srivastava, D. Atlas, “Effect of Finite Radar Pulse Volume on Turbulence Measurements,” Journal of Applied Meteorology, Vol. 13, pp.472~480, Jun. 1974.

[12] T. S. Durrani, C. A. Greated, “Statistical Analysis and Computer Simulation of Laser Doppler Velocimeter Systems,” IEEE Transactions on Instrumentation and Measurement, Vol. 22, No. 1, pp.23~34, Mar. 1973.

[13] W. K. George, J. L. Lumley, “The Laser-Doppler Velocimeter and Its Application to the Measurement of Turbulence,” Journal of Fluid Mechanics, Vol 60, No. 2, pp.321~362, Sep. 1973.

[14] J. L. Garbini, F. K. Forster and J. E. Jorgensen, “Measurement of Fluid Turbulence Based on Pulsed Ultrasound Techniques. Part 1. Analysis,” Journal of Fluid Mechanics, Vol. 118, pp.445~470, May 1982.

[15] J. L. Garbini, F. K. Forster and J. E. Jorgensen, “Measurement of Fluid Turbulence Based on Pulsed Ultrasound Techniques. Part 2. Experimental Investigation,” Journal of Fluid Mechanics, Vol. 118, pp.471~505, May 1982.

[16] A.E. Hay, L. Zedel, R. Craig and W. Paul, “Multi-Frequency Pulse-to-pulse Coherent Doppler Sonar Profiler,” Processing of the IEEE OES CMTC 9th working conference on current measurement technology, 2008.

[17] J. Dillon, L. Zedel and A.E. Hay, “Asymptotic Properties of an Autocorrelation Coefficient for Coherent Doppler Sonar,” Journal of atmospheric and oceanic technology, Vol. 28, pp.966~973, Jul. 2011.

[18] C.D.S. Tollefsen and L. Zedel, “Evaluation of a Doppler Sonar System for Fisheries Applications,” ICES Journal of Marine Science, 60, pp.692–699, 2003.

[19] R. Lhermitte, R. Serafin, “Pulse-to-Pulse Coherent Doppler Sonar Signal Processing Techniques”, Journal of Atmospheric and Oceanic Technology, Vol.1, No.4, pp. 293~308, Dec. 1984.

[20] A. Lohrmann, B. Hackett, and L.P. Roed, “High Resolution Measurements of Turbulence, Velocity and Stress Using a Pulse-to-Pulse Coherent Sonar,” Journal of Atmospheric and Oceanic Technology, pp.19-37, 1990.

[21] L. Zedel ,"Modeling Pulse-to-Pulse Coherent Doppler Sonar", Journal of Atmospheric and Oceanic Technology, Vol. 25, pp.1834~1844, Oct. 2008

[22] H.J. Nitzpon, J.C. Rajaonah, C.B. Burckhardt, B. Dousse, and J-J. Meister, "A New Pulsed Wave Doppler Ultrasound System to Measure Blood Velocities Beyond the Nyquist Limit", Ultrasonics, Ferroelectrics, and Frequency Control, IEEE Transactions, Vol. 42, No.2, pp.265-279, Mar. 1995.

[23] R.G.A. Craig, C. Loadman, B. Clement, P.J. Rusello and E. Siegel, "Characterization and Testing of a New Bistatic Profiling Acoustic Doppler Velocimeter: The Vectrino-II," Proceedings of the IEEE/OES/CWTM Tenth Working Conference on Current Measurement Technology, pp.246-252, 2010.

[24] P. Joe and P.T. May, "Correction of Dual PRF Velocity Errors for Operational Doppler Weather Radars," Journal of Atmospheric and Oceanic Technology, pp.429-442, 2003.

[25] A.E. Hay, L. Zedel, R. Craig and W. Paul, "Multi-Frequency, Pulse-to-pulse Coherent Doppler Sonar Profiler," Proceedings of the IEEE/OES/CMTC Ninth Working Conference on Current Measurement Technology, pp.25–29, 2008.

[26] S. Torres, R Passarelli Jr, A Siggia, and and P. Karhunen, "Alternating Dual-Pulse, Dual-Frequency Techniques for Range and Velocity Ambiguity Mitigation on Weather Radars," Journal of Atmospheric and Oceanic Technology, Vol. 27, pp.1461~1475, Sep. 2010.

[27] I. Holleman, and H. Beekhuis, "Analysis and Correction of Dual PRF Velocity Data", Journal of Atmospheric and Oceanic Technology, Vol. 20, pp.443–453, Apr. 2003.

[28] L. Zedel and A.E. Hay, "Resolving Velocity Ambiguity in Multifrequency, Pulse-to-Pulse Coherent Doppler Sonar", IEEE Journal OF Ocean Engineering, Vol. 35, pp.847~851, Oct. 2010.

[29] W.B. Devenport Jr. and W.L. Root, "An Introduction to the Theory of Random Signals and Noise," McGraw-Hill Book Co., Inc., pp.165~167, 1958.

[30] H. Sekiguchi, K. Nozaki and H. Yanagitaira, "Gendai no tuushinkaisenriron, Morikitashuppan Kabushikikaisha," pp.135~139, 1976. (Japanese Language)

[31] M. Abramowitz and I.A. Stegun, "Handbook of Mathematical Functions with Formulas, Graphs, and Mathematical Tables (Tenth Printing)," Courier Co., pp.297, Dec 1972.

[32] A. Papoulis, "Probability, Random Variables, and Stochastic Process (Third Edition)," McGraw Hill, Inc., pp.136, 1991.

CHAPTER 3

COMBINED METHOD OF DOPPLER SONAR

3.1 Combined Method

In order to overcome the disadvantage of CNDS, a long time delay, and the disadvantage of CHDS, velocity ambiguity, CMDS is proposed. The basic structure of CMDS is shown in Figure 3-1. In the data processing unit, both Doppler shift and phase difference are measured. The Doppler shift is used to provide a rough velocity, which includes velocity range information. The phase difference measured by CHDS is used to provide precise velocity information, but precisely measured velocity is limited to a fixed range. In the data fusion block in Figure 3-1, precise and accurate velocity is provided by combining the range information given by CNDS and the more precise details given by CHDS.

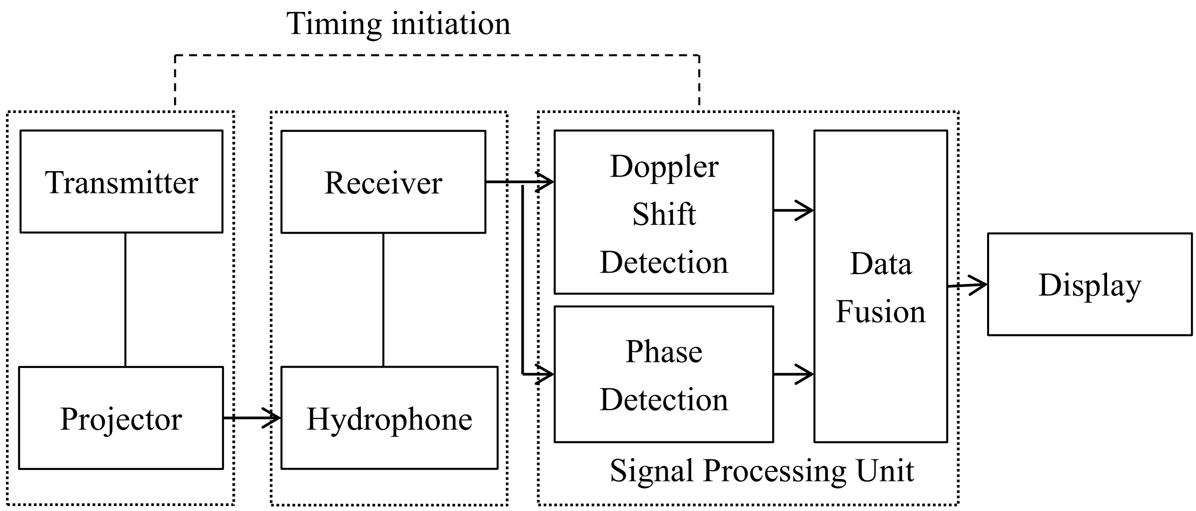

Figure 3-1 Block diagram of combined Doppler system.

3.1.1 Structure of combined method

The aforementioned CHDS can provide accurate velocity information by phase measurement, but it is seriously limited by velocity ambiguity for wider applications. Although lots of methods have been used to extend the range of ambiguity velocity, it still cannot be cancelled. Therefore, CMDS is introduced to take advantage of both CNDS and CHDS to provide accurate and precise velocity information [1], [2]. A functional block diagram of CMDS to measure velocity v is shown in Figure 3-2. At the receiver block, received pulse series are detected and forwarded to CNDS and CHDS. At the start of CNDS, the Doppler shifts of the received pulses are calculated based on Fourier transform, and a coarse velocity (v_n) with error (ε_n) is obtained. In CHDS, phase changes between adjacent pulses are calculated, and the precise velocity (v_h) with measurement error (ε_h) is obtained. In this process, although course velocity is not accurate, it can be used to determine the velocity range for CHDS, which means that it can be used to determine the velocity shift ($2n\Delta v$) of CHDS. Finally, an unlimited and accurate velocity (v_m) is calculated by the addition of the determined velocity shift $2n\Delta v$ and the velocity v_h measured by CHDS.

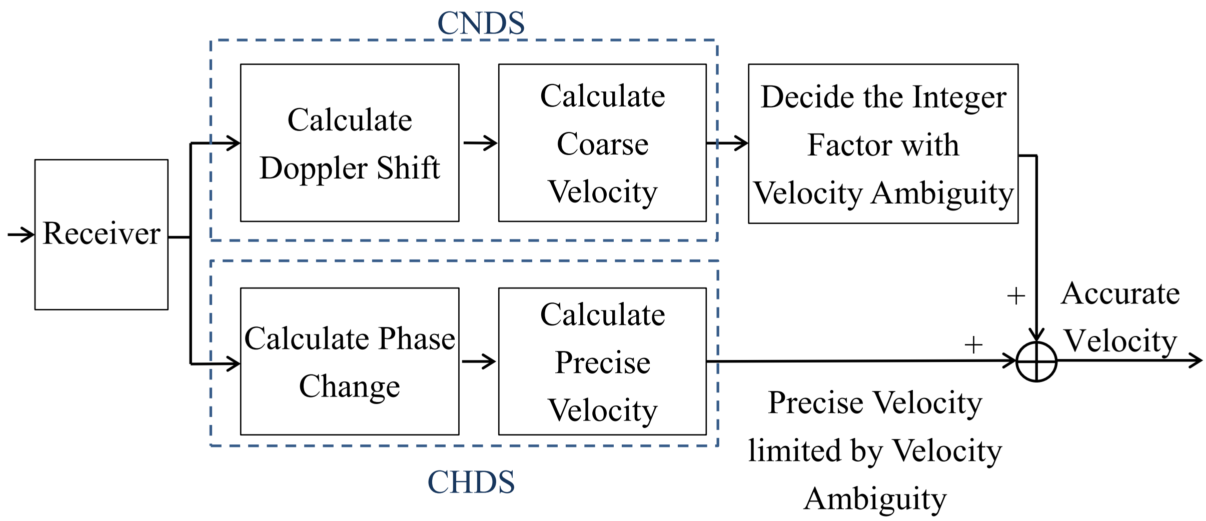

Figure 3-2 Functional block diagram of combined method.

One of the main functions of CMDS is to decide the integer factor n. In order to carry out this calculation, two assumptions are necessary. The first assumption is that the measurement velocity v_h has the same sign as the velocity v_{h0} measured by CHDS without noise. This assumption is only challenged in situations when v_{h0} is near to $\pm\Delta v$. According to this assumption, the sign of v_{h0} can be estimated by v_h. The second assumption is that the absolute value of coarse velocity error ($|\varepsilon_n|$) is less than half the ambiguity velocity Δv. These two assumptions can be expressed as:

$$v_h \times v_{h0} > 0, \tag{3-1}$$

$$|\varepsilon_n| < \frac{\Delta v}{2}. \tag{3-2}$$

In order to make the explanation clear, the basic relationships between measured velocities and true velocity by CNDS and CHDS are shown below:

$$v = v_{h0} + 2n\Delta v = v_h - \varepsilon_h + 2n\Delta v\,, \tag{3-3}$$

$$v = v_n - \varepsilon_n\ . \tag{3-4}$$

Then we get

$$\frac{v_n}{2\Delta v} = \frac{v + \varepsilon_n}{2\Delta v} = \frac{v_h - \varepsilon_h + 2n\Delta v + \varepsilon_n}{2\Delta v} = n + \frac{v_{h0} + \varepsilon_n}{2\Delta v}\ , \tag{3-5}$$

If $\Delta v \geq v_{h0} > 0$, considered with the second assumption, we find

$$-\frac{1}{4} < \frac{v_{h0} + \varepsilon_n}{2\Delta v} \leq \frac{3}{4}\ \ (v_{h0} > 0)\ . \tag{3-6}$$

With Eq. (3-5) and inequality (3-6), one inequality to determine the integer factor n is obtained as

$$n - \frac{1}{4} < \frac{v_n}{2\Delta v} \leq n + \frac{3}{4} \quad (v_{h0} > 0) \quad . \tag{3-7}$$

For the situation $\Delta v < v_{h0} \leq 0$, we can also get the inequality as following:

$$n - \frac{3}{4} < \frac{v_n}{2\Delta v} \leq n + \frac{1}{4} \quad (v_{h0} \leq 0) \quad . \tag{3-8}$$

In the ranges shown in inequalities (3-7) and (3-8), one and only one integer value exists, which means the integer factor n can be determined. With the integer n decided and the precise velocity v_h, the velocity measured by the CMDS can be calculated by Eq. (3-3). According to Eq. (3-3), if the integer n is estimated correctly, CMDS can provide accurate velocity calculations over an unlimited range.

The value of v_{h0} is considered to be a variable limited in the range of $(0,\Delta v]$ in inequality (3-7) and $(-\Delta v,\ 0]$ in inequality (3-8). However, the v_{h0} is fixed by the velocity v. Therefore, the range of error in the second assumption can be extended, and it can be expressed as a function of v_{h0}, which means the measurement error of the integer factor n is also affected by the value of v_{h0}. In order to remove the affection of v_{h0}, a variable shift is introduced in the inequalities of integer factor determination [3].

3.1.2 Procedure of variable shift

As just discussed, integer factor n determined by inequalities (3-7) and (3-8) is affected by the value of measured velocity. This system should be able to provide stable measurement error irregardless of the value of measured velocity. However this isn’t true as the measured error changes when different measured velocities occur. In order to solve this problem, a method of variable shift is introduced.

In a noise-free process, v can be measured by CNDS without noise as v_{n0}, and v_{h0} is the velocity measured by CHDS including the ambiguity velocity. Accordingly, the relationship between v_{n0} and v_{h0} can be expressed as:

$$v_{n0} - v_{h0} = 2n\Delta v \ . \tag{3-9}$$

In the actual process of measurement, each measurement noise, ε_n for CNDS and ε_h for CHDS, should be considered, and the difference between the two measurement values, v_n by CMDS and v_h by CHDS, can be expressed as:

$$v_n - v_h = (v_{n0} + \varepsilon_n) - (v_{h0} + \varepsilon_h) = 2n\Delta v + (\varepsilon_n - \varepsilon_h) \ , \tag{3-10}$$

$$\frac{v_n - v_h}{2\Delta v} = n + \frac{\varepsilon_n - \varepsilon_h}{2\Delta v} \quad . \tag{3-10'}$$

We propose using the left side of Eq. (3-10') as the new decision variable to clear away the error effect generated by the value of v. In the decision algorithm of the integer factor, the inequality used to determine the integer factor n, can be expressed:

$$n - \frac{1}{2} < \frac{v_n - v_h}{2\Delta v} \leq n + \frac{1}{2} \quad . \tag{3-11}$$

In Figure 3-3, a flow chart for the decision algorithm of integer factor n is shown, and the procedure of the decision algorithm is described below.

1) Input the coarse velocity measured by CNDS v_n, the precise velocity measured by CHDS v_h, and the range of ambiguity velocity (Δv).

2) Carry out the variable shift, and calculate $(v_n - v_h)/(2\Delta v)$.

3) Round $(v_n - v_h)/(2\Delta v)$, and decide the integer factor n.

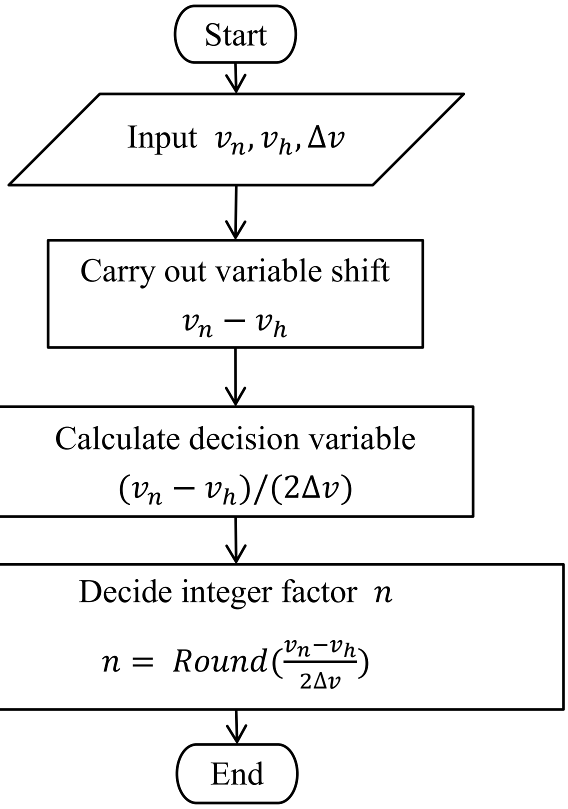

Figure 3-3 Flow chart for decision algorithm of integer factor.

3.2 Adaptive Algorithm

3.2.1 Structure of CMDS using adaptive algorithm

In our previous explanation, we proposed a method of CMDS using a fixed range of ambiguity velocity. This method was proposed to provide accurate and precise velocity information. At high SNRs, this method works well because the absolute value of $(\varepsilon_n - \varepsilon_h)/2\Delta v$ is less than 0.5. However, at low SNRs the error components of CNDS and CHDS, especially ε_n, increase which make the value of $(\varepsilon_n - \varepsilon_h)/2\Delta v$ large enough to direct a wrong estimation of integer factor n. In order to provide accurate and precise velocity at a wide range of SNRs, we propose using CMDS with an adaptive algorithm to decide the optimum range of ambiguity velocity [4].

A functional block diagram of CMDS using the adaptive algorithm for the range of ambiguity velocity is shown in Figure 3-4**.** Signals are received by hydrophone and sent to CNDS and CHDS. In the CNDS, coarse velocity including noise v_n is measured and forwarded to the adaptive algorithm for the range of ambiguity velocity and the decision algorithm for integer factor n. The adaptive algorithm for the range of ambiguity velocity should determine the optimum range of ambiguity velocity (Δv_a) based on the minimum CMDS error. By means of the optimum range of ambiguity velocity and the signal received by hydrophone, the precise velocity including noise v_h is then measured by CHDS. With the use of Δv_a, v_n and v_h, a decision algorithm for integer factor n including a variable shift technique is proposed as inequality (3-11). The variable shift technique changes the range of the variable to a suitable range to eliminate the error effect caused by different measured velocity. After carrying out the variable shift, the most probable integer factor n is decided by the optimum range of ambiguity velocity (Δv_a). Finally, by combining the most probable range of ambiguity velocity $2n\Delta v_a$ and the precise velocity including noise v_h, a precise and accurate measurement of velocity by CMDS v_m is obtained.

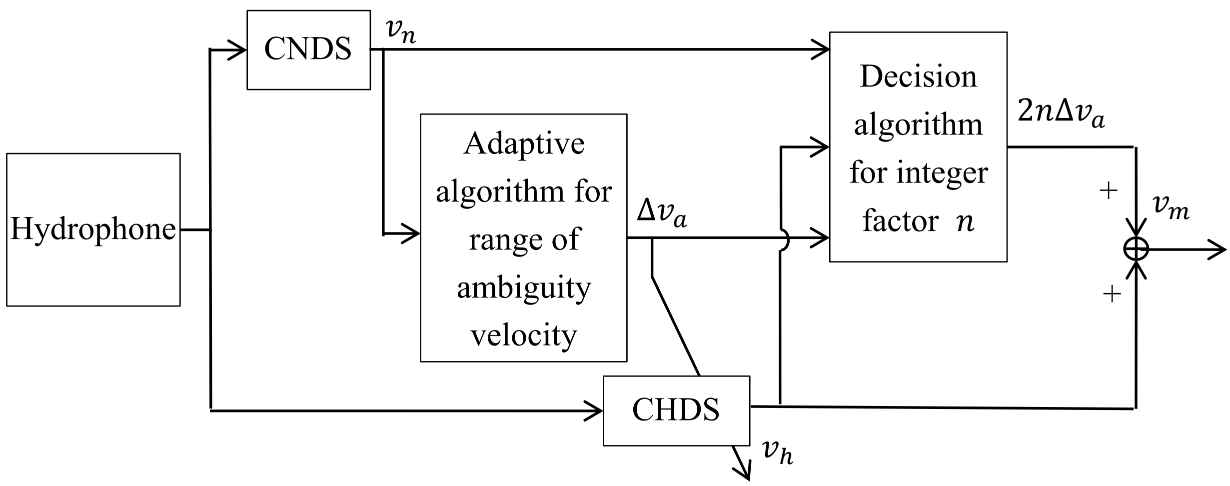

Figure 3-4 Functional block diagram of CMDS using adaptive algorithm.

3.2.2 Method of adaptive algorithm

At low SNR, the CMDS error using a fixed range of ambiguity velocity included many impulsive noises due to wrong decisions for the integer factor n. When the range of ambiguity velocity is wider, the probability of a wrong decision for the integer factor is lower. Therefore, if the range of ambiguity velocity were made larger, the CMDS error using a variable range of ambiguity velocity would become smaller. As shown in Figure 3-5, at low SNRs the measurement error of CMDS with the maximum ambiguity velocity 3.75 m/s is less than other results of CMDS with the ambiguity velocity of 0.75 m/s and 1.87 m/s. On the other hand, the CMDS error also depends on CHDS error. As the range of ambiguity velocity is wider, the CHDS error becomes larger. At high SNRs the measurement error of CMDS with the minimum ambiguity velocity 0.75 m/s is less than the other two in Figure 3-5. Therefore, a wide range of ambiguity velocity does not necessarily reduce the CMDS error. As CMDS with an adaptive algorithm can take advantage of the above two contrary characteristics of the CMDS error at a variable range of ambiguity velocity, it can provide accurate and precise velocity at a wide range of SNRs.

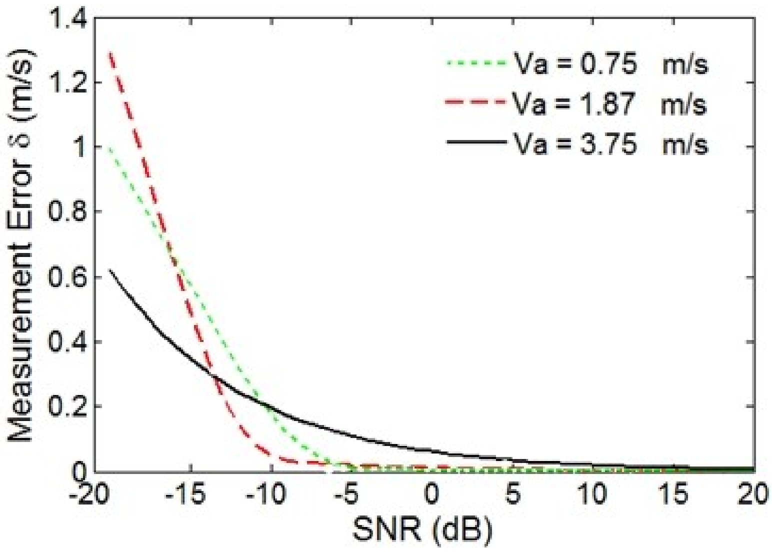

Figure 3-5 Measurement error of CMDS using different ambiguity velocities.

In the process of CMDS using the adaptive algorithm, the most important step is to determine the optimum range of ambiguity velocity based on the minimum CMDS error. A flow chart for the adaptive algorithm for the range of ambiguity velocity is shown in Figure 3-6. From the received signal of hydrophone, SNR is estimated by means of the

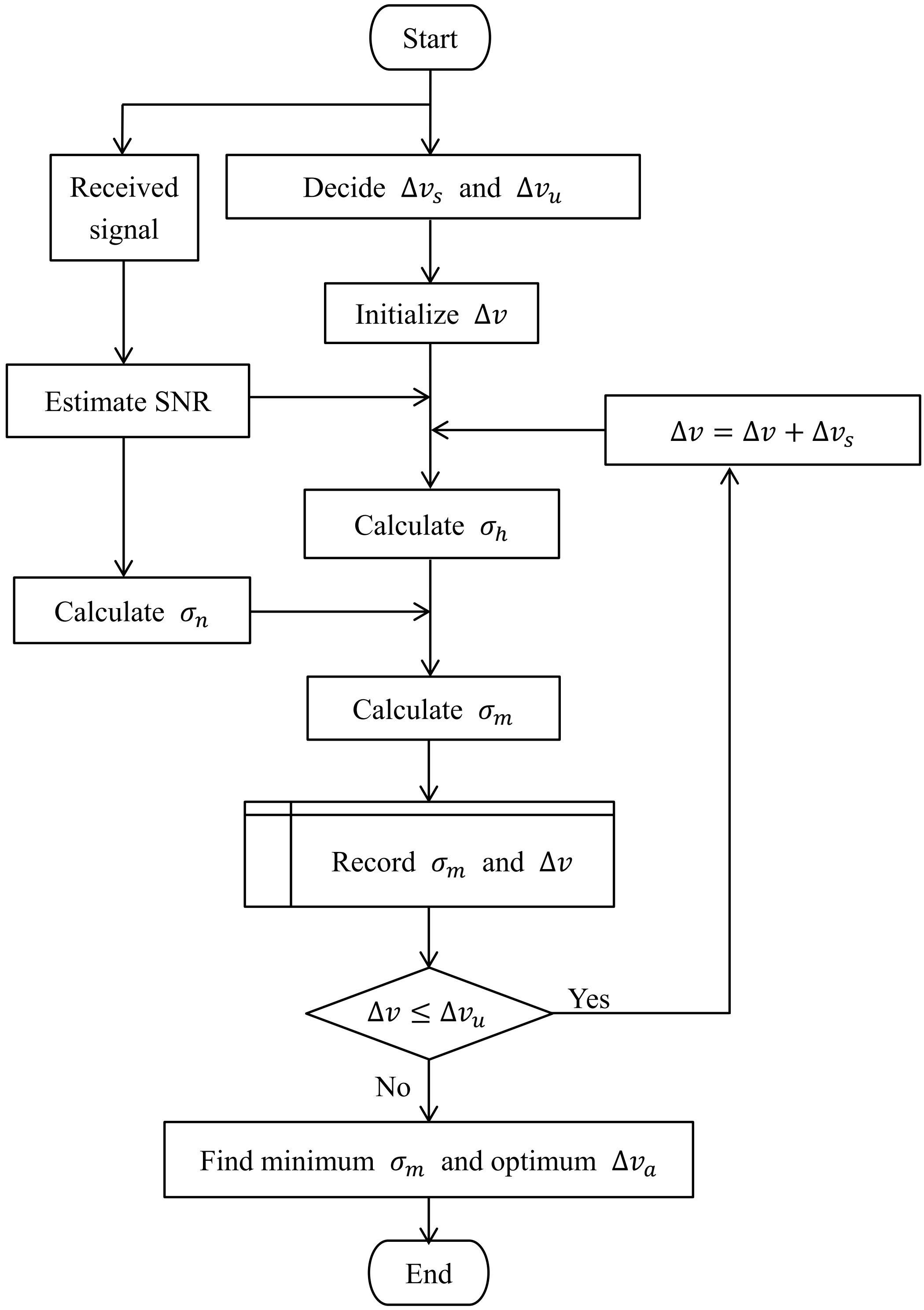

Figure 3-6 Flow chart for adaptive algorithm for the range of ambiguity velocity.

frequency characteristics of the measurement results. Based on the value of SNR, standard deviation (σ_n) of CNDS is calculated. On the other hand, the range of ambiguity velocity of CHDS can be determined using dual time intervals, where the minimum value of the range of ambiguity velocity is zero, and the maximum value of the range of ambiguity velocity is set as Δv_u. Next, the range of ambiguity velocity Δv limited to the range $(0, \Delta v_u]$, is used to calculate the standard deviation of the CHDS error (σ_h) at the estimated SNR. From the results of σ_n, σ_h and Δv, the values of the standard deviation of the CMDS error (σ_m) can be calculated. From 0 to Δv_u at intervals of Δv_s, the CMDS error (σ_m) is obtained for each range of ambiguity velocity. Consequently, the optimum range of ambiguity velocity Δv_a is selected based on the minimum CMDS error σ_m. This method works successfully based on a correct estimation of measurement error for CNDS, CHDS and CMDS. In the next section the error analysis of CMDS will be discussed.

References

[1] P. Liu, N. Kouguchi, "Velocity Measurement by Symbiotic Combination of Conventional and Coherent Doppler Sonars," Proceedings of the OCEANS'13 MTS/IEEE San Diego, 6 pages, 2013.

[2] P. Liu, N. Kouguchi, "Combined Method of Conventional and Coherent Doppler Sonar to Avoid Velocity Ambiguity," the Journal of the Marine Acoustics Society of Japan, Vol.41, No.3, pp.103-112, Jul. 2014.

[3] P. Liu, N. Kouguchi, "Measurement Error Analysis of Combined Doppler Sonar using Adaptive Algorithm," the Journal of the Marine Acoustics Society of Japan, Vol.42, No.1, pp.11-22, Jan. 2015.

[4] P. Liu, N. Kouguchi, "Adaptive Algorithm for Combination Method of Conventional and Coherent Doppler Sonar," Proceedings of the Oceans'15 MTS/IEEE Genova, CD, 6 pages, May 2015.

CHAPTER 4

MEASUREMENT ERROR OF COMBINED METHOD

4.1 Definition of Measurement Error

"Error" in a scientific measurement means the inevitable uncertainty that attends all measurements. "Measurement error" is the difference between a measured value of quantity and its true value. In statistics, errors are not mistakes and they cannot be avoided. One of the best ways to assess the measurement error is to repeat it several times and to examine the different values obtained. However, not all types of errors can be evaluated by statistical analysis using repeated measurement. Therefore, Measurement error can be classified into two groups: random errors, which can be revealed by repeating the measurement; and systematic errors, which cannot [1]. The statistical methods give a reliable estimate of the random errors, but systematic errors are hard to evaluate, and even to detect. In the error analysis of combined method, systematic errors are considered to be much smaller than the required precision and can be ignored.

Mean (or average) is used to find the best estimation of repeated measurement values. If quantity x is measured N times, the best estimation $\bar{x}$ can be expressed as:

$$\bar{x} = \frac{1}{N}\sum_{i=1}^{N} x_i \tag{4-1}$$

where x_i is the result of ith measurement.

Standard deviation is an estimation of the average error of measurements, which can be calculated as:

$$\sigma_x = \sqrt{\frac{1}{N-1}\sum_{i=1}^{N}(x_i - \bar{x})^2} \tag{4-2}$$

If measurements follow Gaussian distribution, about 68 percent of measurements would lie in the range of $\bar{x} \pm \sigma_x$ [2]. In this situation, based on the characteristics of Gaussian distribution, the standard deviation of the mean can be got below.

$$\sigma_{\bar{x}} = \frac{\sigma_x}{\sqrt{N}} \tag{4-3}$$

In the analysis of measurement error of combined method, standard deviation is the basic parameter to evaluate its performance. According to Eq. (4-3), average can decrease the standard deviation. To evaluate the performance of combined method logically, average will not be considered in the error analysis.

4.2 Measurement Error Analysis

4.2.1 Combined method

For CMDS, the measurement error is decided by the accuracy of both CNDS and CHDS. In the case of inequality (3-7), the inequality can also be expressed as:

$$n_e - \frac{1}{4} < \frac{2n_0\Delta v + v_{h0} + \varepsilon_n}{2\Delta v} \le n_e + \frac{3}{4}, \tag{4-4}$$

where v_{h0} is larger than 0, n_0 is the correct value of integer factor n, and n_e is the estimated integer factor. Based on inequality (4-4), the relationship between ε_n and the estimated integer error Δn_e ($\Delta n_e = n_e - n_0$) is obtained as follows:

$$\Delta n_e - \frac{1}{4} - \frac{v_{h0}}{2\Delta v} < \frac{\varepsilon_n}{2\Delta v} \leq \Delta n_e + \frac{3}{4} - \frac{v_{h0}}{2\Delta v}. \tag{4-5}$$

In inequality (4-5), $\varepsilon_n/(2\Delta v)$ is the error factor to estimate the wrong integer number. From Eq. (2-19), the velocity measured by CNDS follows the Gaussian distribution, so the error factor also follows the distribution as shown below:

$$\frac{\varepsilon_n}{2\Delta v} \sim N\left(0, \frac{{\sigma_n}^2}{4\Delta v^2}\right). \tag{4-6}$$

In order to obtain the theoretical error of CMDS, variable conversion from the continuous variable $\varepsilon_n/(2\Delta v)$ to the discrete estimated integer error Δn_e should be carried out. With the integral scales shown in inequality (4-5) as the error factor, the probability of Δn_e occurring can be expressed as [3]:

$$P_{(\Delta n_e)} = \int_{\Delta n_e - \frac{1}{4} - \frac{v_{h0}}{2\Delta v}}^{\Delta n_e + \frac{3}{4} - \frac{v_{h0}}{2\Delta v}} \frac{1}{\sqrt{2\pi}\sigma'_n} e^{\frac{-{\varepsilon'_n}^2}{2(\sigma'_n)^2}} \, d\varepsilon'_n , \tag{4-7}$$

where

$$\varepsilon'_n = \frac{\varepsilon_n}{2\Delta v}, \qquad \sigma'_n = \frac{\sigma_n}{2\Delta v} \qquad \text{and} \qquad \Delta n_e \in \boldsymbol{Z}.$$

The standard deviation of CMDS is expressed as:

$$\sigma_m = \sqrt{\frac{1}{N}\sum_{i=1}^{N}(v_m - v_0)^2}$$

$$= \sqrt{E_1 + E_2 + E_3}\ , \tag{4-8}$$

where

$$E_1 = \frac{1}{N}\sum_{i=1}^{N}(v_{hi} - v_{h0})^2\,;$$

$$E_2 = \frac{1}{N}\sum_{i=1}^{N} 4(\Delta n_{ei})^2\,\Delta v^2; \tag{4-9}$$

$$E_3 = \frac{1}{N}\sum_{i=1}^{N} 4\Delta n_{ei}\Delta v(v_{hi} - v_{h0})\,; \tag{4-10}$$

$N \to \infty$;

Δn_{ei} is the estimated integer error of ith calculation;

v_{hi} is the measurement result of ith calculation by CHDS.

E_1 is the expression of variance for CHDS. E_2 and E_3, expressed in Eq. (4-9) and Eq. (4-10), are difficult to analyse directly. Therefore, expressions with the probability of the estimated integer error are introduced. We set the number such that $\Delta n_{\mathrm{e}i} = q$ occurs as M_q, then Eq. (4-9) and Eq. (4-10) are changed to be:

$$E_2 = \sum_{q\in Z}\frac{M_q}{N}q^2(2\Delta v)^2\ , \tag{4-11}$$

$$E_3 = \frac{1}{N}\sum_{q\in \boldsymbol{Z}}\ \sum_{i:\Delta n_{ei}=q} 4q\Delta v(v_{hi} - v_{h0})$$

$$= \sum_{q \in \boldsymbol{Z}} \frac{M_q}{N} 4q\Delta v \ \{\frac{1}{M_q} \sum_{i:\Delta n_{ei}=q} (v_{hi} - v_{h0})\}$$

$$= \sum_{q \in Z} \frac{M_q}{N} 4q\Delta v\left(\bar{v}_{hq} - v_{h0}\right), \tag{4-12}$$

where the summation of all M_q $(q \in \boldsymbol{Z})$ is N; $\bar{v}_{hq}$ is the mean value of measured velocity by CHDS, while the conventional method provides the integer estimation error q. When $N \to \infty$, M_q/N is the probability of the estimated integer error q happening. Therefore, with the probability of the estimated integer error shown in Eq. (4-7), Eq. (4-11) and Eq. (4-12) can be expressed as:

$$E_2 = \sum_{q \in Z} P_{(q)} (2q\Delta v)^2 \ , \tag{4-13}$$

$$E_3 = \sum_{q \in Z} P_{(q)} 4q\Delta v\left(\bar{v}_{hq} - v_{h0}\right). \tag{4-14}$$

With the integer q replaced by Δn_e in Eq. (4-13) and Eq. (4-14), E_2 and E_3 can be expressed as:

$$E_2 = \sum_{\Delta n_e \in Z} P_{(\Delta n_e)} (2\Delta n_e \Delta v)^2 \ , \tag{4-15}$$

$$E_3 = \sum_{\Delta n_e \in Z} P_{(\Delta n_e)} 4\Delta n_e \Delta v\left(\bar{v}_{h\Delta n_e} - v_{h0}\right). \tag{4-16}$$

In Eq. (4-16), $\bar{v}_{h\Delta n_e}$ is the mean value of measured velocity by CHDS, while the conventional method provides the integer factor estimation with error Δn_e. If the number of measured data is large enough, the value of $\bar{v}_{h\Delta n_e}$ approximates v_{h0}, and the value of E_3 can be ignored. Consequently the standard deviation of CMDS in the case of inequality (3-7) is:

$$\sigma_m = \sqrt{\sigma_h{}^2 + \sum_{\Delta n_e \in Z} P_{(\Delta n_e)}(2\Delta n_e \Delta v)^2}\ . \tag{4-17}$$

For the case of inequality (3-8), the inequality can also be expressed as:

$$n_e - \frac{3}{4} < \frac{2n_0\Delta v + v_{h0} + \varepsilon_n}{2\Delta v} \le n_e + \frac{1}{4}\ , \tag{4-18}$$

where v_{h0} is not larger than 0. The inequality of the error factor $\varepsilon_n/(2\Delta v\,)$ is then obtained as:

$$-\Delta n_e - \frac{1}{4} + \frac{v_{h0}}{2\Delta v} < -\frac{\varepsilon_n}{2\Delta v} \le -\Delta n_e + \frac{3}{4} + \frac{v_{h0}}{2\Delta v}\ . \tag{4-19}$$

Because $\varepsilon_n/(2\Delta v)$ follows a Gaussian distribution, $-\varepsilon_n/(2\Delta v\,)$ has the same distribution as $\varepsilon_n/(2\Delta v\,)$ shown in Eq. (4-6). Therefore, the probability of the discrete estimated integer error Δn_e can be expressed as:

$$P^-_{(\Delta n_e)} = \int_{-\Delta n_e - \frac{1}{4} + \frac{v_{h0}}{2\Delta v}}^{-\Delta n_e + \frac{3}{4} + \frac{v_{h0}}{2\Delta v}} \frac{1}{\sqrt{2\pi}\sigma_n'} e^{\frac{-\varepsilon_n'^{\,2}}{2(\sigma_n')^2}}\, d\varepsilon_n'\ . \tag{4-20}$$

Based on the same data processing technique, the standard deviation of CMDS in the case of $v_{h0} \le 0$ is shown as:

$$\sigma_m^- = \sqrt{\sigma_h{}^2 + \sum_{\Delta n_e \in Z} P^-_{(\Delta n_e)}(2\Delta n_e \Delta v)^2}\,. \tag{4-21}$$

Compared with Eq. (4-7) and Eq. (4-20), if the absolute values of v_{h0} in different directions are the same, the relationship between $P_{(\Delta n_e)}$ and $P^{-}_{(\Delta n_e)}$ can be expressed as:

$$P_{(-\Delta n_e)} = P^{-}_{(\Delta n_e)}. \tag{4-22}$$

According to Eq. (4-22), the relation between σ_m^- and σ_m can be calculated as:

$$\begin{aligned}
\sigma_m^- &= \sqrt{{\sigma_h}^2 + \sum_{\Delta n_e \in \boldsymbol{Z}} P^{-}_{(\Delta n_e)} (2\Delta n_e \Delta v)^2} \\
&= \sqrt{{\sigma_h}^2 + \sum_{\Delta n_e \in \boldsymbol{Z}} P_{(-\Delta n_e)} (2\Delta n_e \Delta v)^2} \\
&= \sqrt{{\sigma_h}^2 + \sum_{\Delta n_e \in \boldsymbol{Z}} P_{(\Delta n_e)} (2\Delta n_e \Delta v)^2} \\
&= \sigma_m \quad .
\end{aligned} \tag{4-23}$$

Based on Eq. (4-23), if the absolute values of v_{h0} in the cases of inequality (3-7) and (3-8) are the same, the standard deviations are also the same, which means that the standard deviation of CMDS is independent of the velocity direction. But as the expression of $P_{(\Delta n_e)}$ contains the parameter v_{h0}, which means the measurement error for CMDS by inequality (3-7) and (3-8) is affected by the value of measured velocity.

4.2.2 Effect of variable shift

As discussed in Chapter 3.1.2, with variable shift CMDS can erase the affection of measured velocity according to inequality (3-11). In order to obtain the measurement error numerically derived by the variable shift process, Eq. (3-3) and Eq. (3-4) are substituted into the inequality (3-11). Accordingly, the inequality (3-11) is expressed as follows:

$$n_e - \frac{1}{2} < \frac{2n_0\Delta v + \varepsilon_n - \varepsilon_h}{2\Delta v} \le n_e + \frac{1}{2},$$

$$n_{\mathrm{e}} - n_0 - \frac{1}{2} < \frac{\varepsilon_{\mathrm{n}} - \varepsilon_{\mathrm{h}}}{2\Delta v} \le n_{\mathrm{e}} - n_0 + \frac{1}{2},$$

$$\Delta n_e - \frac{1}{2} < \frac{\varepsilon_n - \varepsilon_h}{2\Delta v} \le \Delta n_e + \frac{1}{2}\,. \tag{4-24}$$

In the inequality (4-24), $\varepsilon_t = (\varepsilon_n - \varepsilon_h)/(2\Delta v)$ is the error factor used to decide a wrong integer factor.

The measurement errors by CNDS, ε_n, and by CHDS, ε_h, are different velocity errors processed by CNDS and CHDS respectively. The velocity by CNDS is measured from the Doppler shift frequency, but the velocity by CHDS is measured from the coherent phase shift. Accordingly, we assume that the measurement errors by CNDS, ε_n, and by CHDS, ε_h, are statistically independent. Based on this assumption, the probability density function of the error factor, ε_t, can be obtained using the convolution integral of two random variables and is expressed as [4]:

$$p_t(\varepsilon_t) = \int_{-\infty}^{\infty} p_n\left(\varepsilon_t + \frac{\varepsilon_h}{2\Delta v}\right) p_h\left(\frac{\varepsilon_h}{2\Delta v}\right) d\,\frac{\varepsilon_h}{2\Delta v}\,. \tag{4-25}$$

Eq. (4-25) shows the probability density function of the new error factor obtained using the variable shift.

Next, in order to obtain the probability of the decided integer error, Δn_e, we use the following:

$$P_{t(\Delta n_e)} = \int_{\Delta n_e - \frac{1}{2}}^{\Delta n_e + \frac{1}{2}} p_t(\varepsilon_t)\, d\varepsilon_t. \tag{4-26}$$

As in the calculation process of the error for CMDS without variable shift shown in Eq. (4-17), the standard deviation of CMDS error using variable shift can be expressed as:

$$\sigma_{mt} = \sqrt{\sigma_h{}^2 + \sum_{\Delta n_e \in Z} P_{t(\Delta n_e)} (2\Delta n_e \Delta v)^2} \ . \tag{4-27}$$

In Figure 4-1 one example of the standard deviation error by CMDS using variable shift with 0.188 m/s of ambiguity velocity at 3dB SNR is shown. One can see that CMDS error using variable shift is reduced and becomes flat. Our proposed data processing technique of variable shift calculation, to clear away the error effect generated by the value of measured velocity, is proved to be effective.

4.2.3 Error reduction effect of adaptive algorithm

The core calculation in the adaptive algorithm is to find the optimum range of ambiguity

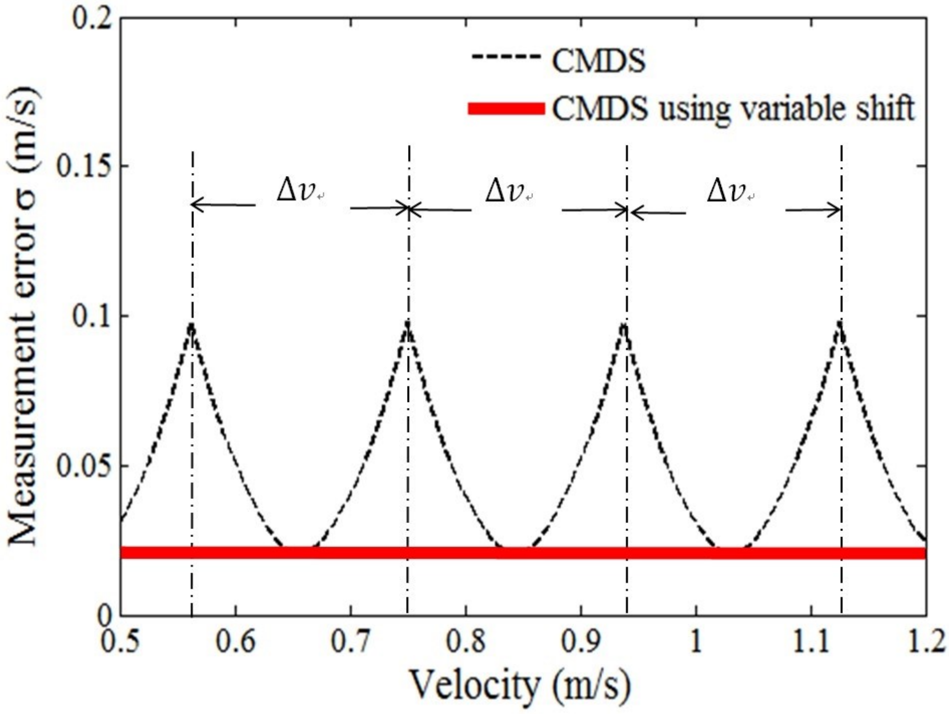

Figure 4-1 Error reduction effect of variable shift at 3 dB SNR.

velocity, Δv_a, from the minimum CMDS error at any SNR shown before the End in Figure 3-6. First, the CMDS error (σ_m) at one SNR is obtained from 0 to Δv_u at intervals of Δv_s.Then the minimum CMDS error (σ_{ma}) can be selected for the SNR, and the optimum range of ambiguity velocity, Δv_a, can be obtained. Next, when the value of SNR is changed to a new value, a new minimum CMDS error can be calculated. Consequently, the minimum CMDS error and the optimum range of ambiguity velocity are simultaneously obtained. This calculation process can be expressed as

$$\Delta v_a = \underset{\Delta v \in (0\ \Delta v_u]}{arg\ min}\, \sigma_m(SNR, \Delta v) \quad . \tag{4-28}$$

Next, we determine the standard deviation of CHDS error using the optimum range of ambiguity velocity. Eq. (2-70) shows the standard deviation of CHDS error using the range of ambiguity velocity. Therefore, Δv in Eq. (2-70) is changed to Δv_a. As a result of the change, the standard deviation of the CHDS error using the optimum range of ambiguity velocity is obtained as

$$\sigma_{ha} = \frac{\Delta v_a}{\pi} \times \sqrt{\int_{-\pi}^{\pi} \phi^2 p_d(\phi) d\phi} \quad . \tag{4-29}$$

In Eq. (4-27), σ_{mt} is the standard deviation of CMDS error using a fixed range of ambiguity velocity and the variable shift. Consequently, Δv and σ_h in Eq. (4-27) are replaced by Δv_a and σ_{ha}; then the CMDS error using the optimum range of ambiguity velocity can be expressed as

$$\sigma_{ma} = \sqrt{{\sigma_{ha}}^2 + \sum_{\Delta n_e \in Z} P_{t(\Delta n_e)} (2\Delta n_e \Delta v_a)^2} \, . \tag{4-30}$$

4.3 Evaluation of Measurement Error

4.3.1 Results of simulation

(1) Conditions

In order to evaluate the performance of CMDS, computer simulations were carried out. In our simulation the hydrophone is considered as a fixed point, and the projector is moving towards the hydrophone with a constant velocity as shown in Figure 4-2. The sign of the projector velocity is negative when the projector moves away from the hydrophone and positive when moving toward.

To evaluate the performance of CMDS, some basic conditions are used in the simulation shown in Table 4-1. The slow moving velocity, -0.270 m/s, was selected as the half speed of our experimental moving device. The fast moving velocity, -2.500 m/s, was selected as a common speed of a moving device on or under the sea. Other conditions are set to use the experimental facilities in our laboratory. For CHDS the velocity ambiguity determined by the time interval of 20 ms is 0.188 m/s. Two moving velocities, -0.270 and -2.500 m/s, are larger than the velocity ambiguity. Therefore, CMDS is adopted to make the measurement.

In this simulation, the received signal is set as the transmitted signal with a time delay and white Gaussian noise. According to a variation of white Gaussian noise, the received signals are generated of various SNRs. Specifically there are 100 received pulses every two seconds in our simulation conditions. The definition of SNR is as follows [5]:

$$SNR=\frac{\text{average signal power}}{\text{average noise power}}=\frac{\frac{1}{t_0}\int_0^{t_0} S(t)^2\,dt}{\frac{1}{t_0}\int_0^{t_0} N_a(t)^2 dt}\quad, \tag{4-31}$$

where

$S(t)$ is the square pulse used in the error analysis;

$N_a(t)$ is the generated white Gaussian noise; and

t_0 is the pulse length.

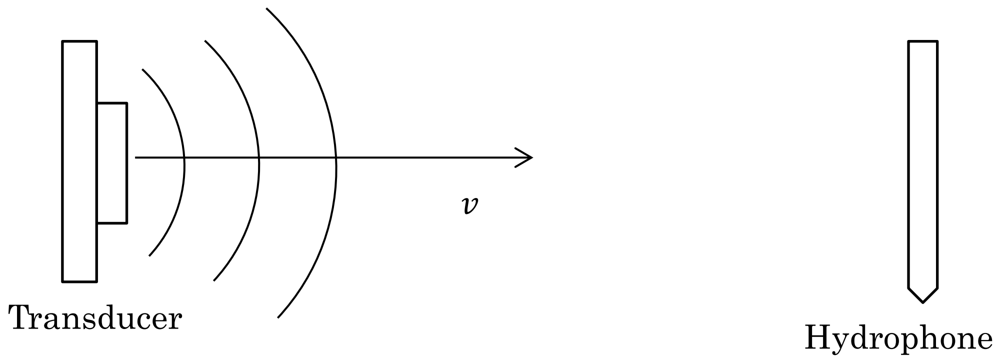

Figure 4-2 Simulation schematic.

Table 4-1 Simulation conditions

Moving speed (m/s)	-0.270	-2.500
Pulse envelope	Square	
Pulse length (ms)	0.6	
Carrier frequency (kHz)	200	
Time interval (ms)	20	
Sampling frequency (MHz)	10	
Sound speed (m/s)	1500	
Simulation Time (s)	2	

In calculating the phase difference of two adjacent pulses, a phase calculation shown in section 2.2.2 (1) needs a low pass filter. For the digital signals, there are other filters to choose [6]. We chose the Butterworth filter is for use in the program.

The frequency response of the Butterworth filter is maximally flat (i.e. has no ripples) in the passband and rolls off towards zero in the stopband. When viewed on a logarithmic Bode plot the response slopes off linearly towards negative infinity. Butterworth filters have a monotonically changing magnitude function with ω, unlike other types of filter that have non-monotonic ripple in the passband and/or the stopband. Compared with a Chebyshev Type I/Type II filter or an elliptic filter, the Butterworth filter has a slower roll-off, and thus will require a higher order to implement a particular stopband specification, but Butterworth filters have a more linear phase response in the pass-band than Chebyshev Type I/Type II and elliptic filters can achieve.

For the low pass Butterworth filter, the bandwidth is from 0 Hz to 10 kHz, and the filter order is set as 4. With these parameters, the amplitude-frequency characteristics of the filter are shown in Figure 4-3.

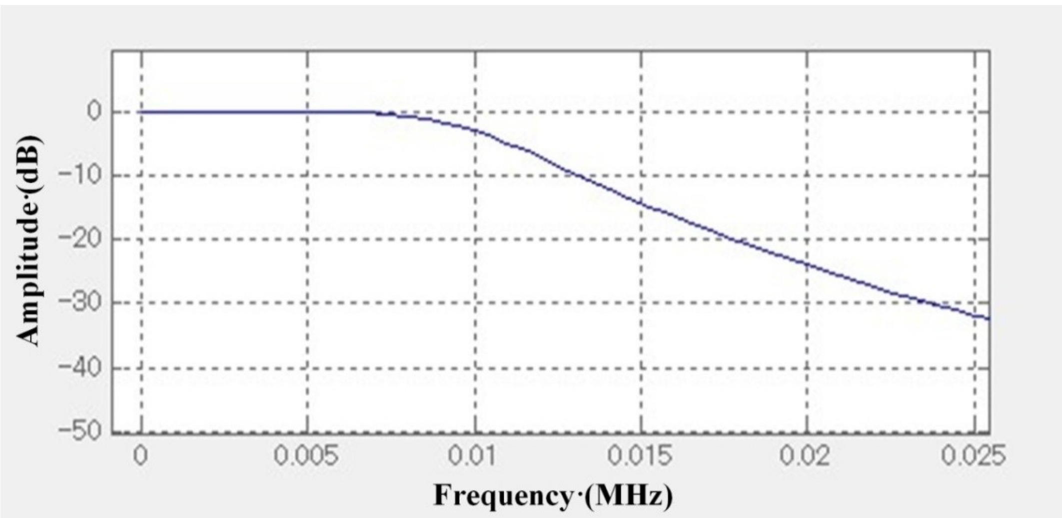

Figure 4-3 Amplitude-frequency characteristics of low pass filter.

(2) Results

Before performing the numerical analysis, the independence of the two measurement errors by CNDS and CHDS at the SNR of -10 dB was carried out by use of the chi square statistical test. As a result of the test, it was verified that the above two measurement errors were statistically independent based on 1 % level of statistical significance.

With the conditions shown in Table 4-1, the theoretical standard deviations of the three methods, CNDS, CHDS and basic CMDS, are shown in Figure 4-4. In Figure 4-4, at the low SNRs (less than-2.0 dB), the difference of the standard deviation between CMDS and CNDS is small, but at the middle SNRs (from -2.0 dB to 5.0 dB), the velocity measured by CMDS is better than CNDS. When the measurement is carried out at the high SNRs, larger than 5.0 dB, CMDS can be as precise as CHDS without velocity ambiguity. The standard deviations of -0.270 and -2.500 m/s measured by CMDS are slightly different at the middle range of SNR, because the two different velocities have different integration intervals in Eq. (4-7). From the results shown in Figure 4-4, the standard deviation of the measurement error by CNDS is about four times the standard deviation by CMDS at the SNR of 5 dB at the velocity of -2.500 m/s. In the case where the standard deviation by CNDS was the same value as by CMDS, the number of samples by CNDS required sixteen times the number by CMDS.

In Figure 4-4, it shows that the error effect of the value of measured velocity is serious, shown as the red line and red dash line. The basic CMDS using fixed ambiguity velocity can provide velocity as precise as CHDS at high SNRs. At low SNRs, because of wrong estimation of integer factor, impulsive noise occurs, and it make the measurement result noisy than CHDS.

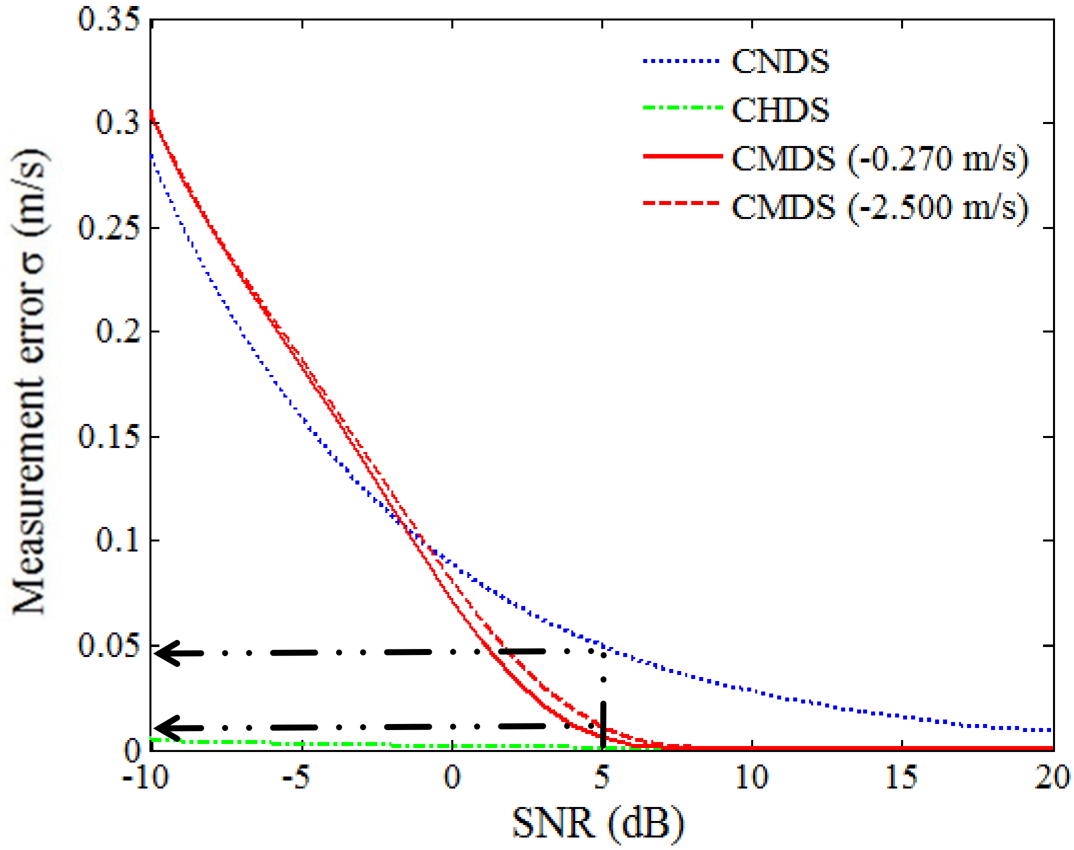

Figure 4-4 Theoretical measurement errors of three methods at different SNRs.

In Figure 4-5 one example of the velocity -0.270 m/s measured by means of CNDS, CHDS and CMDS at the SNR of -1.0 dB is shown. The velocity of CHDS is precise and stable, but it deviates a couple of ambiguity velocity ($2\Delta v$) from the true velocity (v_0). The velocity of CMDS includes one large impulsive behavior. This impulsive behavior is generated due to the wrong estimation of the integer factor n. Except for this one impulse, the velocity of CMDS can be as stable as that of CHDS, and becomes accurate.

Figure 4-6 a) ~ f) show the theoretical and simulation errors of the three methods at different SNRs at -0.270 and -2.500 m/s velocities using a fixed ambiguity velocity of 0.188 m/s. From the results of the comparison between the theoretical and simulated errors, these two methods corresponded well to each other at these two different velocities. Three theoretical equations (Eq. (2-19), Eq. (2-69), Eq. (4-17)) correctly represented the measurement error are and will be able to use them to evaluate the performance of systems. Measurement errors of CHDS, shown in Figure 4-6 b) and e), are much less than the errors measured by CNDS shown in Figure 4-6 a) and d). However, because of the limitation of velocity ambiguity, the measurement results of CHDS are not correct as shown in Figure 4-5. At low SNRs, less than 5 dB, measurement errors of CMDS, shown in Figure 4-6 c) and f), are almost the same as the errors measured by CNDS. However, at high SNRs, larger than 5 dB, CMDS can provide velocity information as precise as CHDS and the measurement results are not affected by velocity ambiguity. These theoretical and simulation results of measurement error show that basic CMDS using a fixed ambiguity velocity can only provide accurate and precise velocity at high SNRs. Therefore, CMDS using adaptive algorithm and variable shift will be evaluated in the simulation.

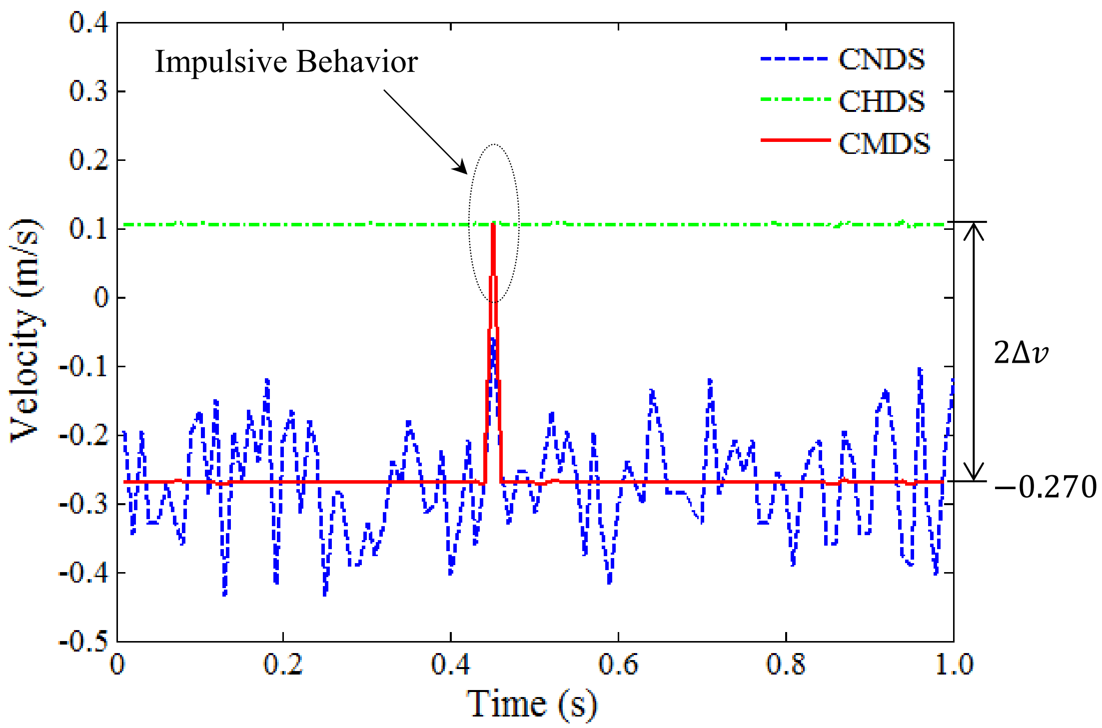

Figure 4-5 Simulation results of -0.270 m/s using three methods at -1.0 dB SNR.

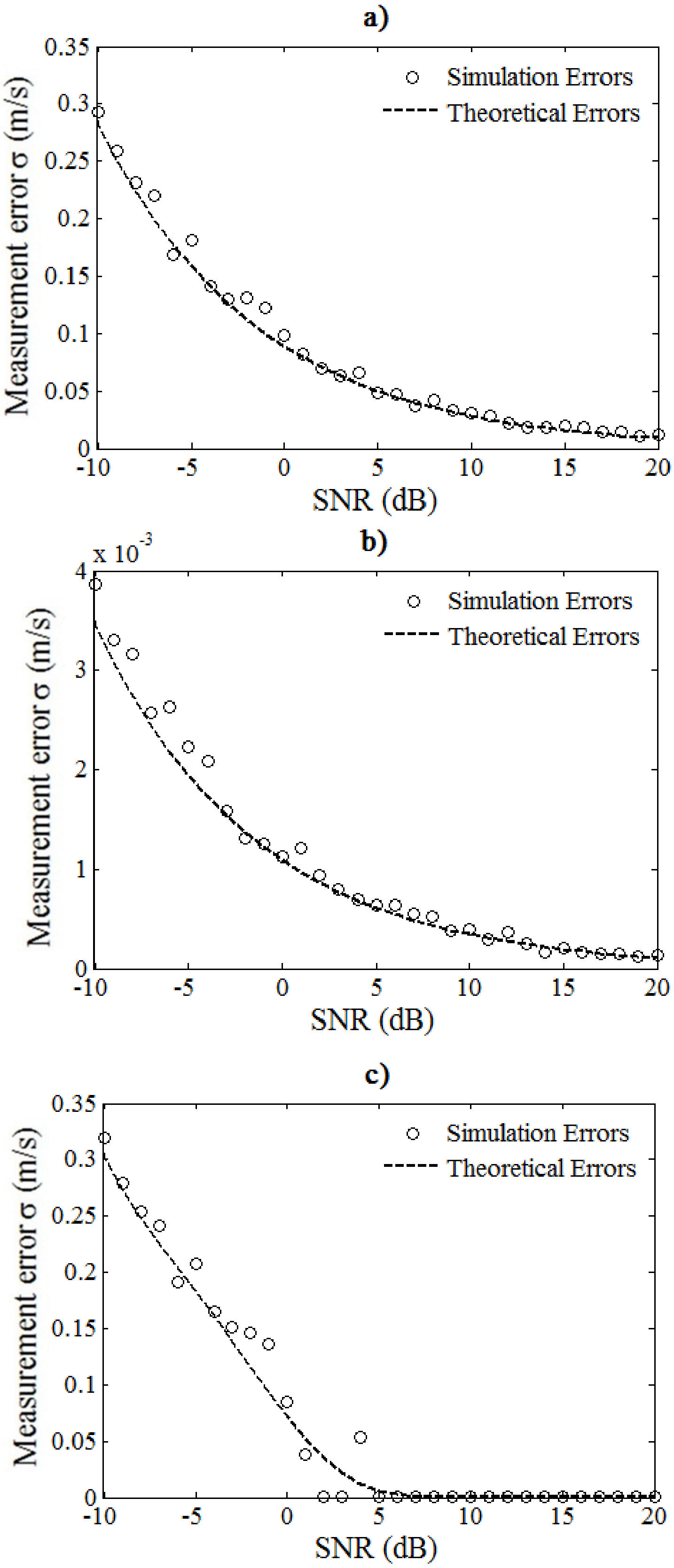
a)
Simulation Errors
Theoretical Errors
Measurement error σ (m/s)
SNR (dB)
b)
x 10^-3
Simulation Errors
Theoretical Errors
Measurement error σ (m/s)
SNR (dB)
c)
Simulation Errors
Theoretical Errors
Measurement error σ (m/s)
SNR (dB)

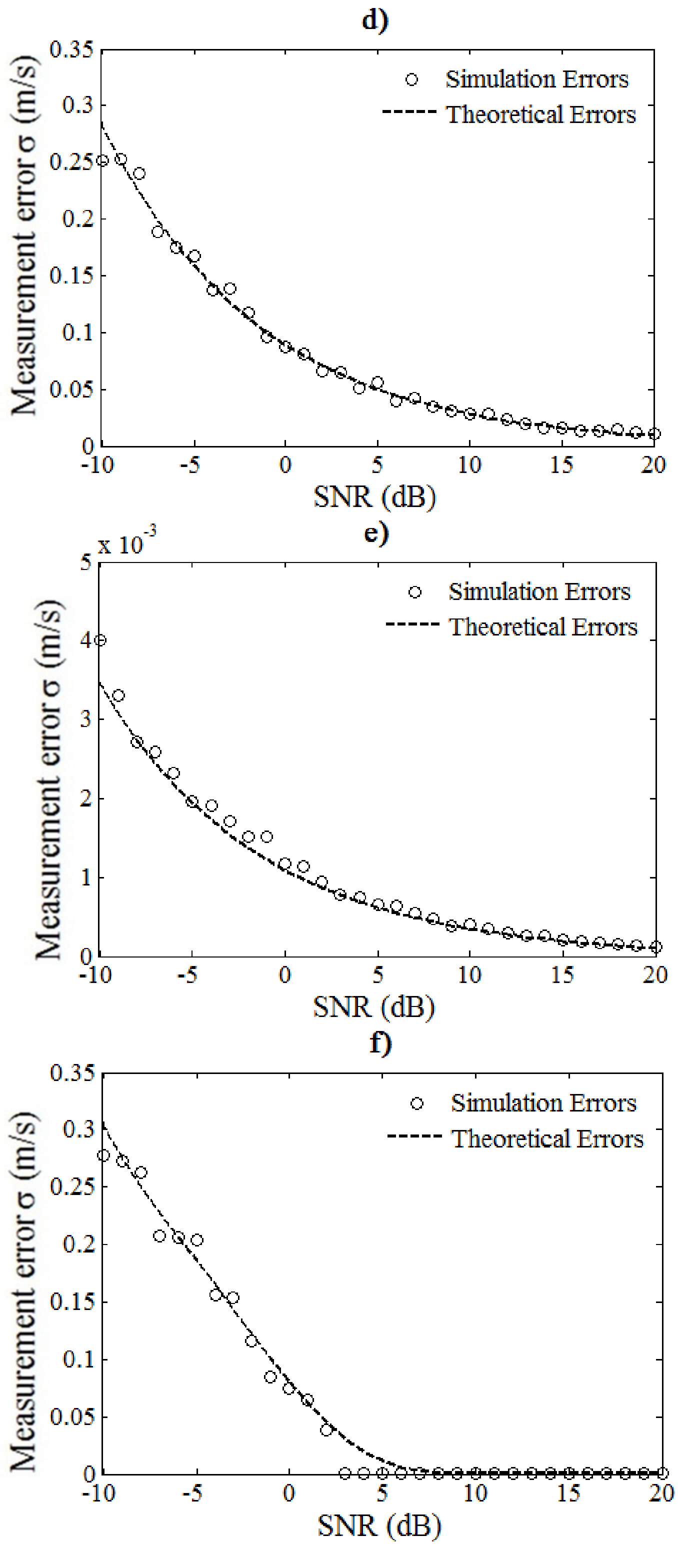

Figure 4-6 Simulation and theoretical errors of three methods. a), CNDS (-0.270 m/s); b), CHDS (-0.270 m/s); c), CMDS (-0.270 m/s); d), CNDS (-2.500 m/s); e), CHDS (-2.500 m/s); f), CMDS (-2.500 m/s).

In Figure 4-7, the relationship between CMDS error and the range of ambiguity velocity is shown, and there is only one optimum range of ambiguity velocity based on the minimum CMDS error, shown as the circle point. For a smaller range of ambiguity velocity, less than 1.163 m/s, the impulsive noises are overwhelming which directs a large measurement error of CMDS. With a larger range of ambiguity velocity, greater than 1.163 m/s, the CHDS error grows progressively which also increase the measurement error of CMDS. Accordingly, the optimum value of the range of ambiguity velocity was identified as 1.163 m/s, and the minimum CMDS error was obtained as 0.045 m/s. From these numerical conditions, the optimum ambiguity velocities and the minimum CMDS errors using the adaptive algorithm were calculated at wide SNRs. The relation between the optimum range of ambiguity velocity and the value of SNR is shown in Figure 4-8. In Figure 4-8, as the value of SNR becomes smaller, the optimum ambiguity velocity

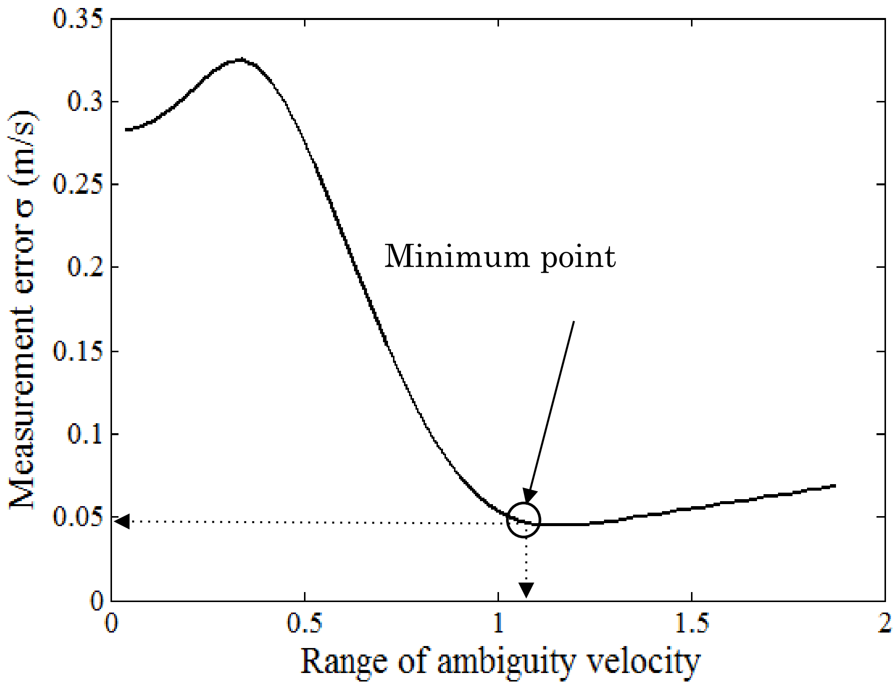

Figure 4-7 One example of CMDS error using variable range of ambiguity velocity at -10 dB SNR.

becomes larger. The reason for this is that CNDS provides a larger measurement error at the lower range of SNRs and it needs a larger ambiguity velocity to decrease the probability of impulsive noise.

Both the numerical and theoretical standard deviations of CNDS, CHDS, and CMDS errors using fixed ambiguity velocity, and CMDS using the adaptive algorithm at different SNRs are shown in Figure 4-9. Figure 4-9 a) shows the comparative results of measurement errors between four types of Doppler sonar. In particular, in order to present the effect of the adaptive algorithm, the CHDS error and the CMDS using the adaptive algorithm are magnified and shown in Figure 4-9 b). In Figure 4-9 a) and b), it is clear that CMDS error using the adaptive algorithm becomes considerably smaller than the CMDS error using fixed ambiguity velocity. Especially, at low SNRs, the proposed adaptive algorithm had a profound effect in reducing the measurement error.

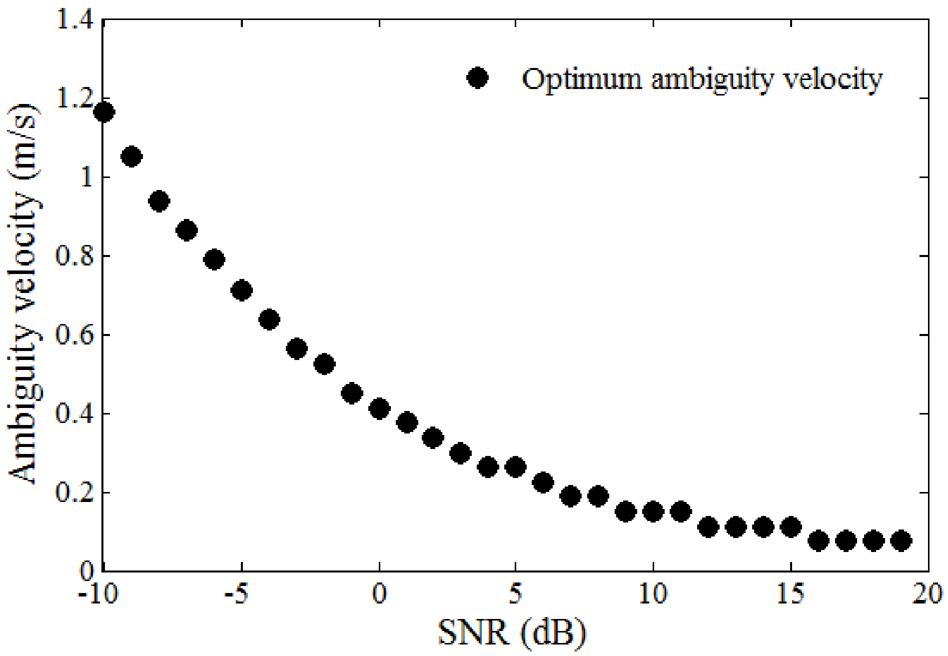

Figure 4-8 Optimum ambiguity velocities of CMDS using adaptive algorithm at different SNRs.

a)

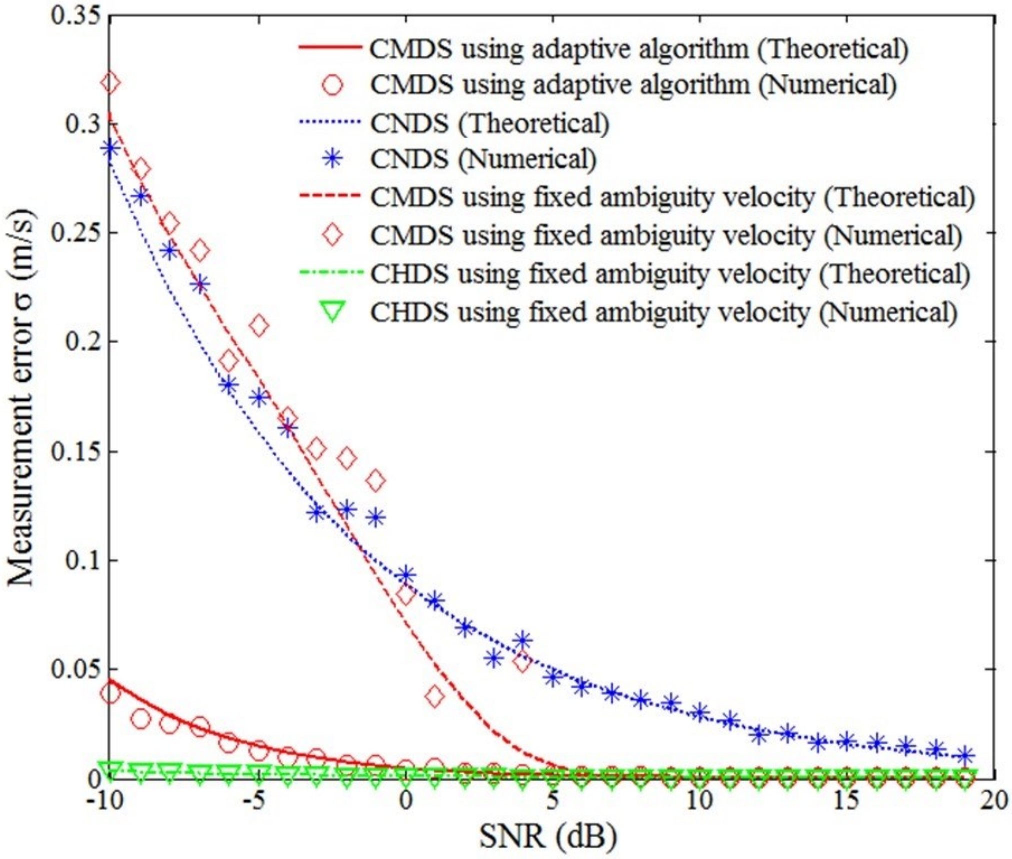

b)

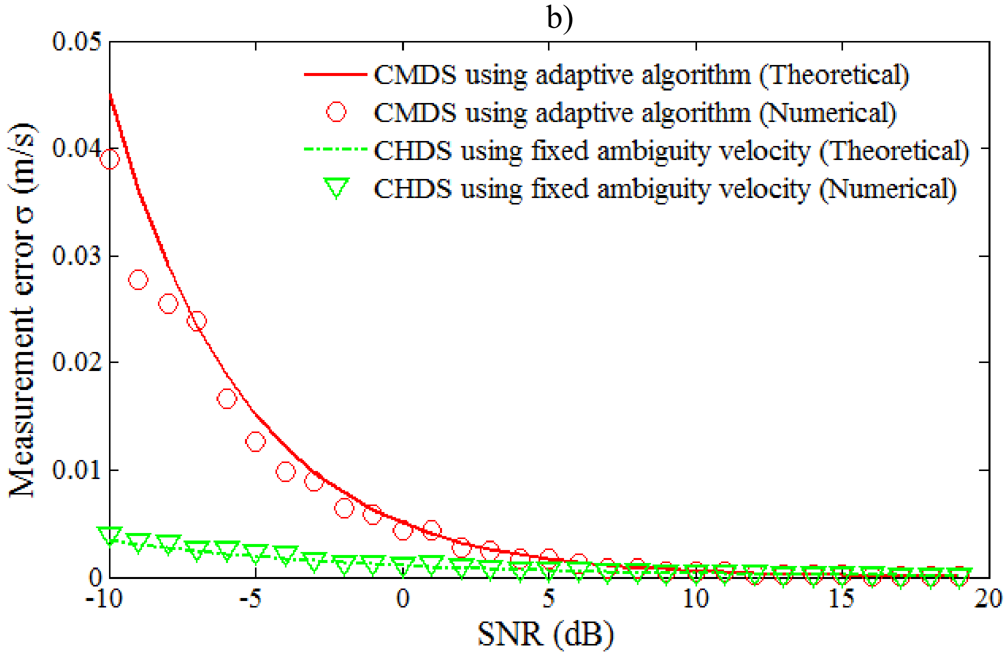

Figure 4-9 a) Comparative results of measurement errors between four types of Doppler sonar. b) Comparative results of measurement errors between two types of Doppler sonar.

Table 4-2 Theoretical and numerical averaged measurement errors by four types of Doppler sonar

Method \ SNR (dB)		-10~ -4	-5~ -1	0 ~ 4	5 ~ 9	10~14	15~19	-10~19
CNDS	$\overline{\sigma_T}$	0.214	0.120	0.068	0.038	0.021	0.012	0.079
	$\overline{\sigma_N}$	0.229	0.132	0.068	0.038	0.022	0.014	0.084
CMDS using fixed ambiguity velocity	$\overline{\sigma_T}$	0.251	0.139	0.039	0.002	0.000	0.000	0.072
	$\overline{\sigma_N}$	0.257	0.161	0.036	0.001	0.000	0.000	0.076
CMDS using adaptive algorithm	$\overline{\sigma_T}$	0.031	0.010	0.003	0.001	0.000	0.000	0.008
	$\overline{\sigma_N}$	0.027	0.009	0.003	0.001	0.000	0.000	0.007
CHDS	$\overline{\sigma_T}$	0.003	0.002	0.001	0.000	0.000	0.000	0.001
	$\overline{\sigma_N}$	0.003	0.002	0.001	0.001	0.000	0.000	0.001

$\overline{\sigma_T}$: Theoretical standard deviation error (m/s), $\overline{\sigma_N}$: Numerical standard deviation error (m/s)

Table 4-2 shows the quantitative results of the theoretical and numerical errors by these four methods. In Table 4-2, the averaged standard deviation errors by these four methods were calculated at every 1 dB SNR from -10 to 19 dB. At the comparatively lower range of SNRs from -10 to 4 dB, the effectiveness of the adaptive algorithm was clearly seen, and the adaptive algorithm reduced the measurement error to one tenth that of the CMDS error using fixed ambiguity velocity. At the higher range of SNRs from 5 to 19 dB, the measurement error, except for CNDS, was almost the same and fairly small. At the wide range of SNRs from -10 to 19, the measurement error by CMDS using adaptive algorithm was about one tenth the measurement of error by CMDS using fixed ambiguity velocity and by CNDS.

Theoretical and simulation results were carried out to evaluate the performance of the CMDS using a fixed and adaptive ambiguity velocity. The simulation results fit the theoretical results well in the situation of white Gaussian noise, which means that the proposed theoretical analysis can be used to evaluate the performance of CMDS systems.

The theoretical and numerical results prove that, CMDS using adaptive algorithm can substantially reduce measurement error compared with CNDS, and it can overcome the disadvantage of velocity ambiguity in CHDS. Consequently, CMDS using adaptive algorithm can provide accurate and precise velocity at a wide range of SNRs.

4.3.2 Results of experiment

The basic structure of experiment system for CMDS is shown in Figure 4-10. The system is established by waveform generator, amplifiers, projector, hydrophone and data acquisition card. The square pulse is generated by the waveform generator with a carrier frequency of 200 kHz and is sent at different time intervals. Then the pulse is amplified by the amplifier and transmitted by the projector in the water tank. The sound signal is received by the hydrophone and amplified by another amplifier. Both the transmitted and received signals are sampled by the NI acquisition card. The speed information

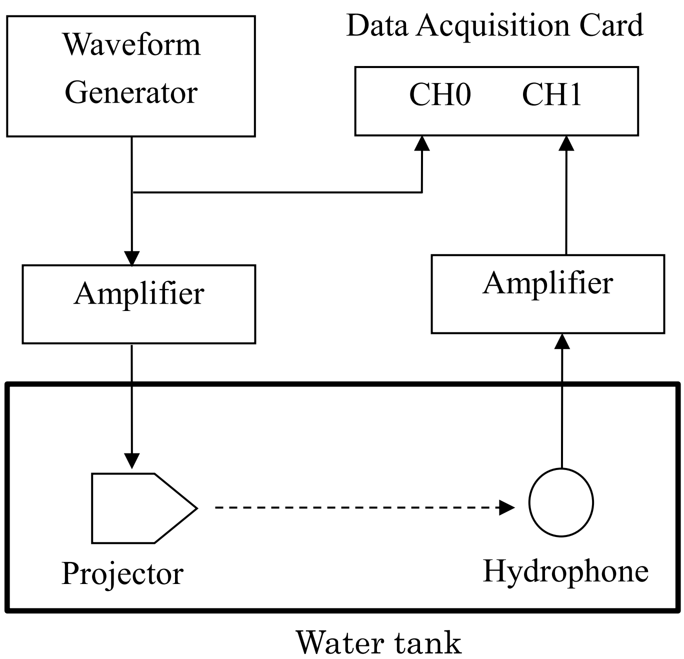

Figure 4-10 System structure of experiment.

is generated by a three dimension moving device with an accuracy of 1 mm/s. In this section, first the experiment system will be introduced in detail, and then the experiment results shown.

(1) Experiment system

a. Waveform generator

Wave Factory 1973 (short as WF1973) is a wave function generator produced by NF Corporation, which is shown in Figure 4-11. WF1973 is a multifunctional generator based on direct digital synthesizers. As a 1-channel generator, the basic features of WF1973 are shown below [7]:

① Highest frequency: 30 MHz (sine wave), 15 MHz (square wave, pulse)

② Frequency accuracy: ±(3 ppm + 2 pHz), high resolution of 0.01 μHz. 10 MHz external frequency reference can be used.

③ Maximum output voltage: 20 Vp-p/open, 10 Vp-p/50 Ω.

④ The Arbitrary Waveform Editor (short as ARB Editor) is software that supports WF1973 Multifunction Generator to generate arbitrary wave function.

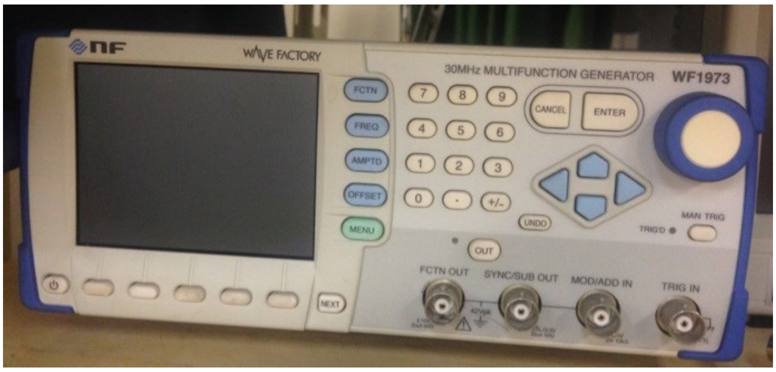

Figure 4-11 Waveform generator WF1973.

b. Amplifier

Figure 4-12 High speed bipolar amplifier HSA4011.

Figure 4-13 Differential amplifier measure league 5307.

In the experiment system, there are two amplifiers to amplify the transmitted and received signals. High speed bipolar amplifier HAS4011, shown in Figure 4-12, is used to enlarge the power of the transmitted signal and differential amplifier Measure League 5307, shown in Figure 4-13, is used to amplify the received signal from the hydrophone.

The high speed bipolar amplifier HAS4011 is a high-speed, wideband power amplifier with a frequency range from DC to 1 MHz and a maximum output of 50 VA [8]. The frequency characteristic is almost flat in the range of DC to 1 MHz with little overshoot or sag of step response waveforms. Its ability to amplify a direct current allows not only asymmetric waveforms between positive and negative polarities but also waveforms with a direct current superimposed to be transmitted correctly.

The Measure League 5307 is a differential amplifier commonly used for wide band that realizes a frequency range of DC to 10 MHz [9]. Although it has a wide frequency range, it also has low noise (4 $nV/\sqrt{Hz}$ typical), low drift (8 $\mu V/°C$ typical), a low distortion factor (0.02 % max), and obtains a maximum gain of 1000 times at a 50 Ω load (2000 time with no-load). In addition to the wide band range, it also has superior pulse response with very little overshoot and ringing. A 1 MHz low-pass filter can be inserted if necessary and the frequency band can be controlled to 1 MHz while maintaining the desire pulse response. This model can select either the differential input or the single-ended input. The single-ended input is available to cancel the DC offset up to $\pm$5 V and to select the reverse or the non-reverse amplitude mode. When the differential is used, a high common model voltage of $\pm$10 V and a large common-mode rejection ratio of 120 dB are obtained and complete protection from excessive input is provided by the input protector. As the input impedance is 1 MΩ, the probe for the oscilloscope can be used. If the internal sort plug in the unit needs to be changed, input impedance is changeable to 100 MΩ and the common-mode rejection ratio deterioration with the unbalance of the single source impedance can be minimized. The output impedance is 50 Ω and this unit can drive a 50 Ω load up to $\pm$5 V (the full power band width is from DC to 3 MHz) and stabilized operation is possible even under capacity load conditions. With wide functions, the Measure League 5307 can be widely used, such as a wide range preamplifier or differential amplifier.

c. Projector

Projector TC2111 which is shown in Figure 4-14 is a compact low cost echo sound transducer, made by RESON Co. shown in Table 4-3 [10].

Figure 4-14 Production of TC2111.

Table 4-3 Technical specifications of TC2111

Resonant Frequency	200 kHz ± 3 kHz
Transmitting Sensitivity	163 dB ± 3 dB (re 1 μPa/V at 1 m)
Impedance	200 Ω ±60 Ω at 200 kHz
Max Input Power	50 W (at 1 % duty cycle)
Operating Temperature Range	+2 ℃ to +35 ℃
Storage Temperature Range	-30 ℃ to +50 ℃
Beam Shape	+2 ℃ to +35 ℃
Beam Width	-30 ℃ to +50 ℃
Operating Depth	30 m
Survival Depth	50 m

The horizontal directivity and transmitting sensitivity of TC2111 are shown in Figure 4-15 and Figure 4-16 respectively [11].

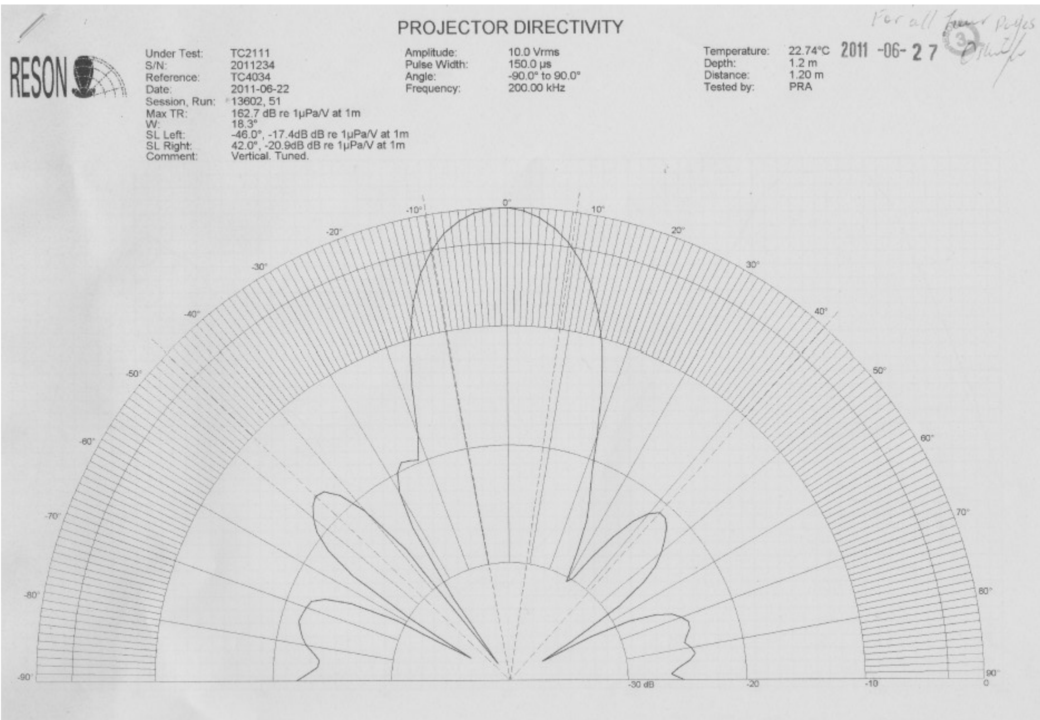

Figure 4-15 Horizontal directivity pattern of TC2111 [11].

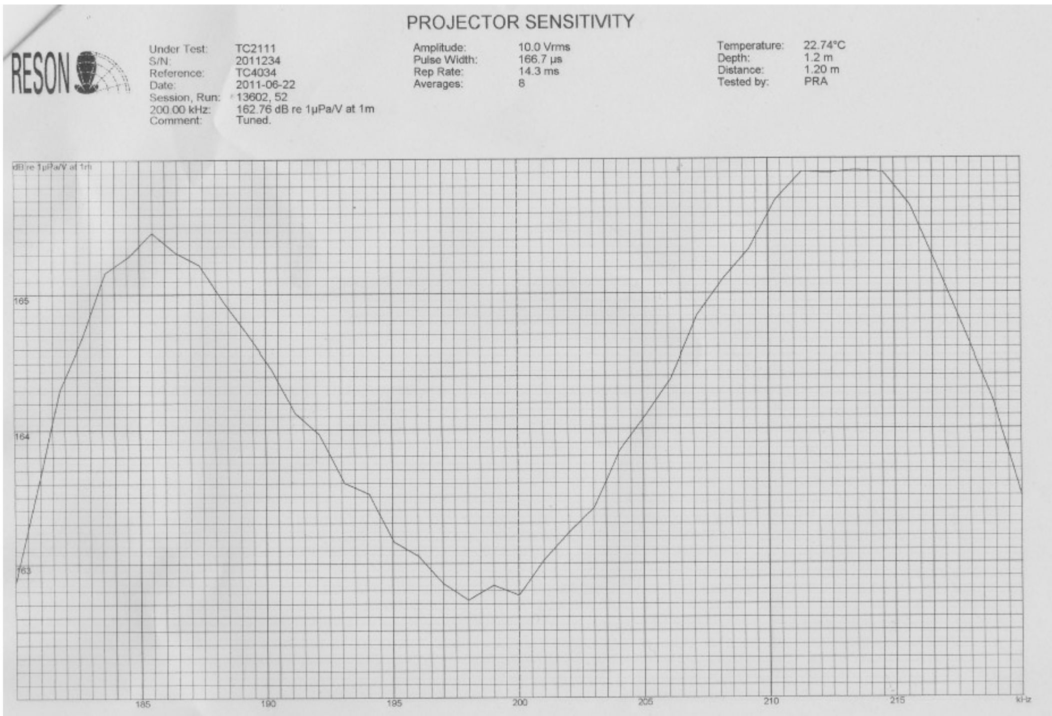

Figure 4-16 Transmitting sensitivity of TC2111 [11].

d. Hydrophone

The hydrophone TC4034 we used is also made by RESON Co., shown in Figure 4-17. The TC4034 broad band spherical hydrophone provides uniform omnidirectional characteristics over a wide frequency range from 1 Hz to 470 kHz. The overall receiving characteristics make the TC4034 an ideal transducer for making absolute underwater sound measurements up to 470 kHz. The wide frequency range also makes the TC4034 perfect for calibration purposes, particularly at higher frequencies. The features of TC4034 are shown in Table 4-4 [10]. The horizontal directivity and the receiving sensitivity of TC4034 are shown in Figure 4-18 and Figure 4-19 respectively [12].

Table 4-4 Technical specifications of TC4034

Usable Frequency Range	1 Hz to 470 kHz (+3, -10 dB)
Linear Frequency Range	1 Hz to 250 kHz (+2, -4 dB)
Receiving Sensitivity	-218 dB±3 dB (at 250 kHz, re 1μV/Pa)
Horizontal Directivity	Omnidirectional ±2 dB (at 100 kHz)
Vertical Directivity	>270° ±3 dB (at 300 kHz)
Nominal Capacitance	3 nF
Operating Depth	900 m
Survival Depth	1000 m
Operating Temperature Range	-2 ℃ to +80 ℃
Storage Temperature Range	-40 ℃ to +80 ℃

Figure 4-17 Production of TC4034.

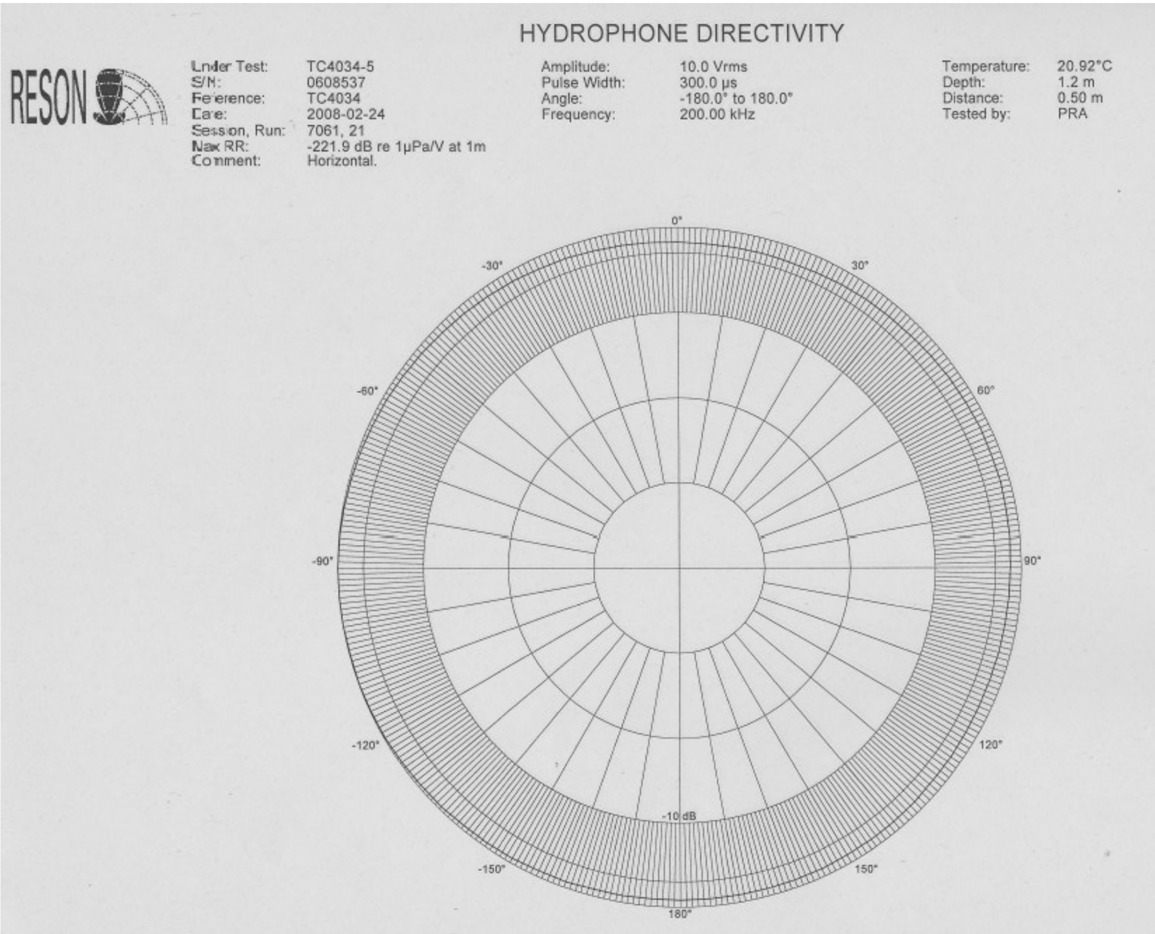

Figure 4-18 Horizontal directivity pattern of TC4034 [12].

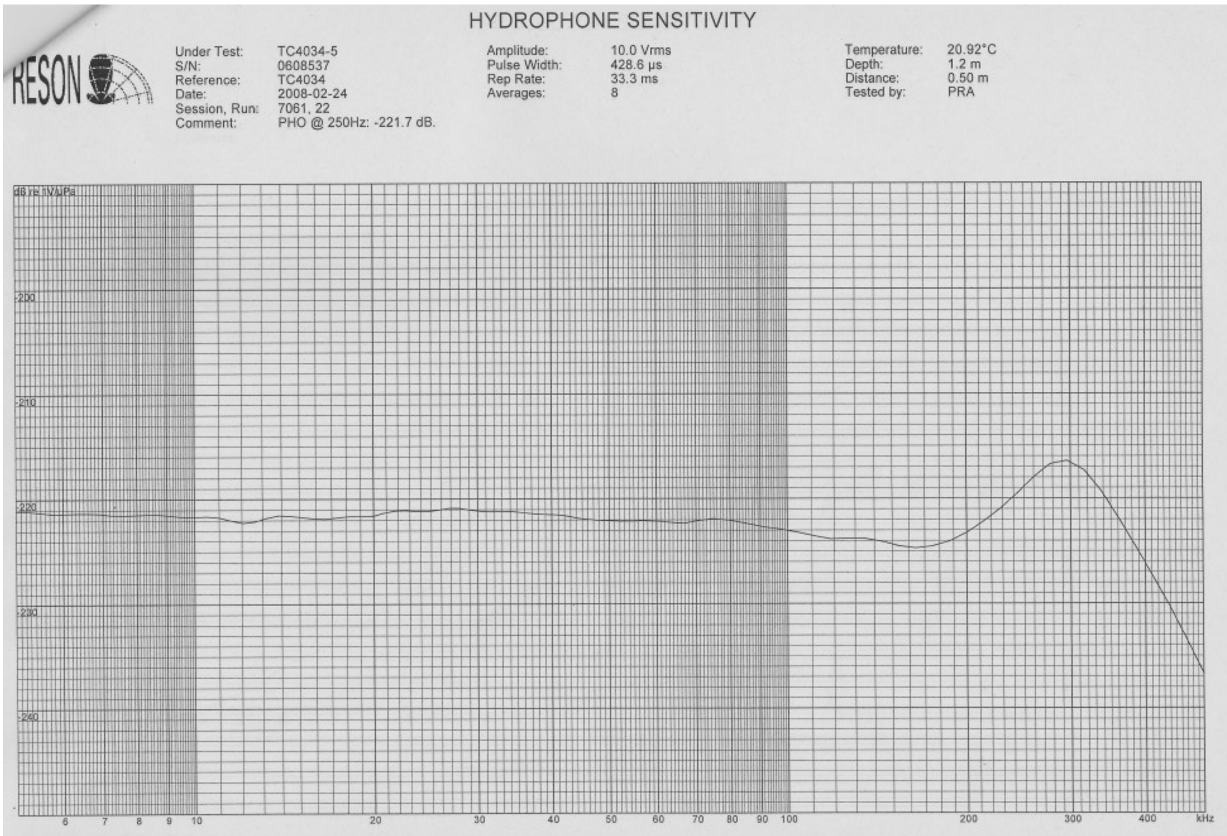

Figure 4-19 Receiving sensitivity of TC4034 [12].

e. Data acquisition card

Data acquisition card NI Pxie-5122 made by National Instruments Corporation is used in the experiment system [13]. NI Pxie-5122 is a high-speed digitizer, which features two 100 million samples per second simultaneously sampled input channels with 14-bit resolution, 100 MHz bandwidth, and up to 512 MB of memory per channel. And the related sampling software, LabVIEW, is used to develop and execute. Generally speaking the sampling frequency and resolution of NI Pxie-5122 are very high. Figure 4-20 shows the NI Pxie-5122, which can be integrated with a general-purpose computer. There are two analog channels, CH0 and CH1, on the board of NI Pxie-5122, with which the transmitted and received signal is input into the high-speed digitizer.

Figure 4-20 High-speed digitizer NI Pxie-5122.

f. Three dimension moving device

The movement information is generated by the three dimension moving device, Super FA made by THK Co., shown in Figure 4-21. The velocity resolution provided by this moving device is 1 mm/s and the highest acceleration is 3m/s^2. In the experiment, only one axis is used [14].

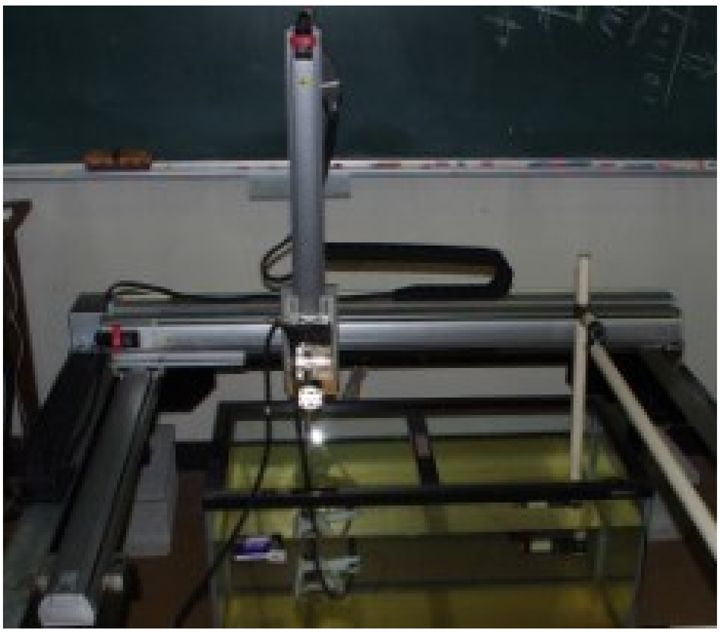
Figure 4-21 Three dimension moving device.

g. Shallow water tank

Experiments are carried out in a shallow water tank, 60 m × 6 m × 2 m. The maximum water depth is 1.5 m, but in our experiment the water depth was kept at 0.9 m. The ground plan and side view of the shallow water tank is shown in Figure 4-22. Figure 4-23 is a photo of the shallow water tank.

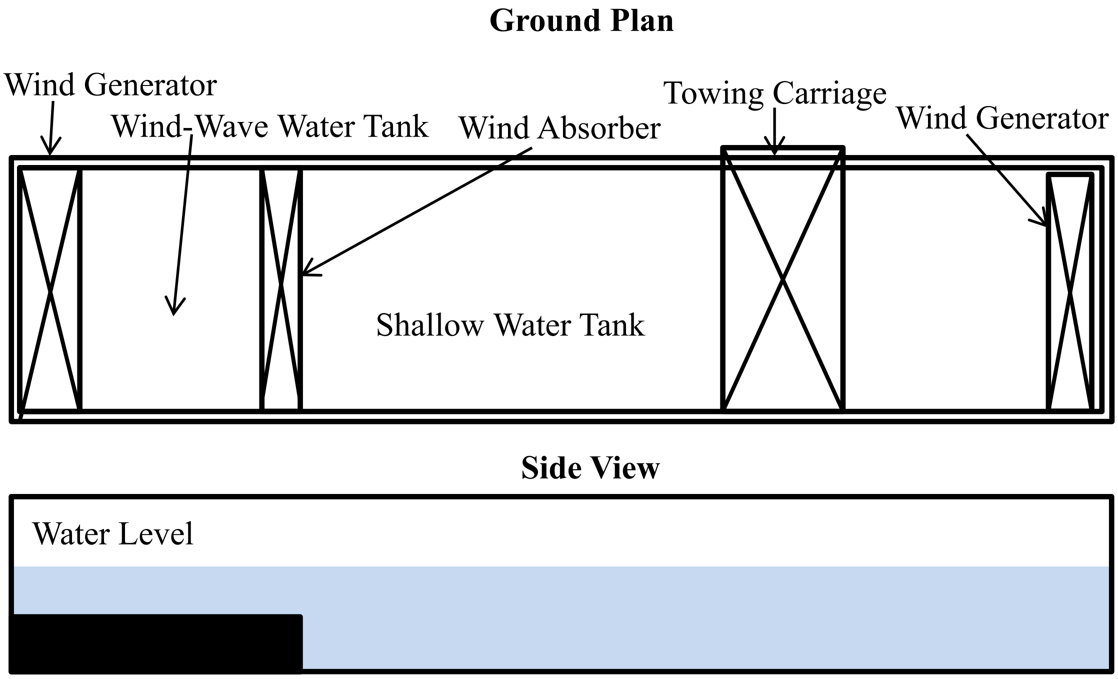

Figure 4-22 Ground plan and side view of shallow water tank.

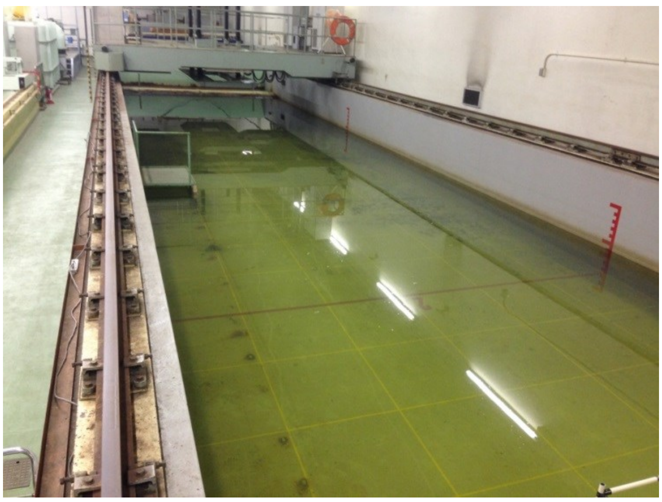

Figure 4-23 Photo of shallow water tank.

h. System structure

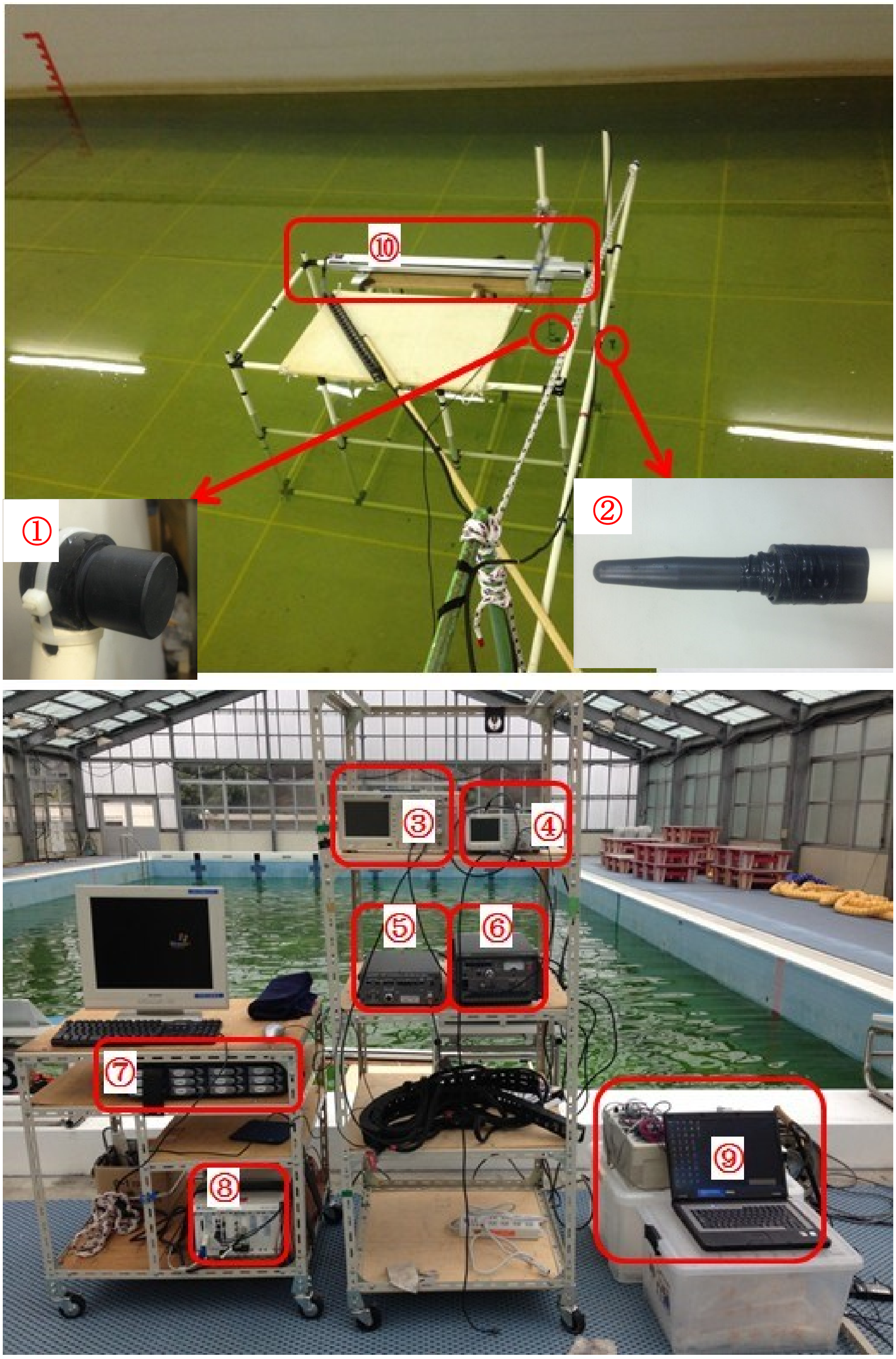

Figure 4-24 Components of experiment system. ①, projector; ②, hydrophone; ③, oscilloscope; ④, waveform generator; ⑤ and ⑥, amplifier; ⑦, high-speed disk; ⑧, NI Pxie-5122 data acquisition card; ⑨, control panel of three dimension moving device; ⑩, one axis of three dimension moving device.

After introducing the characteristics of each component in the experimental system, the whole system is shown in Figure 4-24. The sampled data is stored in the high-speed disc, and will be processed later. Limited by the characteristics of this system, we cannot change the time interval of transmitted pulses automatically. Since we change the time interval manually, one ambiguity velocity is used for a range of SNRs in the experiments.

(2) Experiment results

a. Static experiment

The hydrophone and projector are fixed. In this situation, the velocity is zero. The velocity measurement error is only affected by the noise generated from the electronic device. The three dimension moving device was not used, so the engine was not needed to turn on. Therefore, noise only comes from the signal generator, amplifiers, sensors and the environment. These kinds of noise are normally all considered as white Gaussian noise, which means the analysis of CNDS, CHDS and CMDS using and not using adaptive algorithm should fit the experimental results.

In the experiments, limited by the device we used, it was impossible to change the ambiguity velocity according to each measured SNR immediately. Therefore, instead of an ambiguity for each measured SNR, an ambiguity velocity was used for a range of SNRs. To evaluate the affection from the range of SNRs, experiments were carried out with different ranges of SNRs, and they are shown in Table 4-5.

Table 4-5 Ambiguity velocities used at different ranges of SNRs

Range of SNRs: 2 dB

SNR (dB)	(-12,-10]	(-10,-8]	(-8,-6]	(-6,-4]	(-4,-2]	(-2,0]	(0,2]	(2,4]
A.V. (m/s)	1.163	0.938	0.788	0.638	0.525	0.413	0.338	0.263
SNR (dB)	(4,6]	(6,8]	(8,10]	(10,12]	(12,14]	(14,16]	(16,18]	(18,20]
A.V. (m/s)	0.225	0.188	0.150	0.113	0.113	0.075	0.075	0.075

Range of SNRs: 4 dB

SNR (dB)	(-12,-8]	(-8,-4]	(-4,0]	(0,4]	(4,8]	(8,12]	(12,16]	(16,20]
A.V. (m/s)	1.050	0.713	0.450	0.300	0.188	0.150	0.113	0.075

Range of SNRs: 8 dB

SNR (dB)	(-12,-4]	(-4,-4]	(4,12]	(12,20]
A.V. (m/s)	0.938	0.375	0.150	0.075

Range of SNRs: 16 dB

SNR (dB)	(-12,4]	(4,20]
A.V. (m/s)	0.563	0.113

Range of SNRs: 32 dB (fixed ambiguity velocity)

SNR (dB)	(-12,20]
A.V. (m/s)	0.263

a)-1

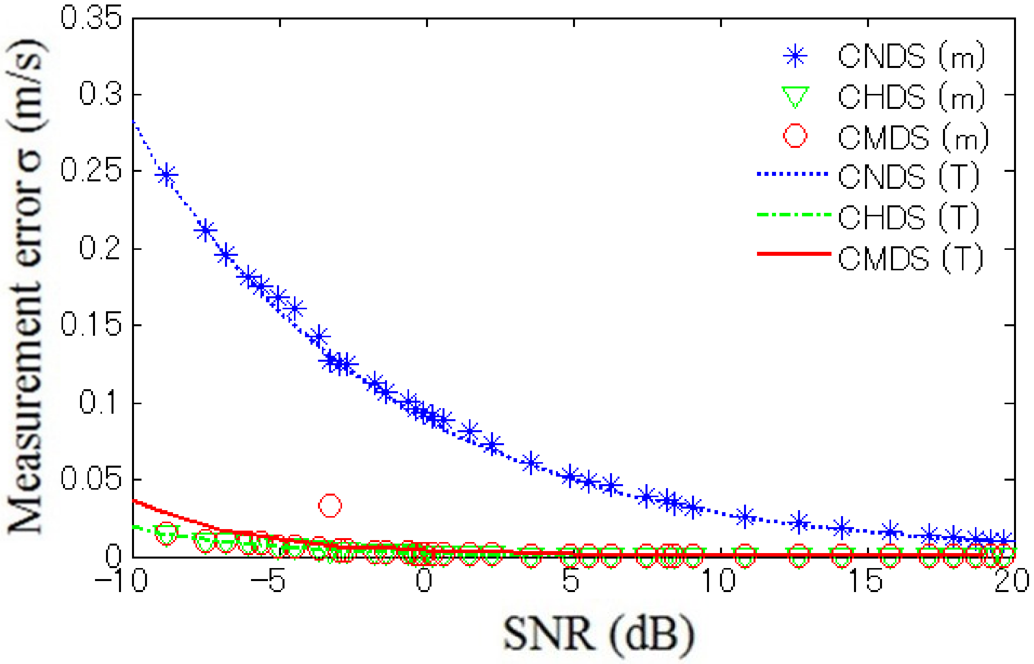
Measurement error σ (m/s)
SNR (dB)
CNDS (m)
CHDS (m)
CMDS (m)
CNDS (T)
CHDS (T)
CMDS (T)
0.35
0.3
0.25
0.2
0.15
0.1
0.05
0
−10
−5
0
5
10
15
20

a)-2

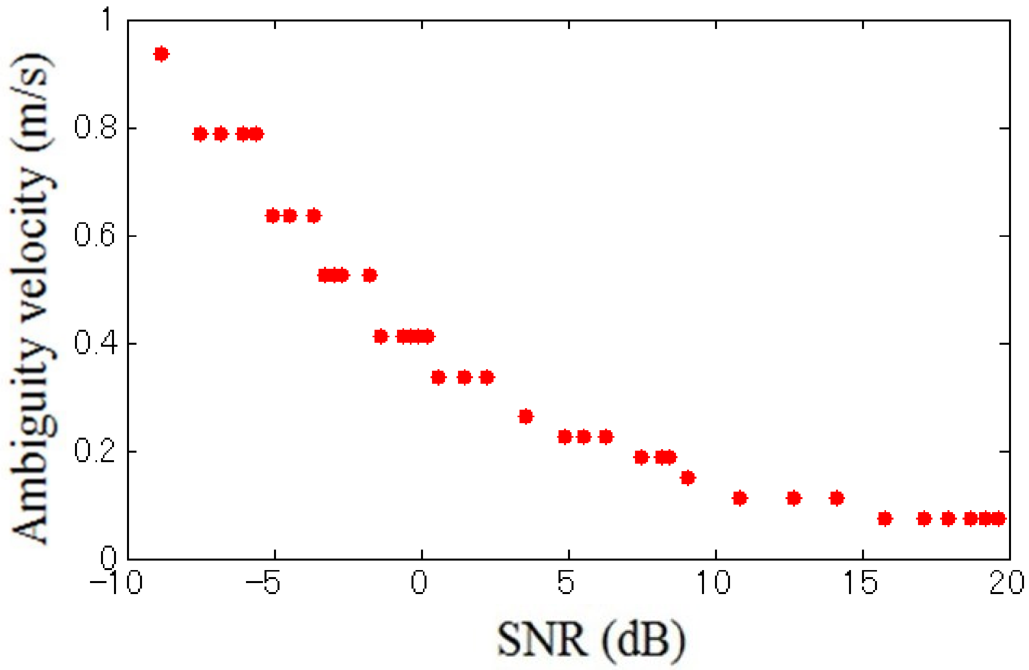
Ambiguity velocity (m/s)
SNR (dB)
1
0.8
0.6
0.4
0.2
0
−10
−5
0
5
10
15
20

b)-1

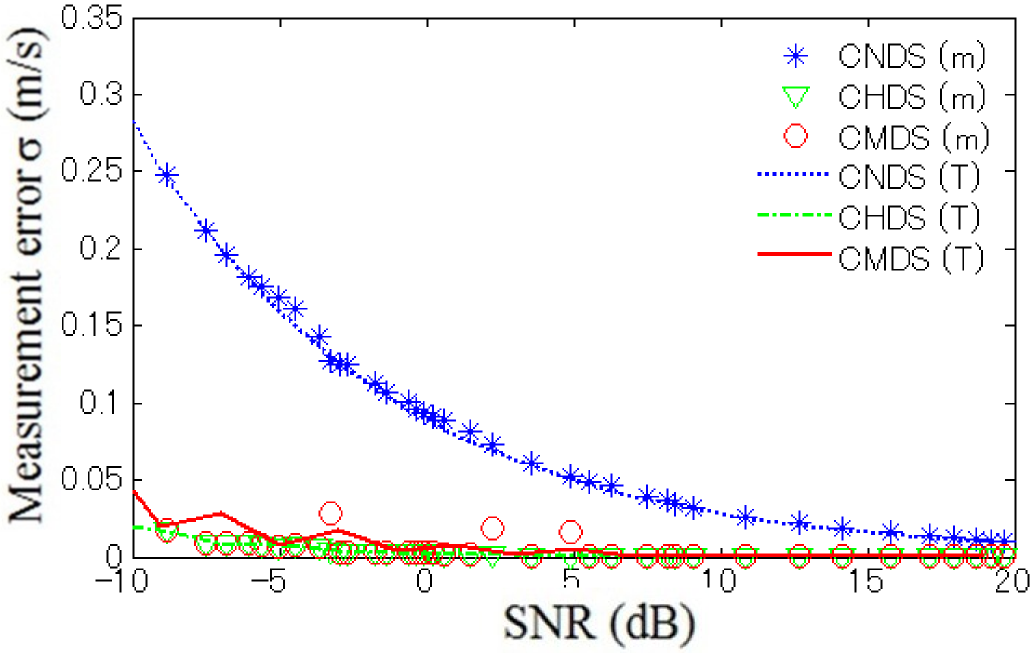

CNDS (m)
CHDS (m)
CMDS (m)
CNDS (T)
CHDS (T)
CMDS (T)
Measurement error σ (m/s)
SNR (dB)
0.35
0.3
0.25
0.2
0.15
0.1
0.05
0
−10
−5
0
5
10
15
20

b)-2

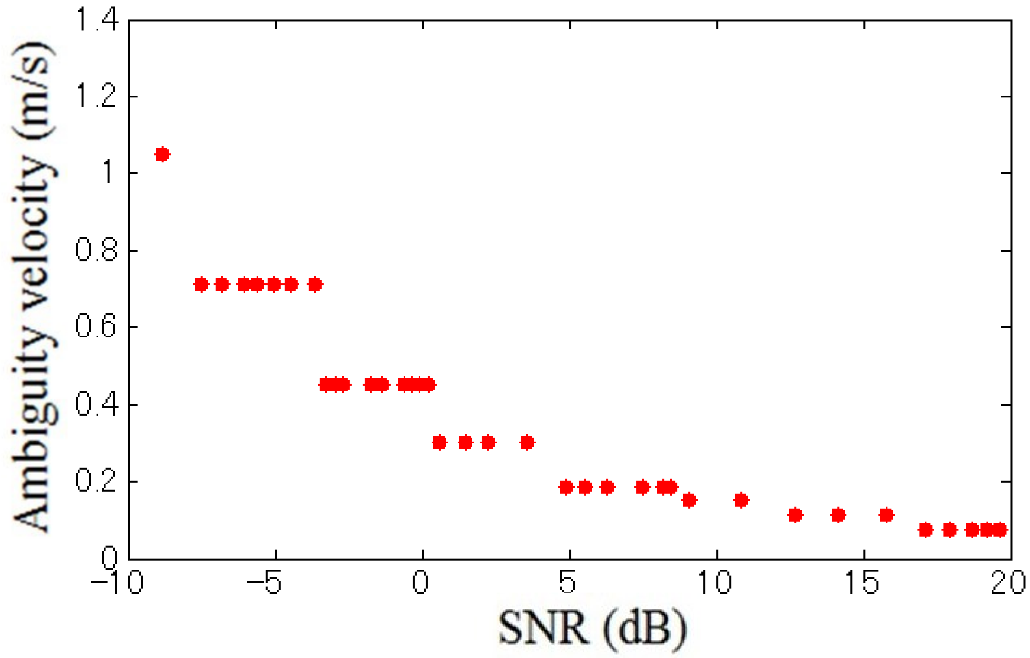

Ambiguity velocity (m/s)
SNR (dB)
1.4
1.2
1
0.8
0.6
0.4
0.2
0
−10
−5
0
5
10
15
20

c)-1

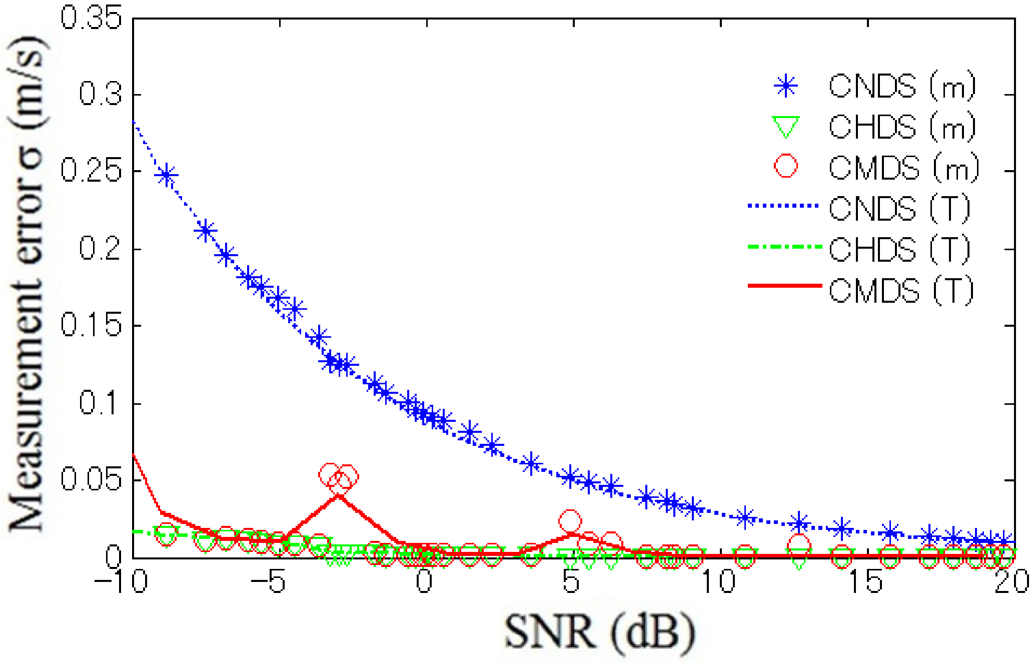

Measurement error σ (m/s)
SNR (dB)
CNDS (m)
CHDS (m)
CMDS (m)
CNDS (T)
CHDS (T)
CMDS (T)

c)-2

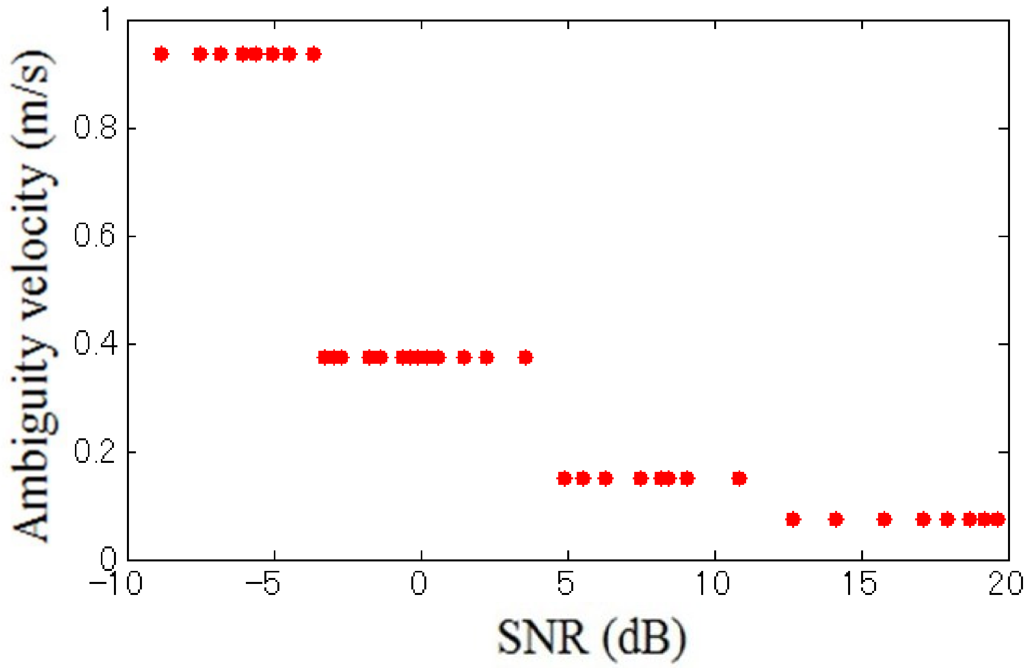

Ambiguity velocity (m/s)
SNR (dB)

d)-1

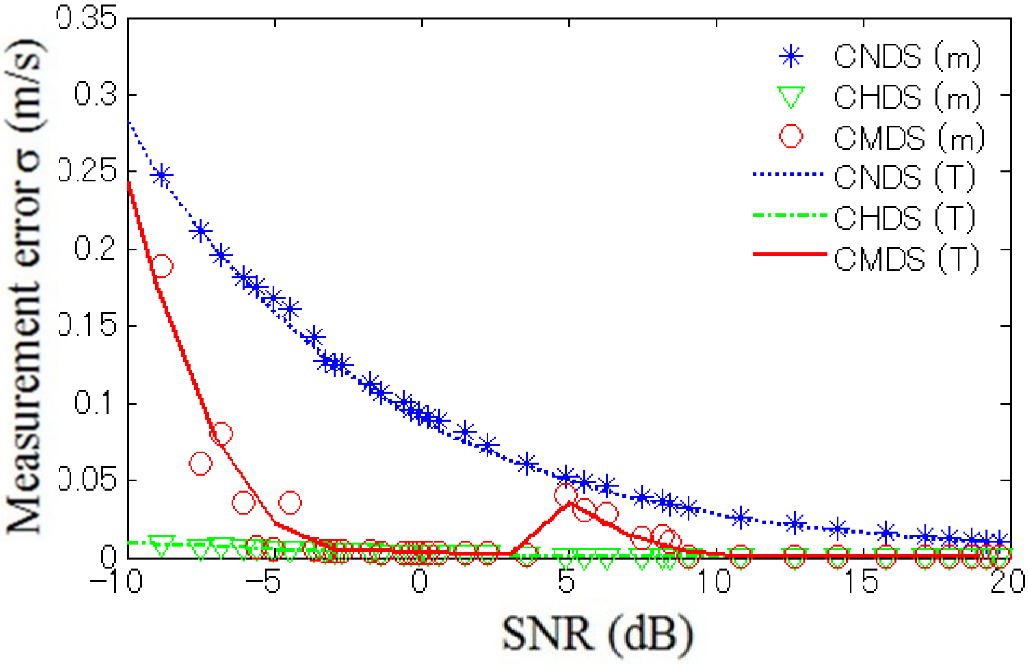

0.35
0.3
0.25
0.2
0.15
0.1
0.05
0
Measurement error σ (m/s)
−10
−5
0
5
10
15
20
SNR (dB)
CNDS (m)
CHDS (m)
CMDS (m)
CNDS (T)
CHDS (T)
CMDS (T)

d)-2

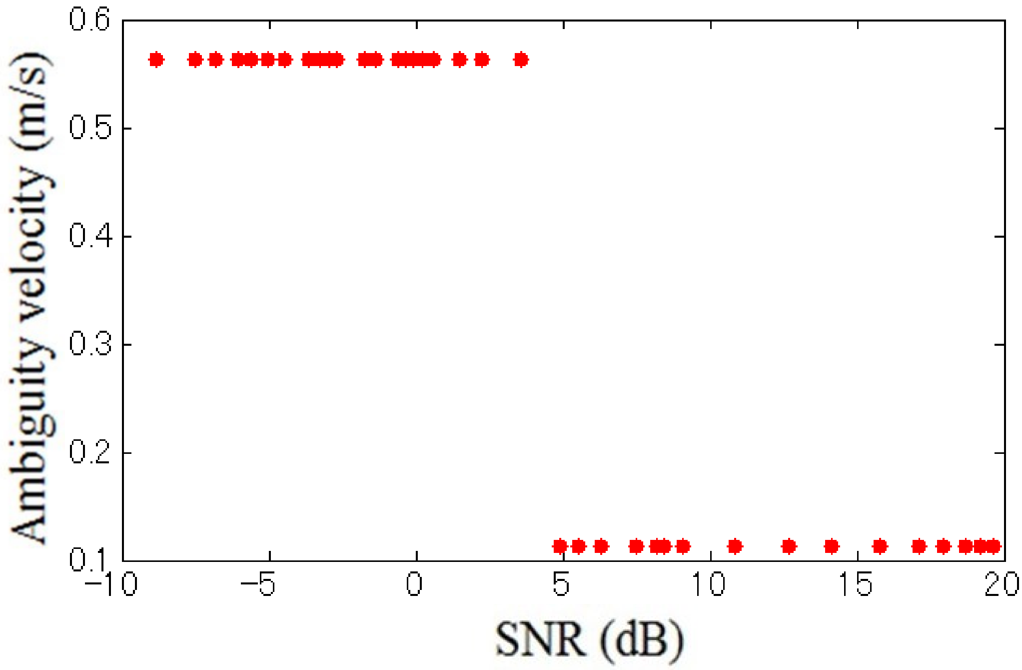

0.6
0.5
0.4
0.3
0.2
0.1
Ambiguity velocity (m/s)
−10
−5
0
5
10
15
20
SNR (dB)

e)-1

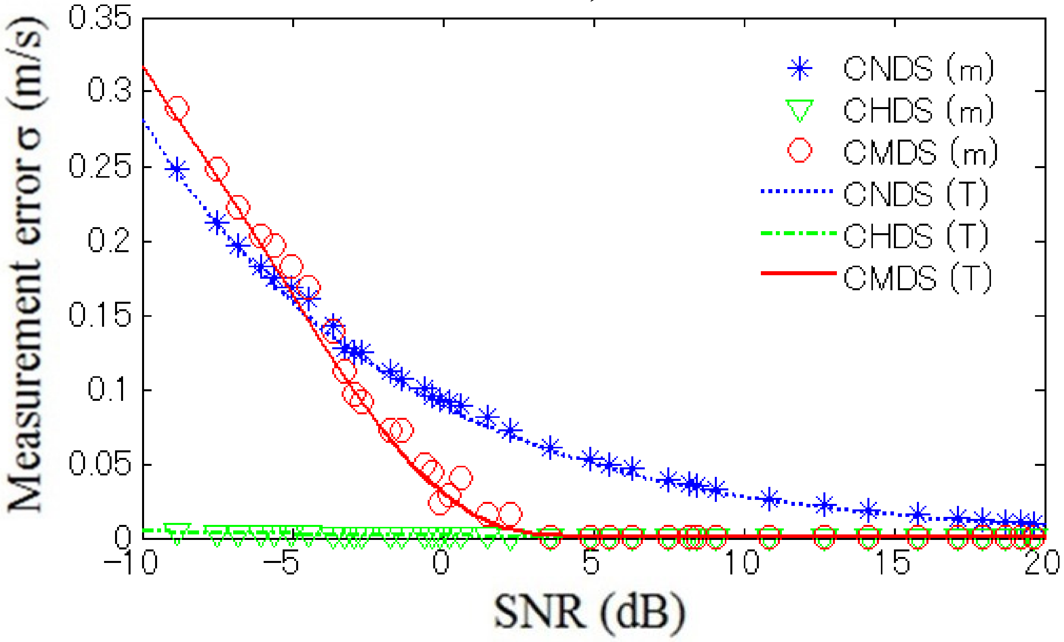

e)-2

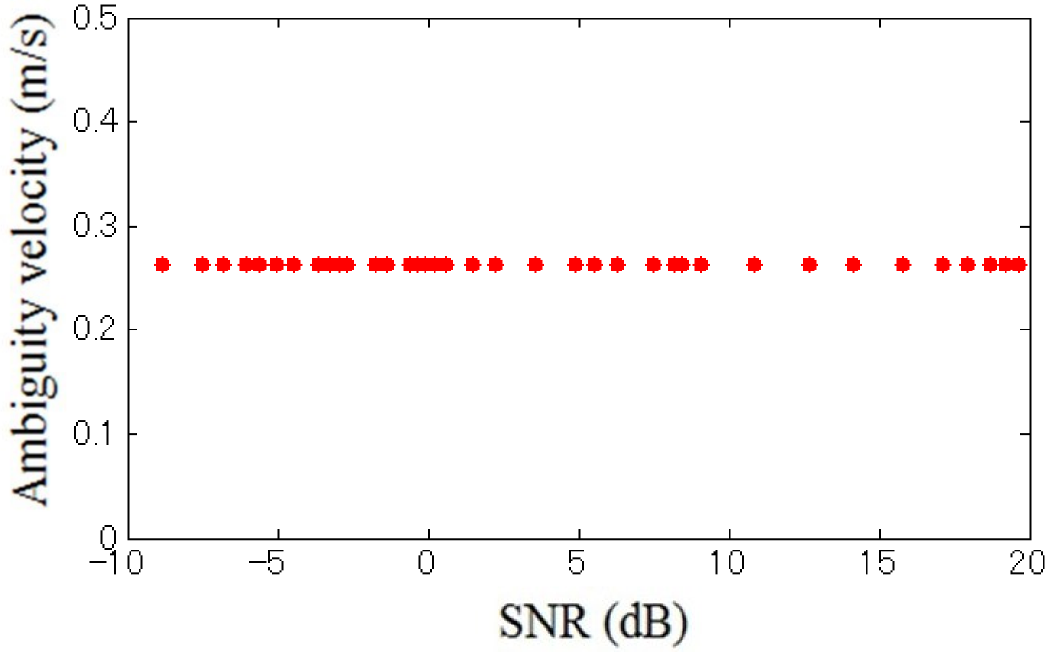

Figure 4-25 Measurement and theoretical errors of CNDS, CHDS and CMDS under different ambiguity velocities at different SNRs. a)-1, measurement errors at the 2 dB range of SNRs; a)-2, used ambiguity velocities; b)-1, measurement errors at the 4 dB range of SNRs; b)-2, used ambiguity velocities; c)-1, measurement errors at the 8 dB range of SNRs; c)-2, used ambiguity velocities; d)-1 measurement errors at the 16 dB range of SNRs; d)-2, used ambiguity velocities; e)-1 measurement errors of CNDS, CMDS and CHDS at one fixed ambiguity velocity of 0.2625 m/s; e)-2, used ambiguity velocities.

Based on the ambiguity velocities used at different ranges of SNRs, the measurement results are shown in Figure 4-25, where “(m)” means measurement result in experiment and “(T)” means theoretical analyzed result. In Figure 4-25, all measurement errors from experimental data fit the theoretical calculation well, which means that the theoretical analysis can be used to evaluate CNDS, CHDS and CMDS systems well when only white Gaussian noise occurs. According to the measurement results of CMDS from Figure 4-25 a) to Figure 4-25 e), we can find that the smaller the range of SNRs is, the better the measurement results will be. Comparing the results in Figure 4-25 a) and Figure 4-25 b), this shows that when the range of SNRs is less than 4 dB, the measurement error will only decrease slightly as the range of SNRs decreases. While comparing the results of CMDS from Figure 4-25 b) to Figure 4-25 e), CMDS using an ambiguity velocity of the 4 dB range of SNRs can provide accurate and precise velocities at a wide range of SNRs. Taking into consideration of both measurement error and the sensitivity to noise, the 4 dB range of SNRs is a good choice for the usage of CMDS using adaptive algorithm.

b. Dynamic experiment

The hydrophone is fixed, the projector is moving with a constant velocity of 0.200 m/s forward and backward to the hydrophone. In this situation, the received signal contains not only white Gaussian noise, but also the noises generated from the 3 dimension moving device and the vibration of the frame and the bar connected with the projector. The generated noise from the 3 dimension moving device is shown in Figure 4-26. In Figure 4-26 a), the yellow line on the oscilloscope is the generated signal from the generator, and the blue line is the received signal from the hydrophone when the engine of the 3 dimension moving device is turn off. The received signal with lots of noise in Figure 4-26 b) is the situation when the engine is turn on. Comparing Figure 4-26 a) and Figure 4-26 b), the noise from the engine of the 3 dimension moving device is large.

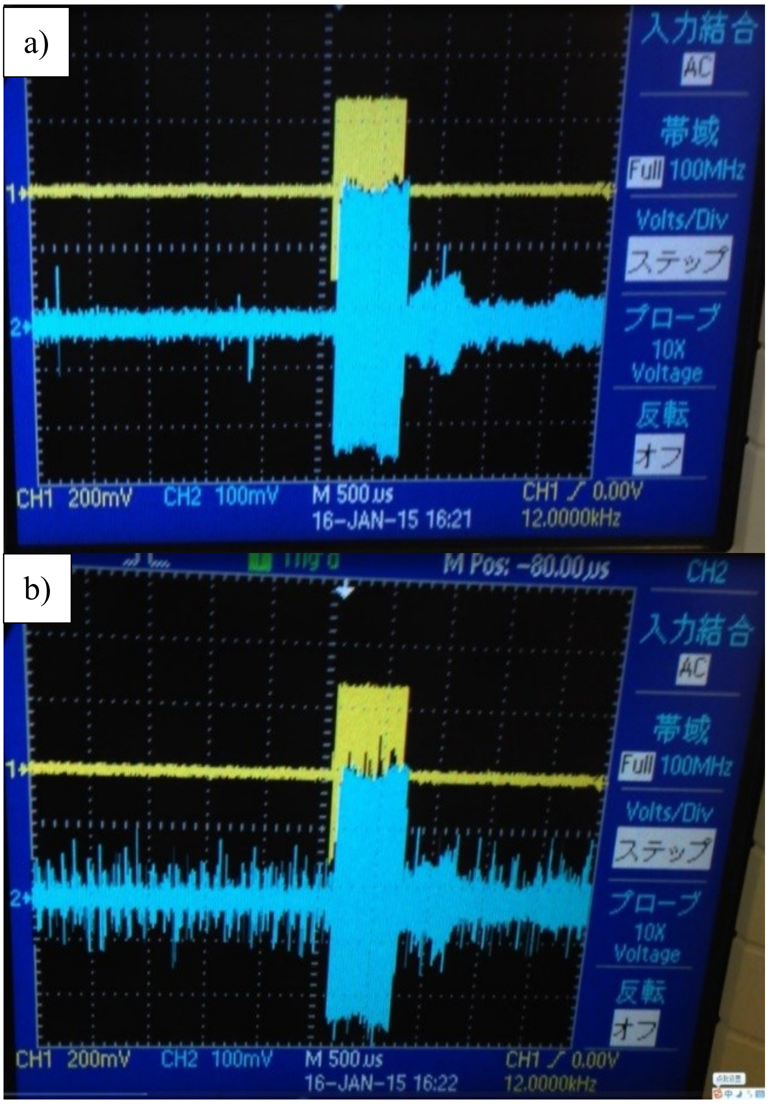

Figure 4-26 Transmitted and received signals with and without engine turn on.

The structure of the installed projector is shown in Figure 4-27. When the moving projector changes direction, the force generated by the three dimension moving device vibrates the bar connected with the projector. This vibration continues even when the acceleration generated from the 3 dimension moving device is zero. The vibration increases the measurement error of CNDS, CHDS and CMDS.

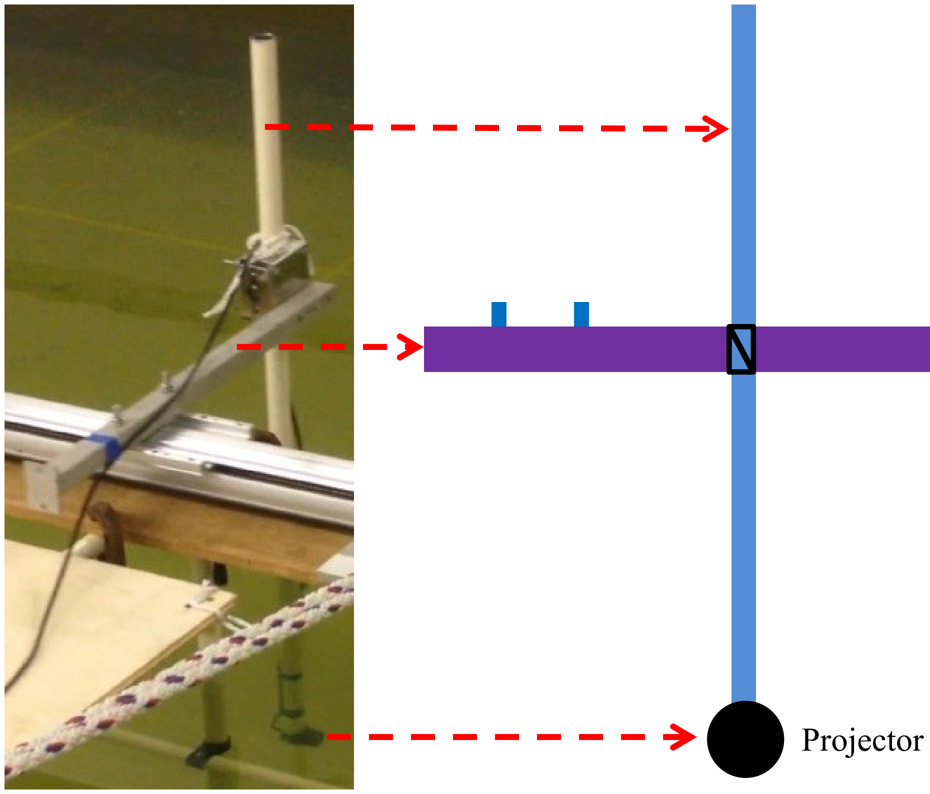

Figure 4-27 Structure of installed projector.

The following figures from Figure 4-28 to Figure 4-43 show measurement results of 0.200 m/s by CNDS, CHDS and CMDS at four SNRs, -11 dB, -2 dB, 5 dB and 13 dB. The ambiguity velocities used at these SNRs are shown in Table 4-5 for every 8 dB from -12 dB to 20 dB. These results are chosen from the smooth moving periods. In these figures, first the velocities measured by CNDS, CHDS and CMDS are shown together in one figure, and then the next three figures show the velocities separately measured by CNDS, CHDS and CMDS.

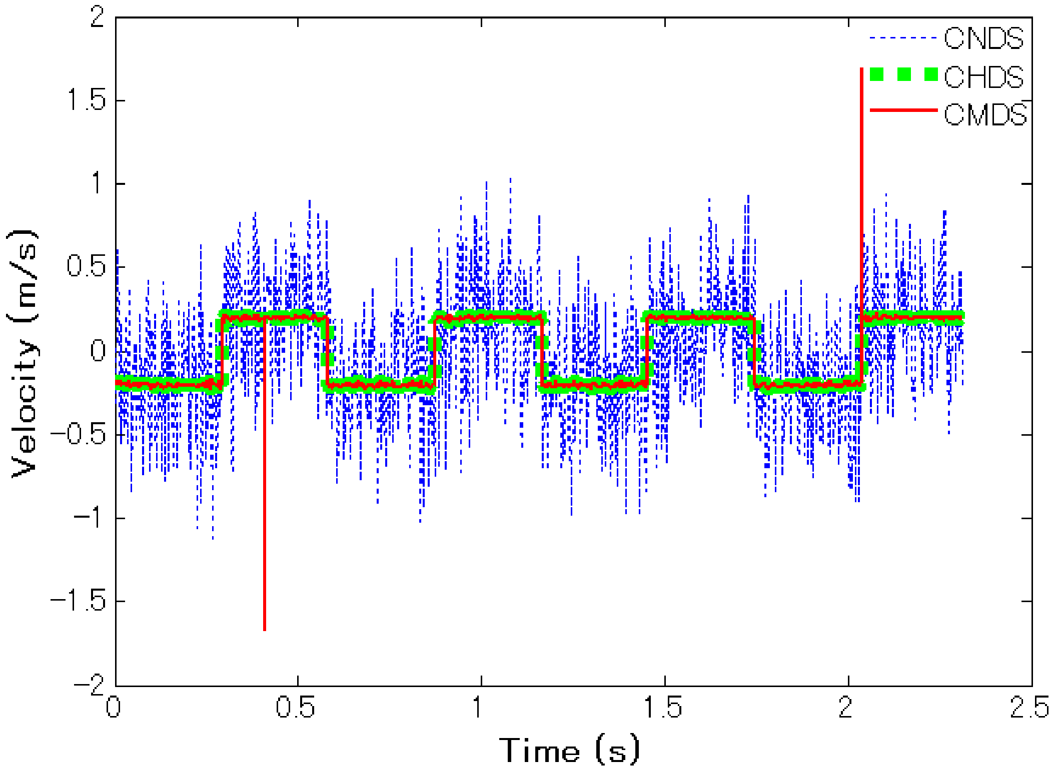

Figure 4-28 Measurement results of 0.200 m/s by CNDS, CHDS and CMDS using the ambiguity velocity of 0.938 m/s at the SNR of -11 dB.

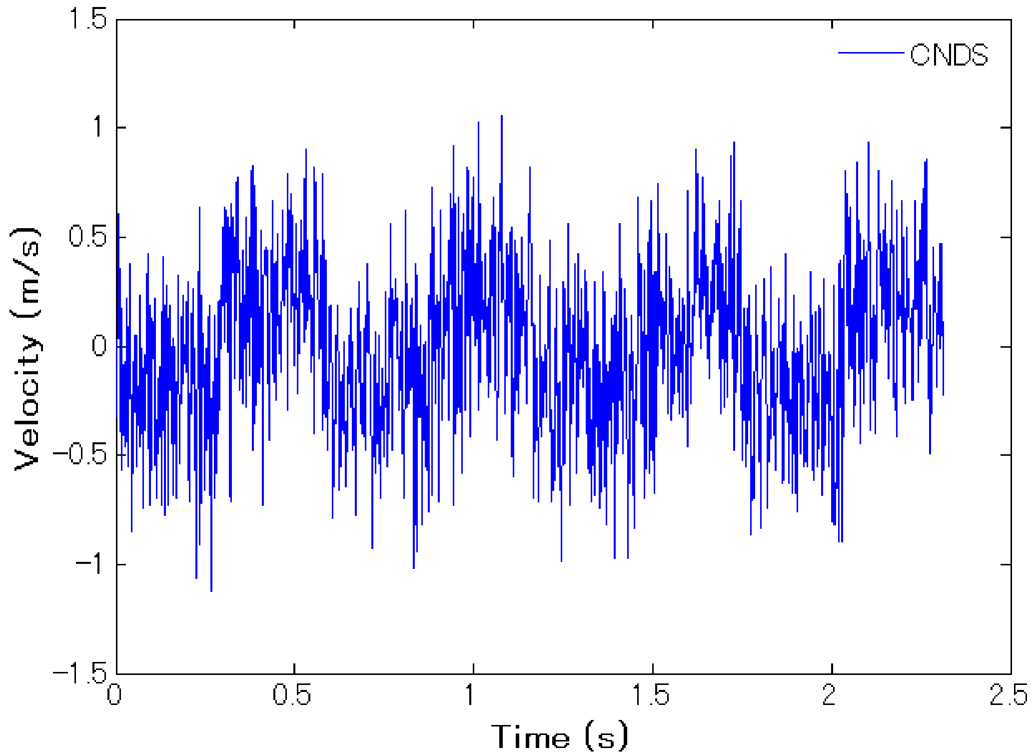

Figure 4-29 Measurement results of 0.200 m/s by CNDS at the SNR of -11 dB.

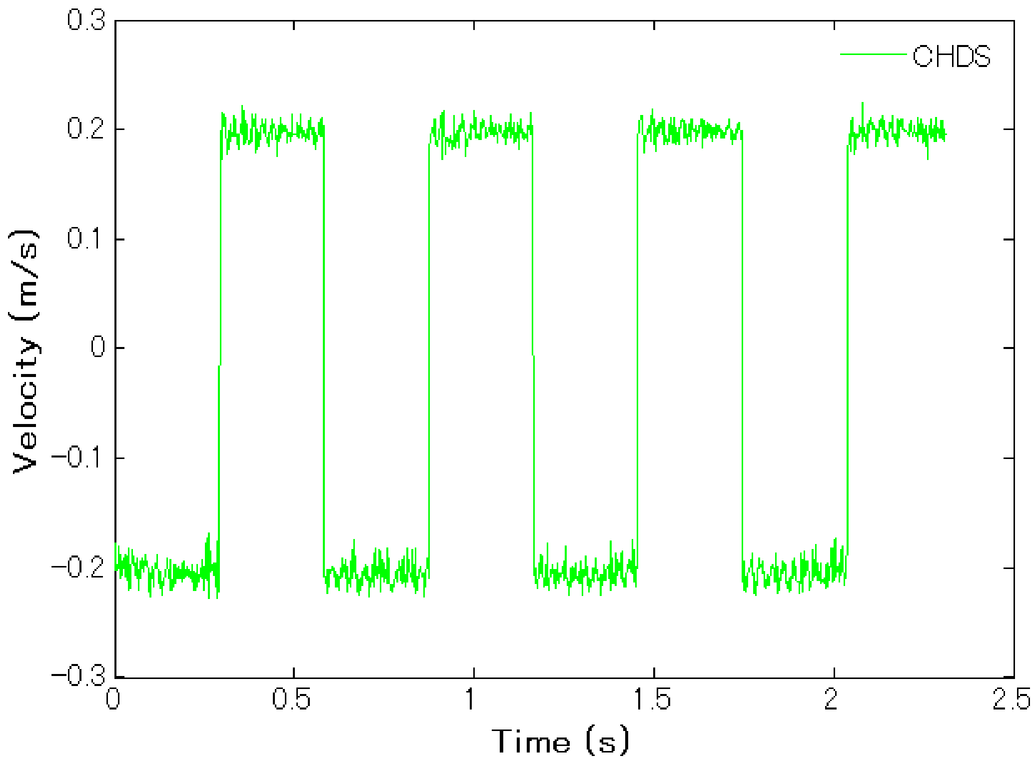

Figure 4-30 Measurement results of 0.200 m/s by CHDS at the SNR of -11 dB.

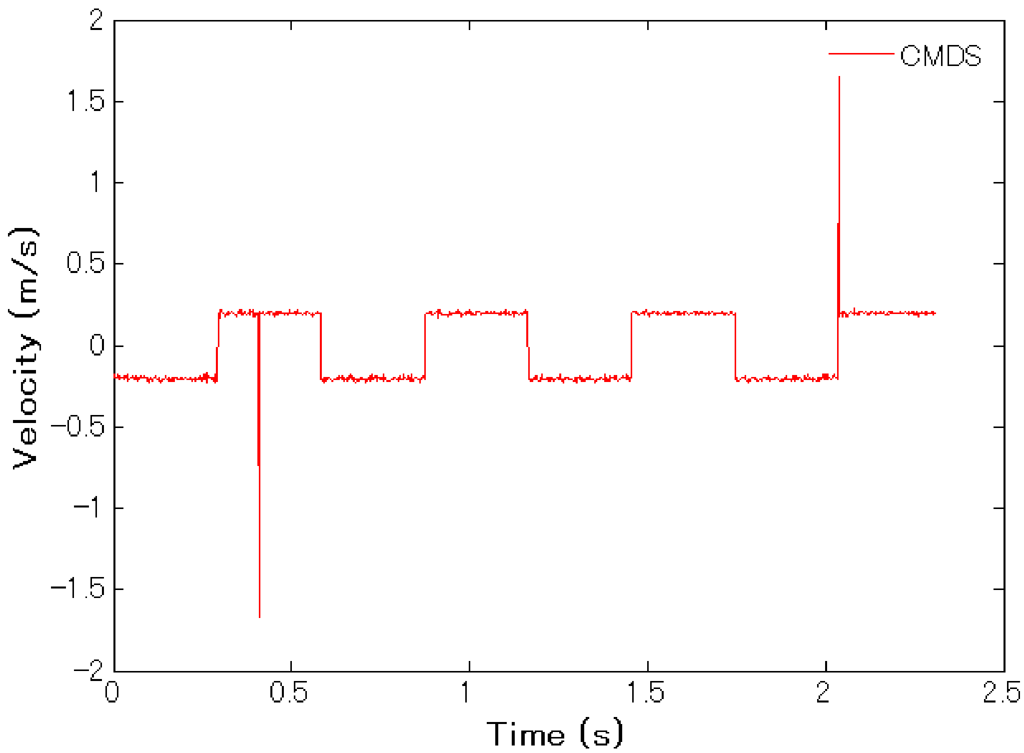

Figure 4-31 Measurement results of 0.200 m/s by CMDS using the ambiguity velocity of 0.938 m/s at the SNR of -11 dB.

From Figure 4-28 to Figure 4-31, the velocities measured by three methods at the SNR of -11 dB are shown. The velocities measured by CNDS (Figure 4-29) are very noisy. Velocities measured by CHDS are more precise than CNDS as shown in Figure 4-30. Although velocities measured by CMDS using the ambiguity velocity of 0.938 m/s can be mostly as precise as CHDS, but because of the wrong estimation of integer factor n impulsive noise occurs.

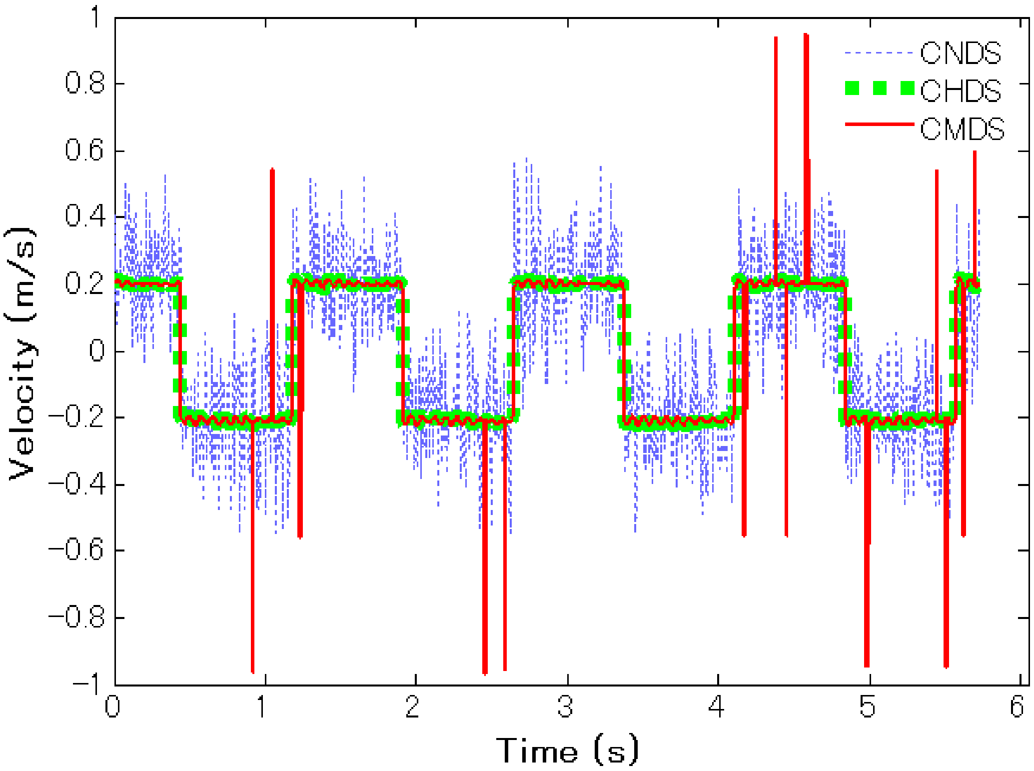

Figure 4-32 Measurement results of 0.200 m/s by CNDS, CHDS and CMDS using the ambiguity velocity of 0.375 m/s at the SNR of -2 dB.

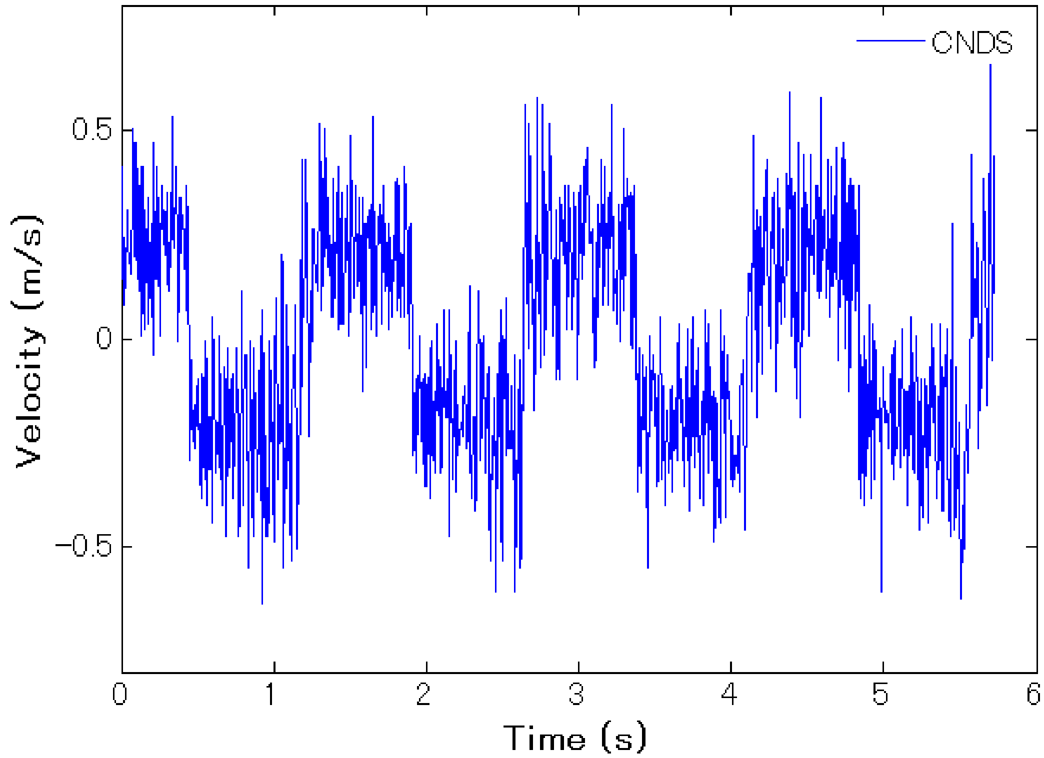

Figure 4-33 Measurement results of 0.200 m/s by CNDS at the SNR of -2 dB.

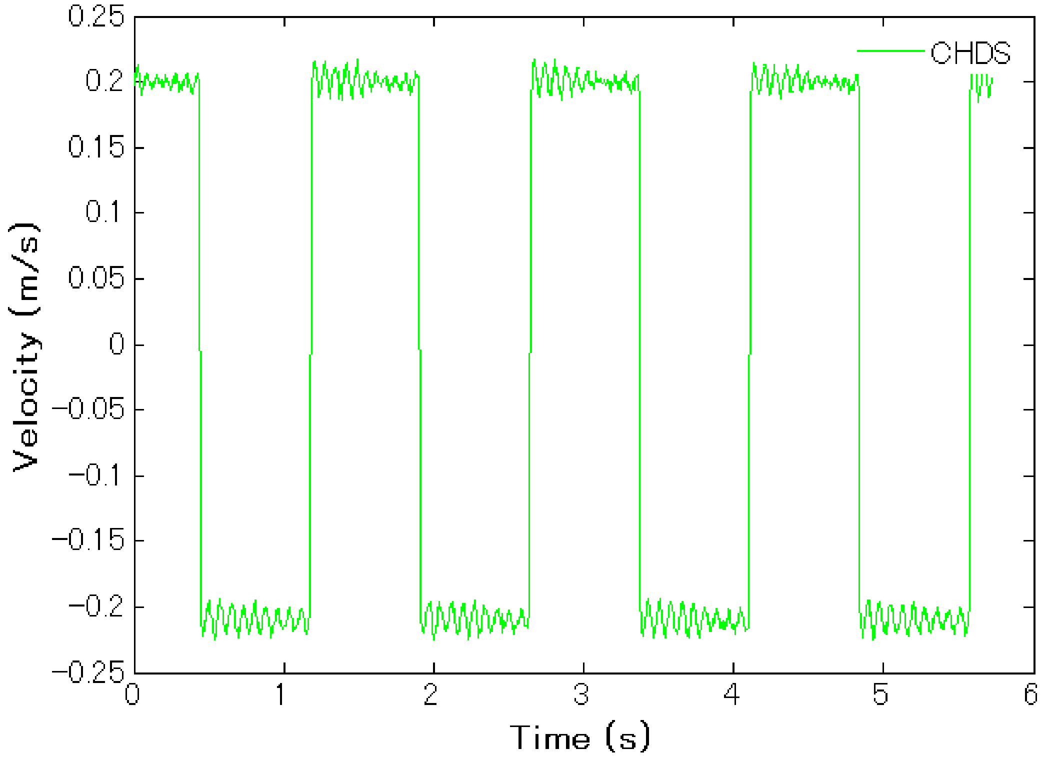

Figure 4-34 Measurement results of 0.200 m/s by CHDS at the SNR of -2 dB.

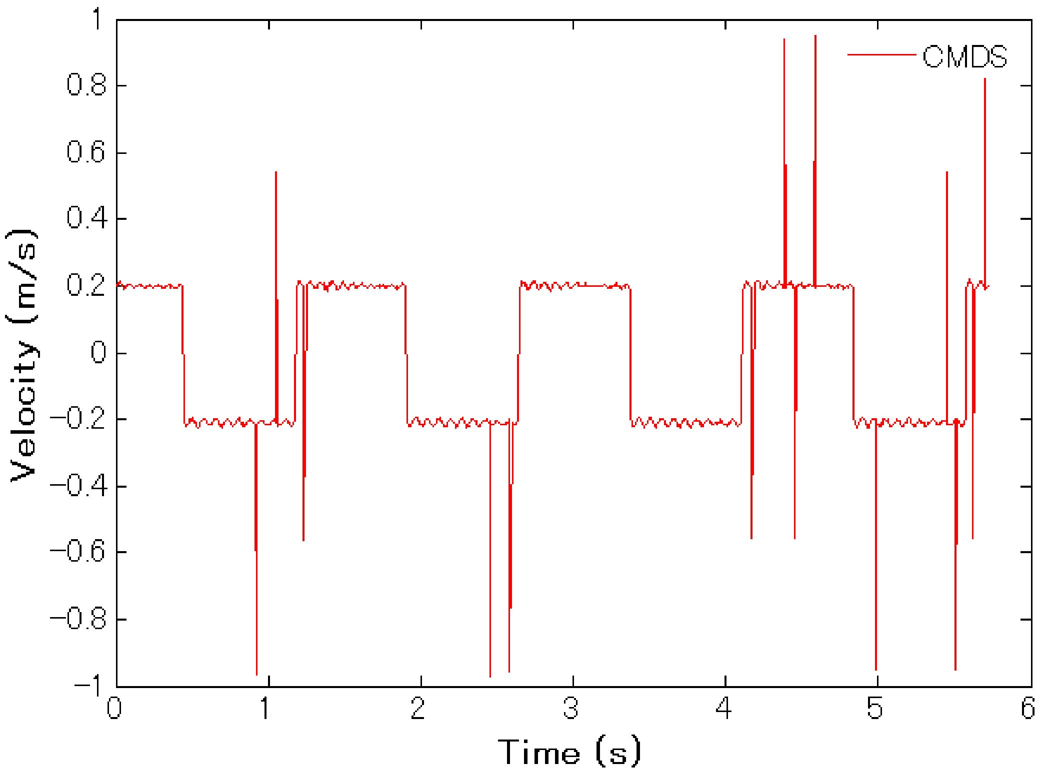

Figure 4-35 Measurement results of 0.200 m/s by CMDS using the ambiguity velocity of 0.375 m/s at the SNR of -2 dB.

From Figure 4-32 to Figure 4-35, the figures present the measurement results at the SNR of -2 dB. Velocities measured by CNDS in Figure 4-33 are noisy, but they are better than the results shown in Figure 4-29. Velocities measured by CHDS shown in Figure 4-34 are much smoother than those of CNDS. In Figure 4-34, the vibration generated from the bar is also obvious. This shows that CHDS can even pick up the vibration information while the projector is moving. Velocities measured by CMDS using the ambiguity of 0.375 m/s are shown in Figure 4-35. It can also provide immediate accurate and precise velocity, but as the ambiguity velocity decreases, the impulsive noise, shown in Figure 4-35, increases.

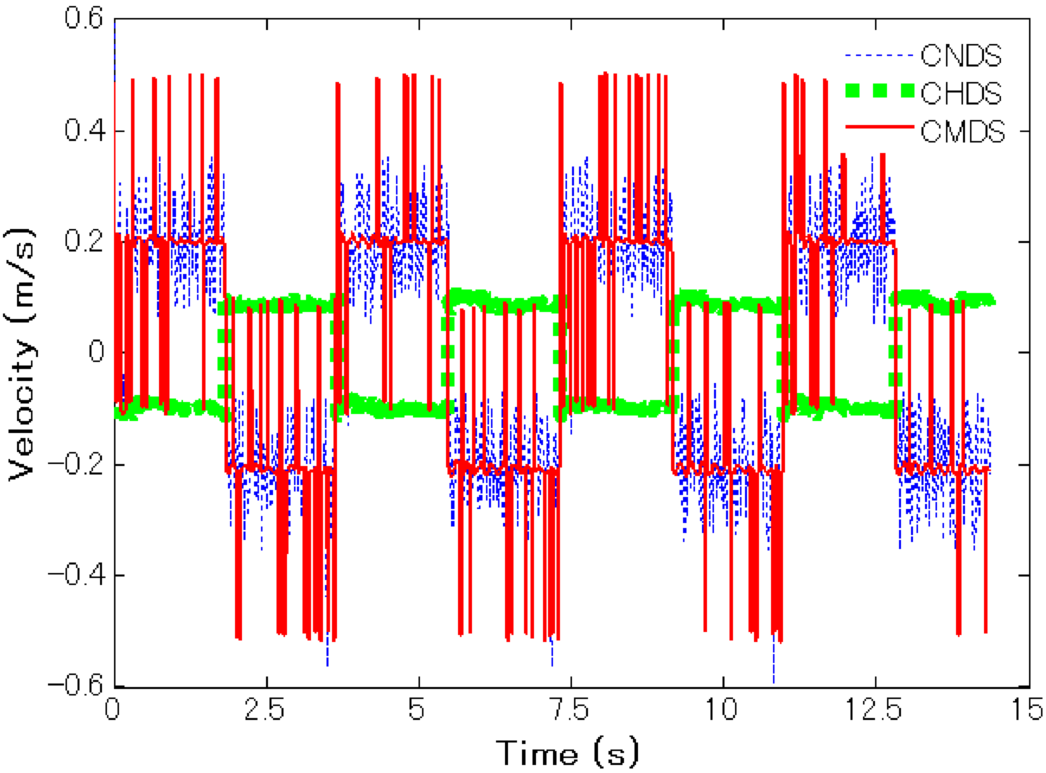

Figure 4-36 Measurement results of 0.200 m/s by CNDS, CHDS and CMDS using the ambiguity velocity of 0.150 m/s at the SNR of 5 dB.

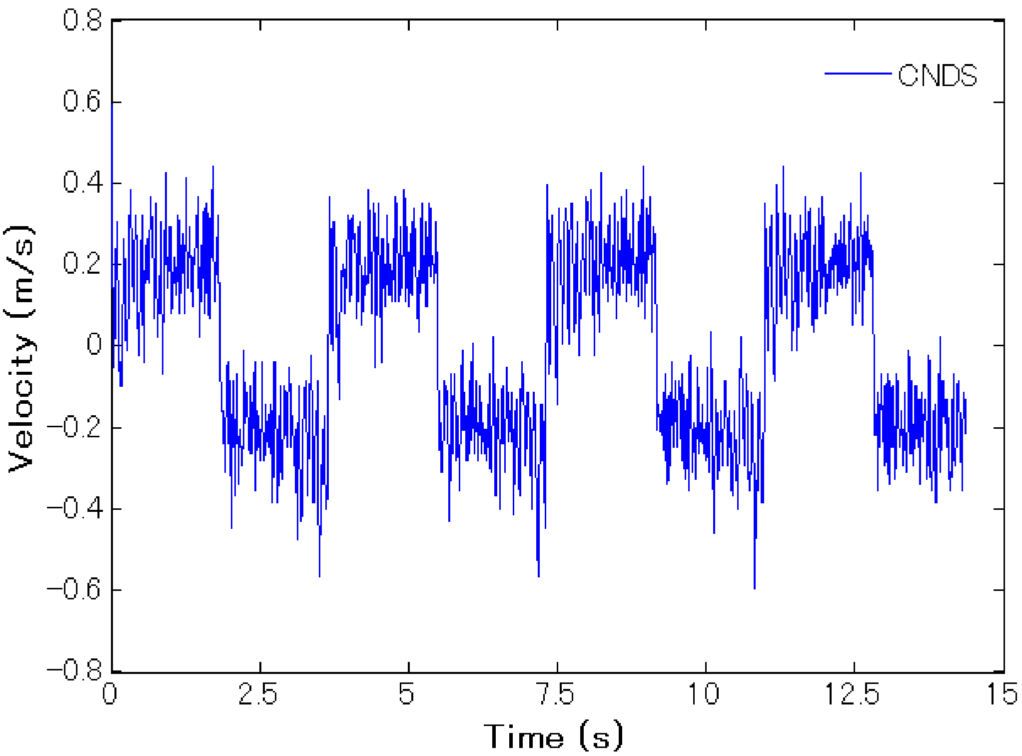

Figure 4-37 Measurement results of 0.200 m/s by CNDS at the SNR of 5 dB.

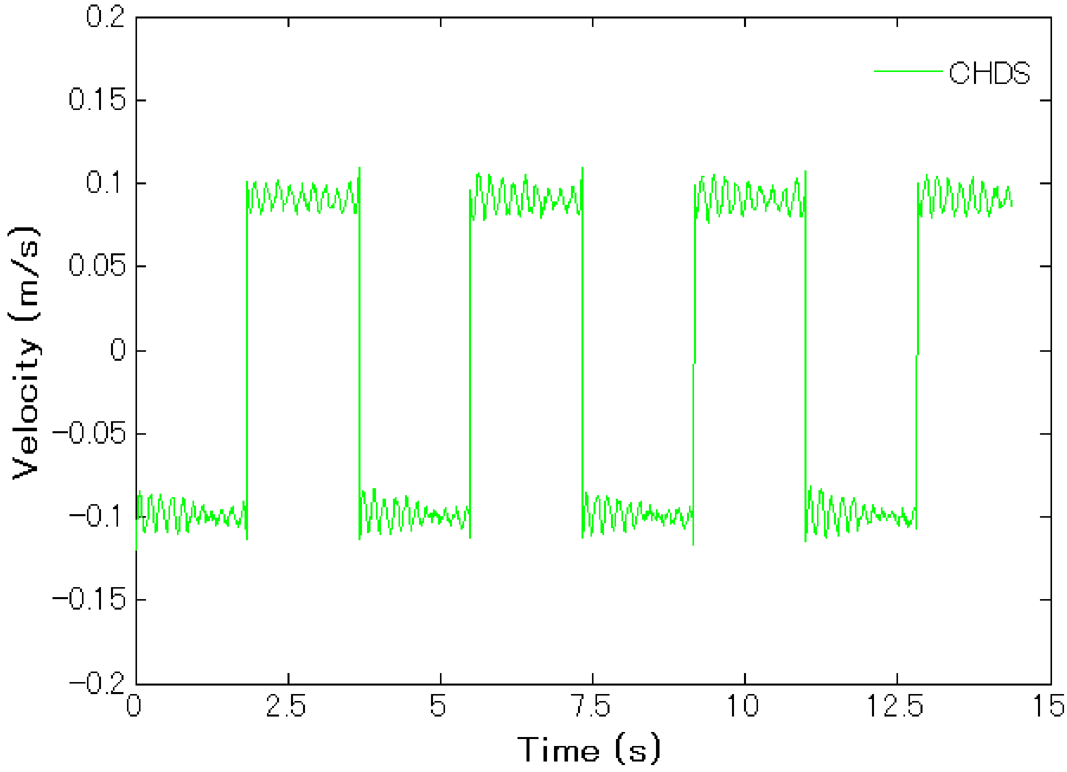

Figure 4-38 Measurement results of 0.200 m/s by CHDS at the SNR of 5 dB.

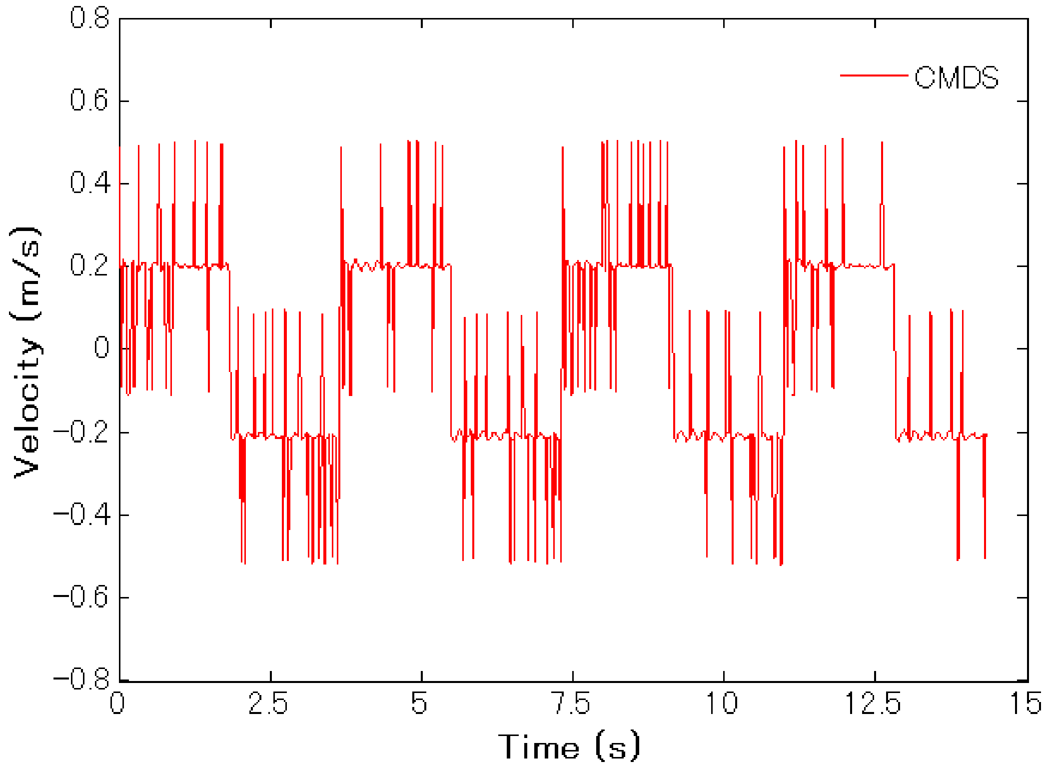

Figure 4-39 Measurement results of 0.200 m/s by CMDS using the ambiguity velocity of 0.150 m/s at the SNR of 5 dB.

From Figure 4-36 to Figure 4-39, the figures present the measurement results at the SNR of 5 dB. Velocities measured by CNDS in Figure 4-37 become precise, compared with the results measured at the SNR of -11 dB and -2 dB. Velocities measured by CHDS shown in Figure 4-38 are much more precise than CNDS, but not correct, because the ambiguity velocity used in CHDS is 0.150 m/s which is less than the measured velocity, so the velocities measured by CHDS cannot reflect the true measured velocity. However, the vibration can be presented in the measurement results of CHDS as a wave. Velocities measured by CMDS using the ambiguity of 0.150 m/s are shown in Figure 4-39. It can provide accurate and precise velocity immediately without velocity ambiguity, but as the ambiguity velocity decreases, the impulsive noise increases, occurs more often.

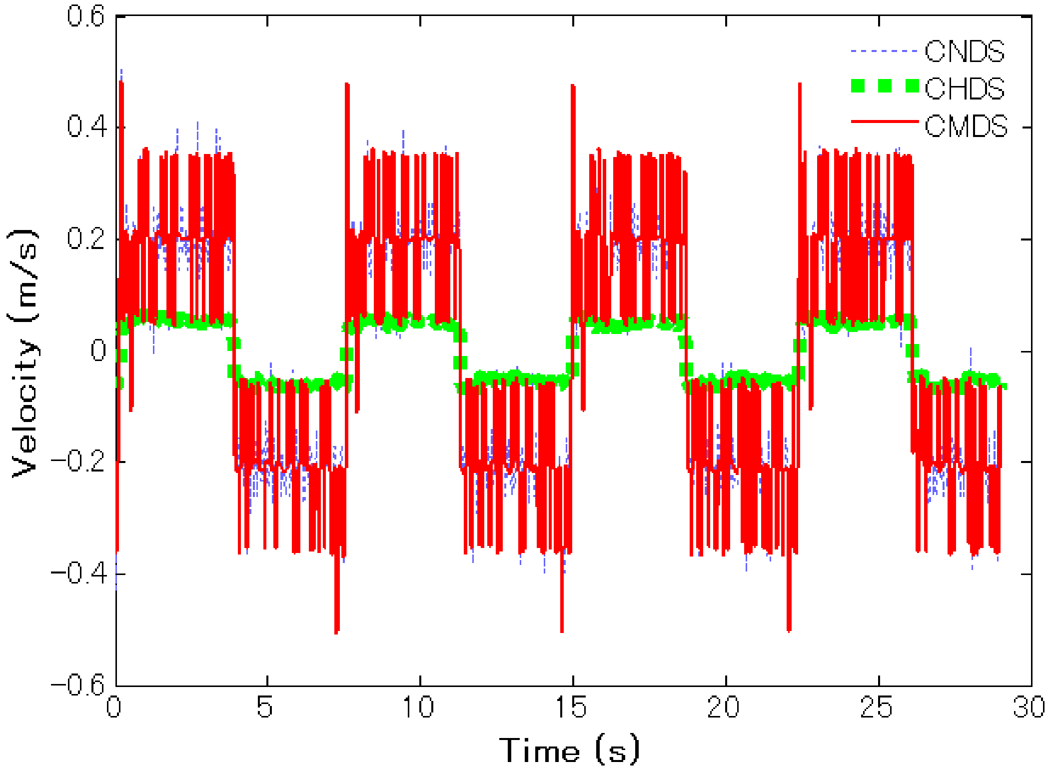

Figure 4-40 Measurement results of 0.200 m/s by CNDS, CHDS and CMDS using the ambiguity velocity of 0.075 m/s at the SNR of 13 dB.

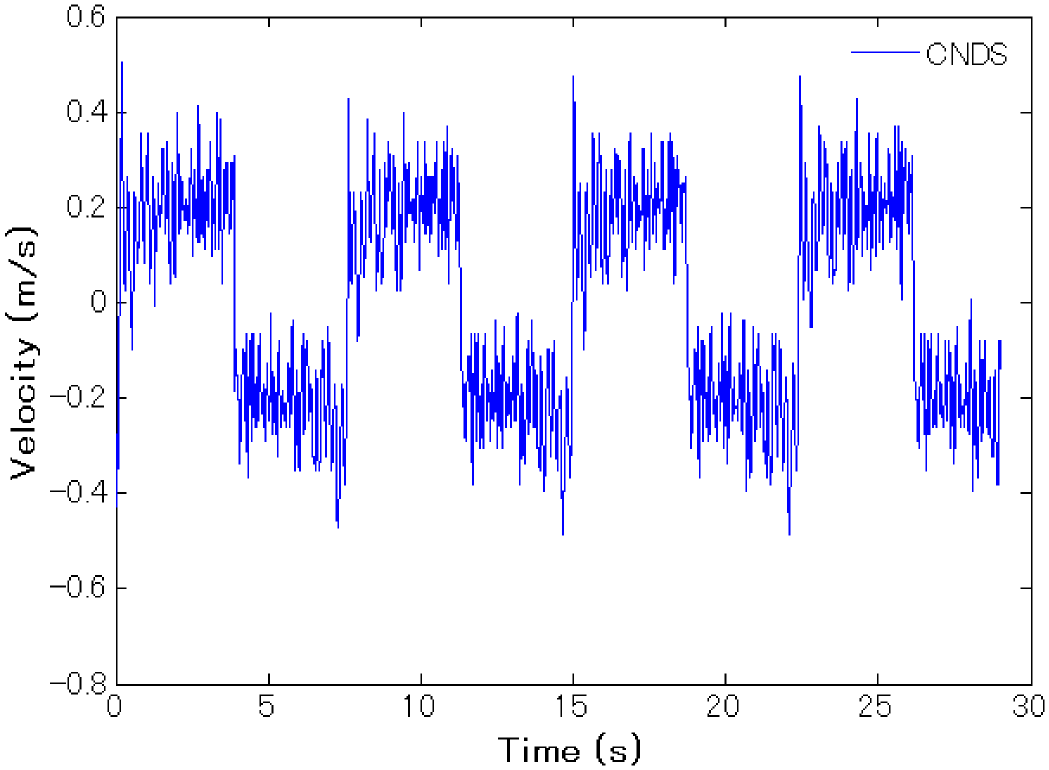

Figure 4-41 Measurement results of 0.200 m/s by CNDS at the SNR of 13 dB.

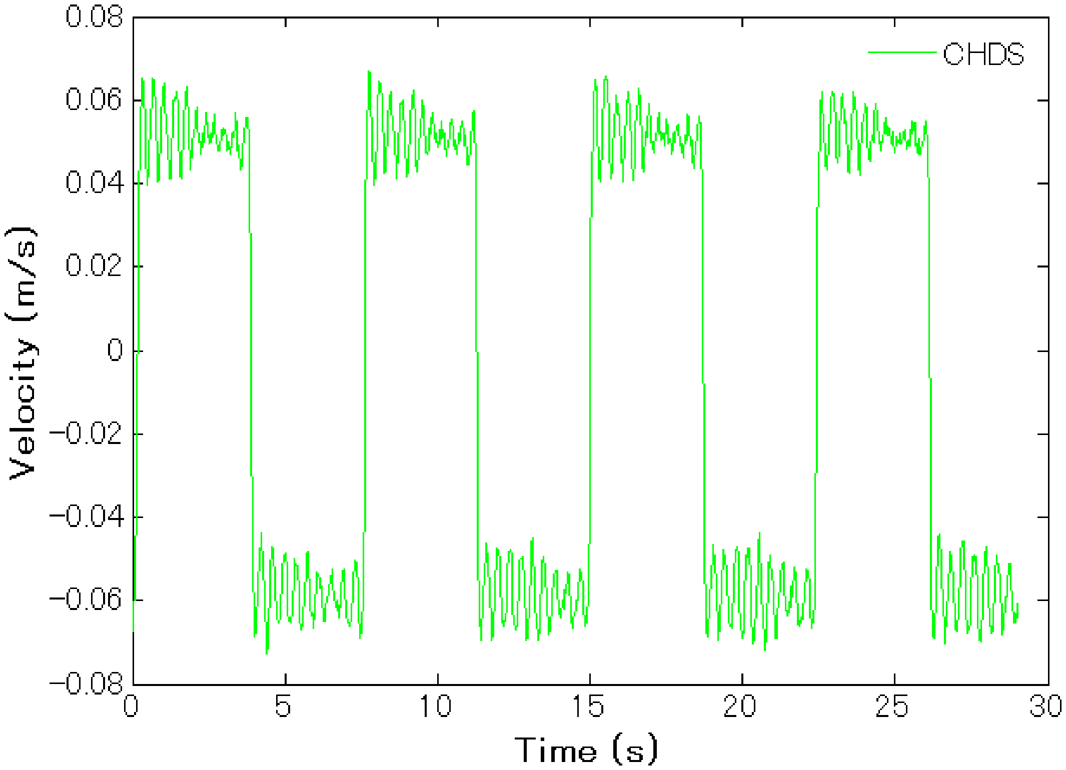

Figure 4-42 Measurement results of 0.200 m/s by CHDS at the SNR of 13 dB.

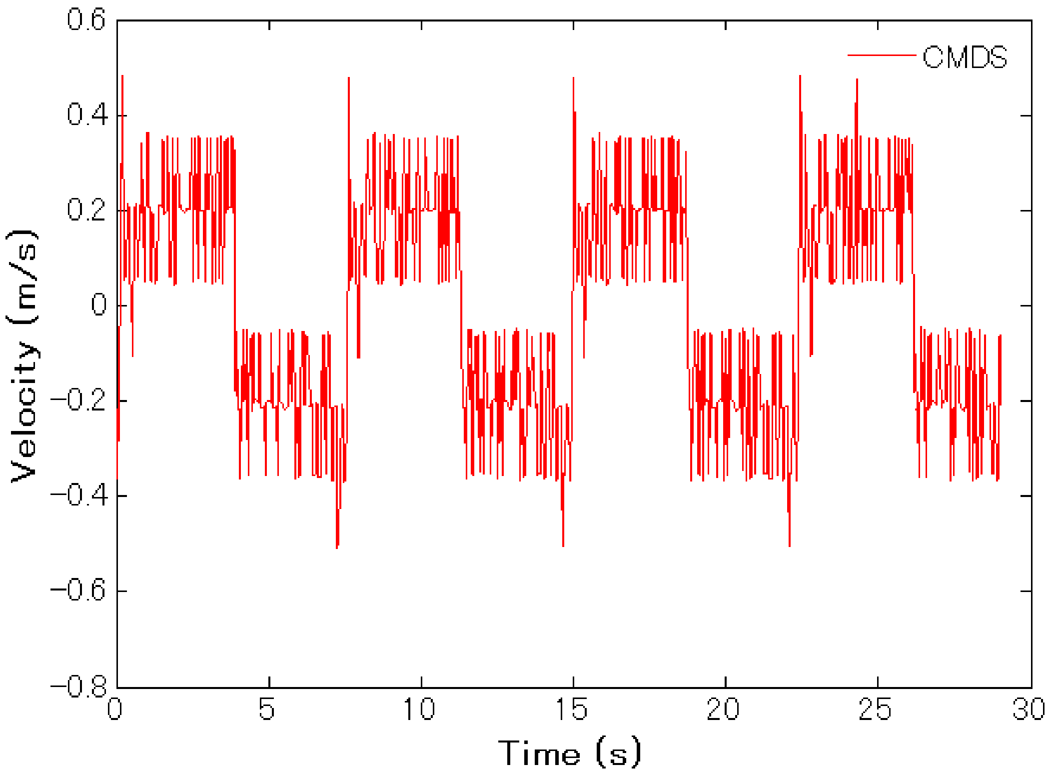

Figure 4-43 Measurement results of 0.200 m/s by CMDS using the ambiguity velocity of 0.075 m/s at the SNR of 13 dB.

From Figure 4-40 to Figure 4-43, the figures present the measurement results at the SNR of 13 dB. Compared with the results shown before, the error of velocities measured by CNDS decrease when the SNRs increase. Velocities measured by CHDS shown in Figure 4-42 are limited by the ambiguity velocity of 0.075 m/s. Velocities measured by CMDS using the ambiguity of 0.075 m/s are shown in Figure 4-43. Because of impulsive noise, velocity measured by CMDS is almost as noisy as CNDS.

Measurement results of CMDS using adaptive algorithm does not work as well as theoretical analysis and the situation where the transducers are fixed. This is a result of the affection of vibration generated by the bar used to connect the projector. The measurement error of CNDS, CHDS and CMDS using different ambiguities shown in Table 4-5 are shown from Figure 4-44 to Figure 4-48.

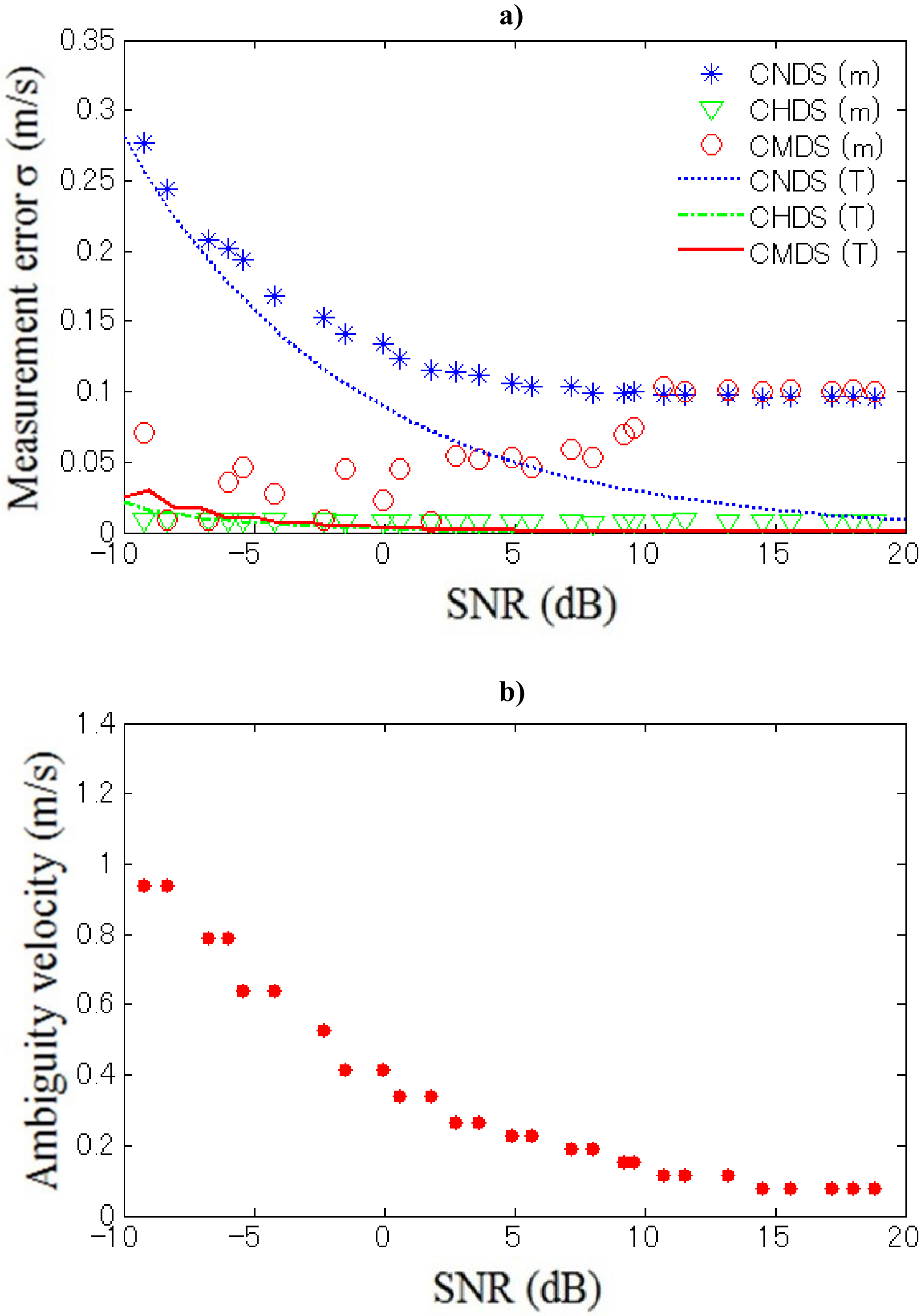

Figure 4-44 Measurement errors of CNDS, CHDS and CMDS under the ambiguity velocities with the range of SNRs as 2 dB. a), measurement errors of three methods; b), used ambiguity velocities.

a)

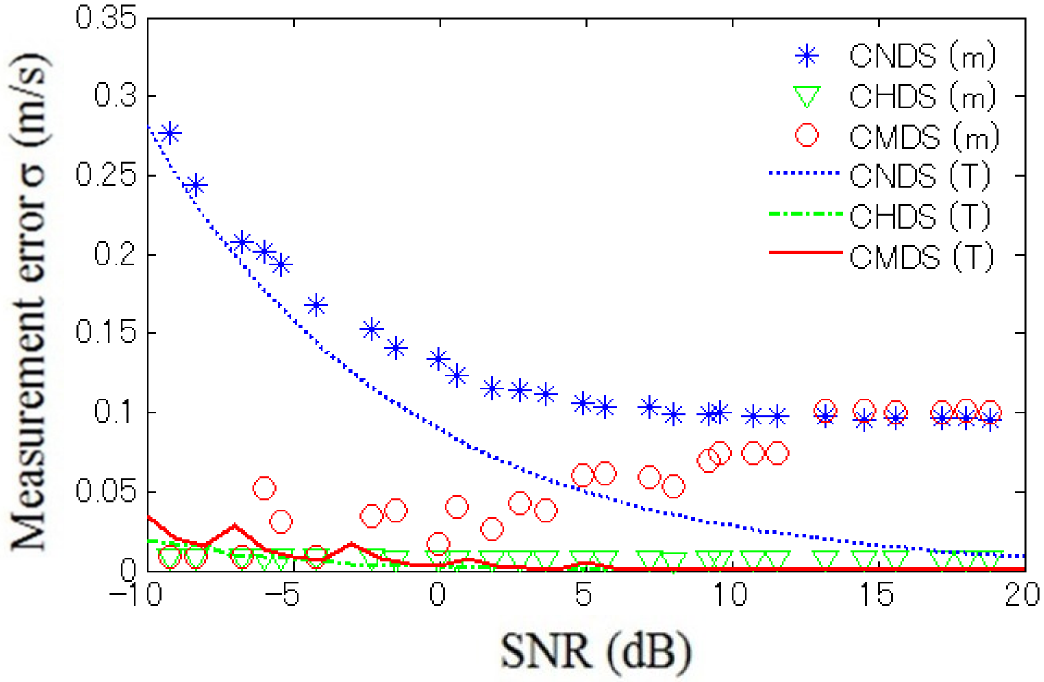

b)

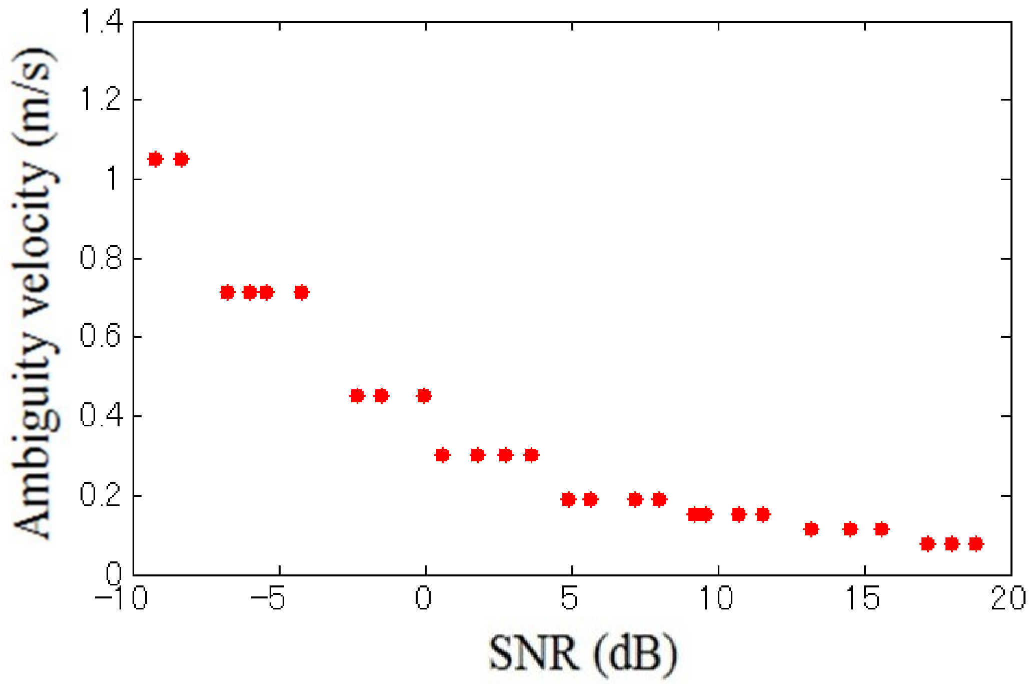

Figure 4-45 Measurement errors of CNDS, CHDS and CMDS under the ambiguity velocities with the range of SNRs as 4 dB. a), measurement errors of three methods; b), used ambiguity velocities.

a)

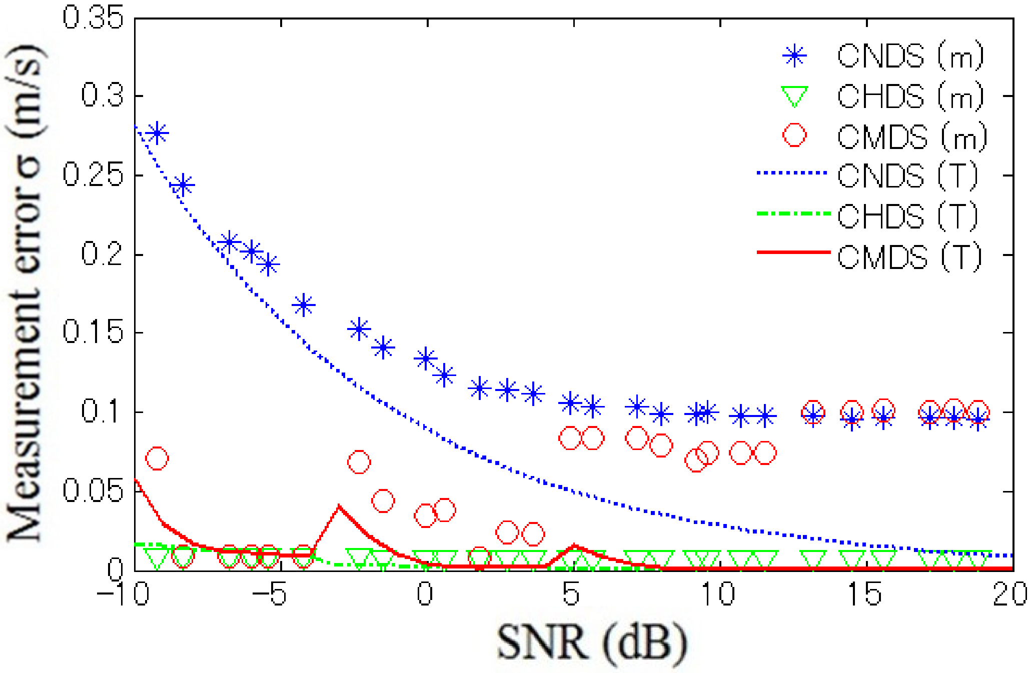

b)

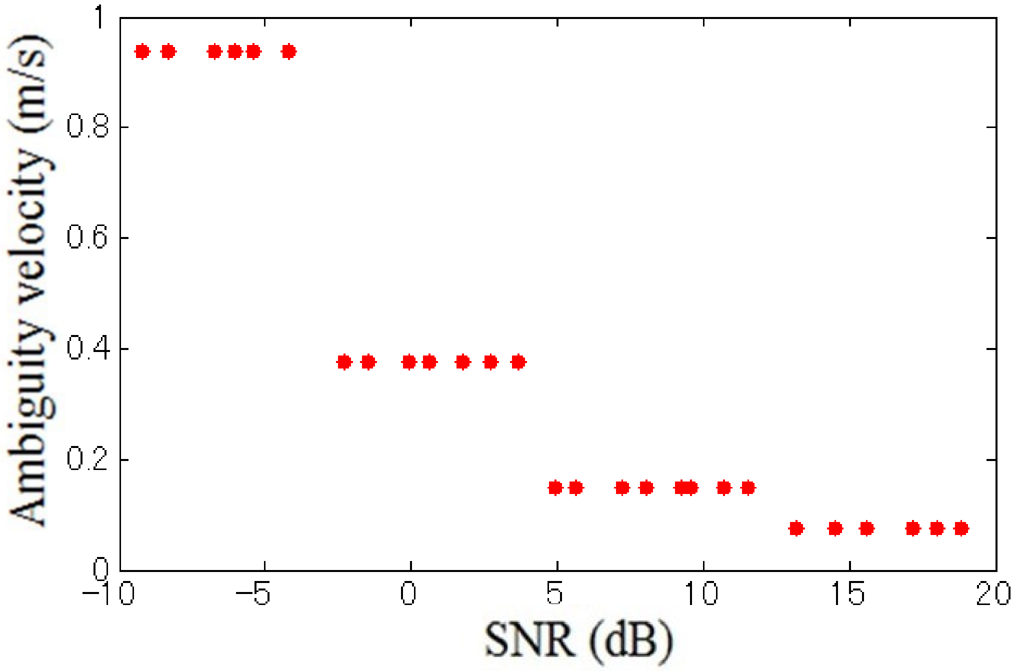

Figure 4-46 Measurement errors of CNDS, CHDS and CMDS under the ambiguity velocities with the range of SNRs as 8 dB. a), measurement errors of three methods; b), used ambiguity velocities.

a)

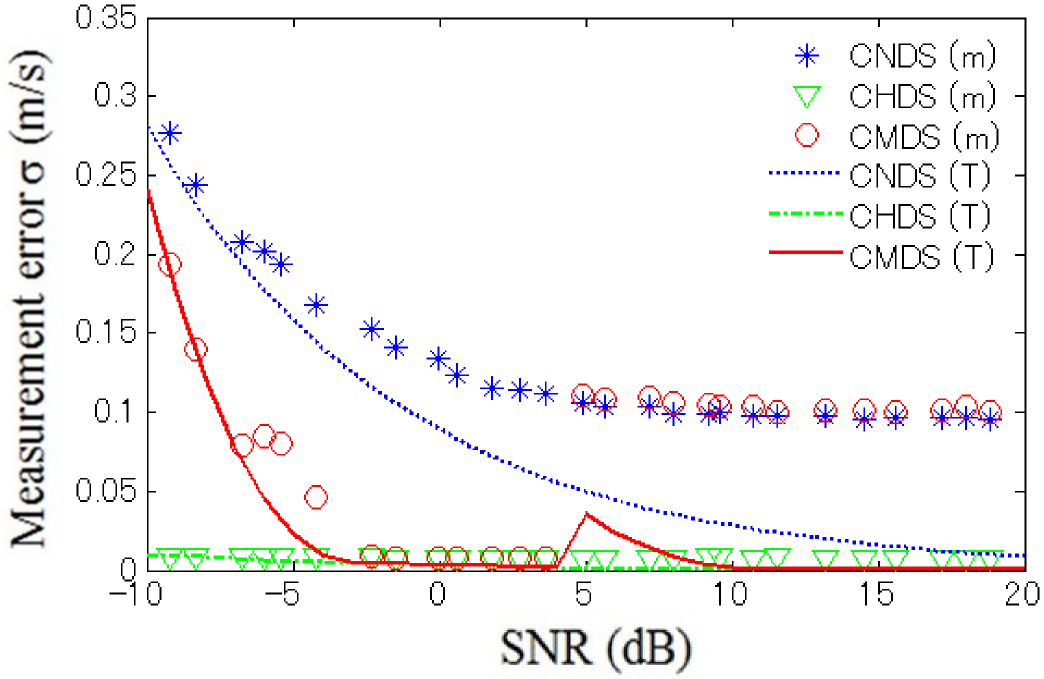

b)

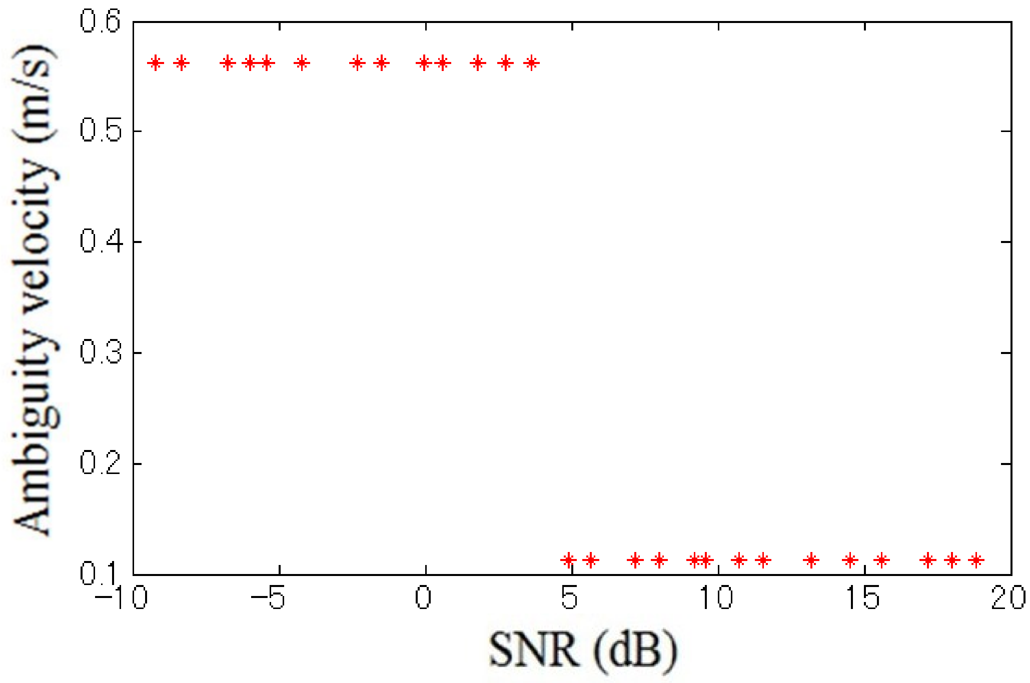

Figure 4-47 Measurement errors of CNDS, CHDS and CMDS under the ambiguity velocities with the range of SNRs as 16 dB. a), measurement errors of three methods; b), used ambiguity velocities.

a)

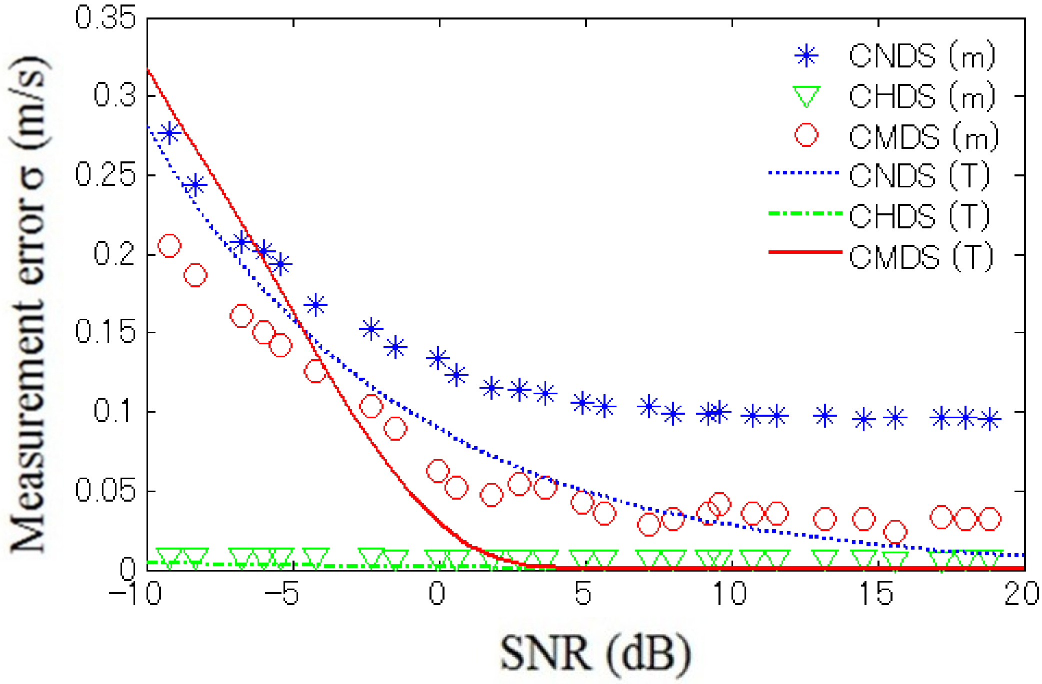

b)

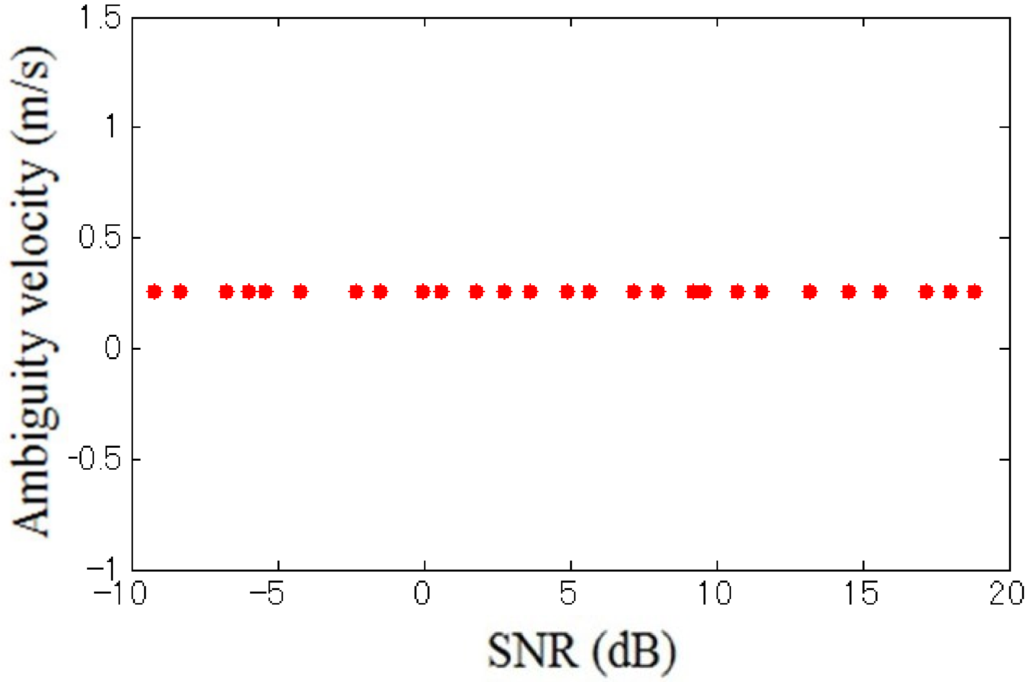

Figure 4-48 Measurement errors of CNDS, CHDS and CMDS under the ambiguity velocities with the range of SNRs as 32 dB. a), measurement errors of three methods; b), used ambiguity velocities.

From Figure 4-44 to Figure 4-48, the velocity measurement error by CNDS is much worse than the theoretical results, especially at the range of high SNRs. Because of the vibration and electro-magnetic noise from three dimension traverser, measurement error of CNDS (blue asterisk) is much larger than theoretical analysis (blue line), especially at high SNRs. Using ambiguity velocities calculated based on theoretical analysis shown in Table 4-5, the probability of wrong estimation for integer factor increases a lot, because of the noisier measurement results of CNDS. With improper ambiguity velocities, measurement results of CMDS are larger than theoretical analysis. According to the measurement error from Figure 4-44 to Figure 4-48, CMDS using the ambiguity velocities determined by adaptive algorithm based on Eq. (4-28) does not perform well in non-white Gaussian noise.

References

[1] J. R. Taylor, “An Introduction to Error Analysis The Study of Uncertainties in Physical Measurements,” Oxford University Press, pp.3-98, 1982.

[2] P. Z. Peebles, “Probability , Random Variables, and Random Signal Principles,” McGraw-Hill Book Company, pp.42-45, 1980.

[3] P.Z. Peebles, “Probability, Random Variables and Random Signal Principles,” McGraw-Hill, Inc., pp.42-45, 1980.

[4] A. Papoulis, “Probability, Random Variables, and Stochastic Process (Third Edition),” McGraw Hill, Inc., pp.136, 1991.

[5] R. S. Berkowitz, “Modern Radar analysis, evaluation, and system design,” John Wiley & Sons, Inc., New York, p.170, 1965.

[6] A.B. Williams, F.J. Taylor, “Electronic Filter Design Handbook (Fourth Edition),” McGraw-Hill, pp.42–52, 2006.

[7] NF Co., “Multifunction Generator WF1973/WF1974 Instruction Manual (Basics),” pp.1.

[8] NF Co., “High Speed Bipolar Amplifier HSA4011 Operation Manual,” pp.1-2.

[9] NF Co., “Measure League Differential Amplifier 5307 Operation Manual,” pp.1-2.

[10] Teledyne RESON Co., “Catalogue for Standard Transducers and Hydrophones,” pp.36, 82.

[11] Teledyne RESON Co., Calibration documents for bought transducer TC 2111.

[12] Teledyne RESON Co., Calibration documents for bought hydrophone TC 4034.

[13] National Instruments Co., “NI PXI/PXIe/PCI-5122 Specifications,” pp.1-5.

[14] THK Co., “Catalogue for Super FA series,” pp.10.

CHAPTER 5

CONCLUSIONS

Combined method of conventional and coherent Doppler sonars (CMDS) is proposed to provide accurate and precise velocity information. This method is proposed to overcome the disadvantages of long time lag for conventional Doppler sonar (CNDS) and velocity ambiguity for coherent Doppler sonar (CHDS). The advantages that large measureable velocity range of CNDS and precise measurement result of CHDS are taken into CMDS. According to the theoretical analysis and experiment results, we can draw some of the following conclusions.

The CMDS was designed to provide accurate and precise velocity information with a short time lag. According to the theoretical analysis, the measurement method and measurement error of CMDS are proposed. With variable shift and adaptive algorithm, the measurement error of CMDS is deduced. Simulation and experiment results of CMDS show that CMDS using adaptive algorithm can provide accurate and precise velocities as CHDS does without velocity ambiguity. The theoretical analyses fit the simulation and experiment results well when the noise is white Gaussian noise. Therefore, the theoretical analysis of CMDS system can be used as a basic method to evaluate the performance.

Although some achievements have been obtained from CMDS, CMDS can be improved if some considerations and proposals are implemented in the future research. They are shown following:

(1) Reducing impulsive noise

Impulsive noise is the specific characteristic of CMDS. When an ambiguity velocity used in CMDS is not appropriate for the measurement error of CNDS, the wrong estimation of integer factor occurs, which directs impulsive noise. The impulsive noise makes the measurement results of CMDS become noisy. If some methods can be introduced to cancel the impulsive noise, CMDS will be improved.

One method is considered to introduce inertial measurement unit sensor. With the acceleration information measured by inertial measurement unit sensor, the impulsive noise can be determined and canceled. Moreover, Kalman filter can also be used to decrease the probability of impulsive noise occurs.

(2) Searching suitable ambiguity velocity

As discussed in Chapter 4, optimum ambiguity velocity at each SNR is calculated based on theoretical analysis in white Gaussian noise according to adaptive algorithm. However, in dynamic experiment, measurement errors of CMDS using calculated optimum ambiguity velocities are larger than theoretical analyses because of vibration and non-white Gaussian noise. Therefore measurement error of CNDS in practical applications should be considered as the basic parameter to determine suitable ambiguity velocities at a wide range of SNRs.

ACKNOWLEDGEMENT

In 2010 I was admitted as an international student of the International Priority Graduate Program: Leadership Development Program for Maritime Sciences in Asia. First of all, I would like to express my deepest gratitude to the Graduate School of Maritime Sciences, Kobe University for the opportunity to pursue advanced studies and research in maritime sciences and for the financial support to make it possible.

I am most grateful to my supervisor, Professor Nobuyoshi Kouguchi for his guidance and support throughout my master and doctoral courses. While doing my research, his extraordinary efforts, tremendous encouragement, most valuable thoughts and advices helped me to complete my dissertation.

Special thanks go to Mr. Ikawa for his helpful support in preparing the experiments of this research.

I also thank all the members of Navigation Cybernetics Laboratory for their assistance.

Finally, my grateful thanks go to my family. I thank them for their love, blessing, and encouragement during my student years.